INFORMATION TO USERS

This manuscript has been reproduced from the microfilm master. UMI films the text directly from the original or copy submitted. Thus, some thesis and dissertation copies are in typewriter face, while others may be from any type of computer printer.

The quality of this reproduction is dependent upon the quality of the copy submitted. Broken or indistinct print, colored or poor quality illustrations and photographs, print bleedthrough, substandard margins, and improper alignment can adversely affect reproduction.

In the unlikely event that the author did not send UMI a complete manuscript and there are missing pages, these will be noted. Also, if unauthorized copyright material had to be removed, a note will indicate the deletion.

Oversize materials (e.g., maps, drawings, charts) are reproduced by sectioning the original, beginning at the upper left-hand corner and continuing from left to right in equal sections with small overlaps.

Photographs included in the original manuscript have been reproduced xerographically in this copy. Higher quality 6" x 9" black and white photographic prints are available for any photographs or illustrations appearing in this copy for an additional charge. Contact UMI directly to order.

ProQuest Information and Learning
300 North Zeeb Road, Ann Arbor, MI 48106-1346 USA
800-521-0600

UMI®

DISSERTATION

DYNAMICS OF ELECTRON TRANSFER REACTIONS IN RUTHENIUM-BASED DONOR-CHROMOPHORE-ACCEPTOR COMPLEXES INVOLVING PHENOTHIAZINE-TYPE DONORS

Submitted by

Bradford R. Limoges

Department of Chemistry

In partial fulfillment of the requirements

For the Degree of Doctor of Philosophy

Colorado State University

Fort Collins, CO

Fall 2001

COLORADO STATE UNIVERSITY

18 September, 2001

We hereby recommend that the dissertation prepared under our supervision by Bradford R. Limoges entitled Dynamics of Electron Transfer Reactions in Ruthenium-based Donor-Chromophore-Acceptor Complexes Involving Phenothiazine-type Donors be accepted as fulfilling in part the requirements for the Degree of Doctor of Philosophy.

Committee on Graduate Work

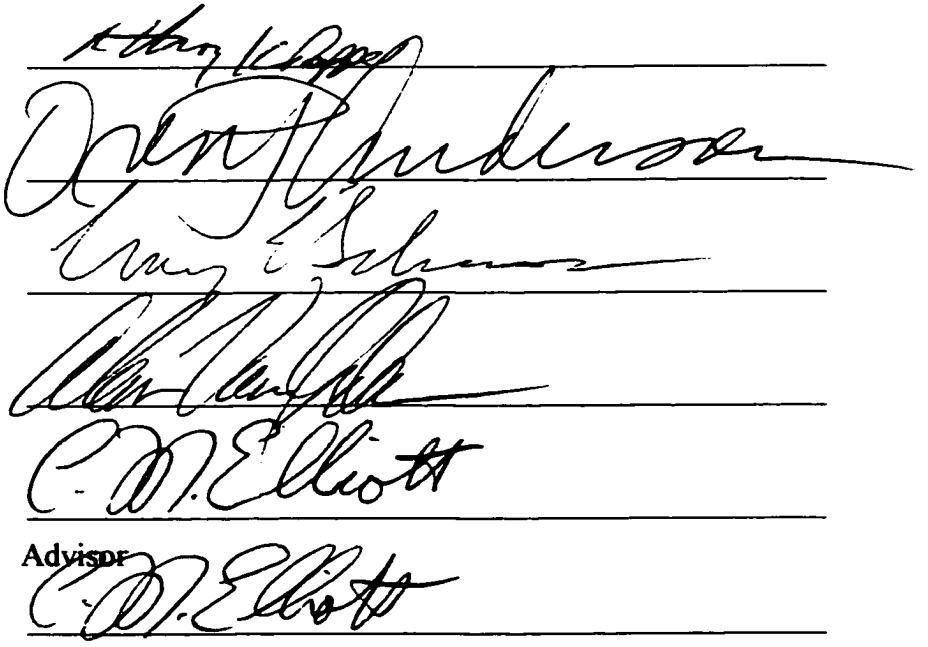

Advisor

Department Head

Abstract of Dissertation

Dynamics of Electron Transfer Reactions in Ruthenium-based Donor-Chromophore-Acceptor Complexes involving Phenothiazine-type Donors

A series of electron donating groups were synthesized to study the effect of driving force on the electron transfer between the donor and a photoexcited trisbipyridineruthenium (II) chromophore. The driving force for the electron transfer reaction is directly related to the oxidation potential of the donor. The findings can be understood in terms of a combination of driving force and a π-π interaction between the donor and the chromophore.

The π-π interaction was investigated to determine its role in the electron transfer reaction. To this end, a series of bipyridine-like ligands were used to make chromophores that either favored or hindered the π-π interaction. The existence of the π-π interaction was shown by spectroscopy and NMR studies. The electron transfer rates for the ligand series reflect both the importance of the π-π interaction and driving force in these systems (ligand substitution affects the emission energy for a chromophore which in turn affects the driving force for the electron transfer reaction).

The effect of the π-π interaction on the electron transfers in donor-chromophore-acceptor complexes was investigated in bimolecular quenching experiments between donor and chromophore-acceptor complexes. The results can be understood in terms of a scheme where a ground state π-π interaction between the donor and the chromophore is the primary mode of electron transfer in these systems. The π-π interaction is also used to explain the high quantum efficiency to the charge-separated state, where both the donor and the acceptor have undergone electron transfers with the chromophore.

Bradford R. Limoges
Department of
Chemistry
Colorado State
University
Fort Collins, CO
Fall 2001

Acknowledgements

I would like to thank my advisor Dr. C.M. Elliott and the rest of the Elliott group for their time and patience and the immeasurable help they have given me over the years. I would especially like to thank Dr. Valerie MacKenzie who built the instrumentation that provided the bulk of the quenching data, and John Weber who had to move and rebuild it. Lastly, I would like to thank my parents who supported my skiing habit for so many years.

Table of Contents

List of Illustrations

Figures:

Schemes:

Tables:

List of Abbreviations

A = acceptor

Acn = acetonitrile

bpppz[a] = benzo[3,2-*a*]-dipyrido[2,1-*e* : 1',2'-*g*] phenazine

bpy = 2,2'-bipyridine

bpy-MV$^{+,b}$ = bpy-methyl viologen acceptor

C^{2+} = chromophore

CS = Charge Separated state (i.e. $D^{+\cdot}$-C^{2+}-$A^{+\cdot}$)

CT = Charge Transfer state (i.e. D-C^{3+}-$A^{+\cdot}$) or Charge Transfer interaction

D = donor

DCE = 1,2-dichloroethane

ddp[a] = dibenzo[3,2-*a* : 2',3'-*c*]-dipyrido[2,1-*e* : 1',2'-*g*] phenazine

dpdpz[a] = dipyridodiphenazine

dppz[a] = dipyrido[3,2-*a* : 2',3'-*c*]phenazine

dmb = 4,4'-dimethyl-2,2'-bipyridine

DQ$^{2+,c}$ = diquaternary amine

GS = Ground State (i.e. D-C^{2+}-A^{2+})

i-biq[a] = bis-isoquinoline

^{3}**MLCT** = Metal to Ligand Charge Transfer state (i.e. D-C^{2+*}-A^{2+}); superscript number denotes spin multiplicity of the state.

phen[a] = 1,10-phenanthroline

φ_2-bpy[a] = 4,4'-diphenyl-2,2'-bipyridine

φ_2-phen[a] = 5,7-diphenyl-1,10-phenanthroline

PNZ[d] = phenazine

POZ[e] = phenoxazine

PSZ[e] = phenoselenazine

PTZ[e] = phenothiazine

$TBAPF_6$ = tetrabutylammonium hexafluorophosphate

t-but[a] = 4,4'-di(t-butyl)-2,2'-bipyridine

tMe-PTZ[e] = 2,4,6,8-Tetramethylphenothiazine

TMPD[d] = *N,N'*-tetramethyl-phenylenediamine

[a] see Figure 3.3.
[b] see Figure 4.2
[c] see Figure 1.8 for a representative DQ^{2+}.
[d] see Figure 2.2.
[e] see Figure 2.1.

Chapter 1:

Background on Ruthenium Based Donor-Chromophore-Acceptor ($D\text{-}C^{2+}\text{-}A^{2+}$) Complexes

Rutheniumtrisbipyridyl-type complexes have been the subject of an active area of research for many years.[1] They have generated considerable interest as models of more complex biological photosynthetic centers,[2] as solar cell dyes,[3,4] and as catalysts,[5,6] to name a few areas of research. A combination of properties such as moderate to long excited state lifetimes, room temperature solution luminescence, and chemical stability[7] make it a useful tool to probe energy and electron transfer reactions.[8] Investigating electron transfers allows one to test the theories advanced by Marcus, Hush, Sutin, and Jortner among others.[9,10,11,12]

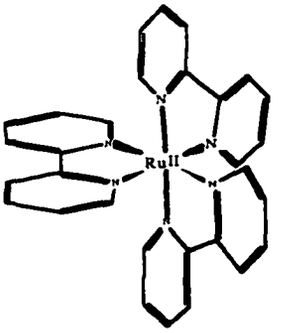

Figure 1.1: $Ru(2,2'\text{-bipyridine})_3^{2+}$ chromophore.

When the $Ru(bpy)_3^{2+}$ (Figure 1.1) chromophore [*bpy* = a bidentate polypyridyl ligand] absorbs a photon, a triplet metal-to-ligand charge-transfer (^{3}MLCT) excited state is quickly reached. This excited state electron is essentially in a ligand based π^* orbital.[13] It can be thought of as localized on a particular *bpy* ligand at any moment in time, but delocalized over the entire ligand system on longer time scales (>25 ps).[14,15] Due to the higher energy content of the molecule, the excited state is both a better oxidizing and better reducing agent than the ground state.

In the absence of a quenching species (one which undergoes energy or electron transfer), the excited chromophore will either non-radiatively relax to the ground state or emit a photon. Because the triplet excited electron is spin forbidden from returning to the singlet ground state, the $Ru(bpy)_3^{2+}$ chromophore has a long excited state lifetime (ca. 1μs). Spin-orbit coupling due to the heavy ruthenium ion allows the electron to relax to the ground state with the emission of a photon.[16]

In the presence of a quencher, the excited state can either non-radiatively relax, emit a photon, or undergo energy/electron transfer to the quencher. The photoemission allows this quenching rate to be measured. The observed lifetime (τ_{obs}) is equal to the sum of the reciprocal of the rates of all pathways from the excited state (eq. 1):

$$\tau_{obs} = 1/k_{nr} + 1/k_r + 1/k_q \qquad (1)$$

where k_{nr}, k_r, k_q are the non-radiative, radiative, and quenching rate constants, respectively. By subtracting the lifetimes in the presence (τ_q) and absence (τ_0) of a quencher gives us the quenching rate (eq. 2):

$$\tau_q - \tau_0 = 1/k_q \qquad (2).$$

It should be noted that k_q is concentration dependant for bimolecular quenching processes

(i.e. when the quencher and chromophore are not linked, ion paired, etc.). A modification of the Stern-Volmer equation (eq. 3) gives the concentration dependence of the quenching:[17]

$$\tau_0/\tau_q = 1 + k_q\tau_0[Q] \qquad (3).$$

As mentioned above, the excited state is both a better oxidizing and reducing agent than the ground state. The excited states redox potentials are obtained from the ground state redox potentials and spectroscopic excited state energy.[1] This assumes that the photochemical and electrochemical orbitals are equivalent. In practice, one takes the electrochemical value of the quencher couple and subtracts from it the appropriate value of the ruthenium couple. The emission onset energy (obtained spectroscopically and expressed in electron volts) is subtracted to obtain a driving force for the electron transfer quenching of the excited state (eqs. 4a-b):

$$(D^{1+/0} - Ru^{2+/1+}) - E_{em} = \Delta G_q \qquad (4a)$$

$$(Ru^{3+/2+} - A^{0/1-}) - E_{em} = \Delta G_q \qquad (4b).$$

In nature, light is converted into energy (in the form of sugars and plant structure) by photosynthesis. One of the key elements of photosynthesis is the ability of chlorophylls to take a photon of light and convert that into an electron and a hole separated spatially. The chromophore absorbs a photon and promotes an electron to the excited state. The electron is transferred to an acceptor and a hole to a donor. The charge is then separated by a series of electron/hole transfers. The initial step of photosynthesis can be modeled by ruthenium based $D\text{-}C^{2+}\text{-}A^{2+}$ complexes, with the charge separated state (CS state) being $D^{+\bullet}\text{-}C\text{-}A^{-\bullet}$.

A quantity that will be discussed throughout is the quantum yield of the charge separated state. This is the fraction of the total excited state generated that produces the charge separated state and is defined as:

$$\varphi_{cs} = [CS]/[Ru^*]_T \qquad (5).$$

Previous work had focused on linked Donor-Chromophore (D-C) complexes,[18] linked Chromophore-Acceptor (C-A) complexes,[19,20,21,22] and linked Donor-Chromophore-Acceptor ($D\text{-}C^{2+}\text{-}A^{2+}$) complexes.[23,24] These complexes were comprised of an essentially $Ru(dmb)_3^{2+}$-type chromophore [dmb= 4,4'-dimethyl-2,2'-bipyridine], an alkyl-linked phenothiazine [4*p*-PTZ] (Figure 1.2a) as the donor, and an alkyl-linked diquaternary amine [4*mn*-DQ^{2+}] (Figure 1.2b). Figure 1.3 gives a representative $D\text{-}C^{2+}\text{-}A^{2+}$ complex. Earlier studies looked at the linkage dependence (and the distance dependence) of the donor and acceptor, the driving force dependence of the acceptor, and the effect of the number of donor units and the nature of the remote ligands in the $C^{2+}\text{-}A^{2+}$ and $D\text{-}C^{2+}$ diads and the $D\text{-}C^{2+}\text{-}A^{2+}$ traids.[18-24]

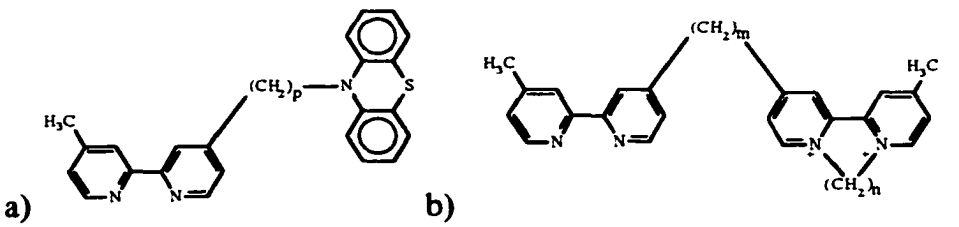

Figure 1.2: a) Linked phenothiazine donor ligand (4*p*-PTZ); b) linked diquaternary amine ligand (4*mn*-DQ^{2+}).

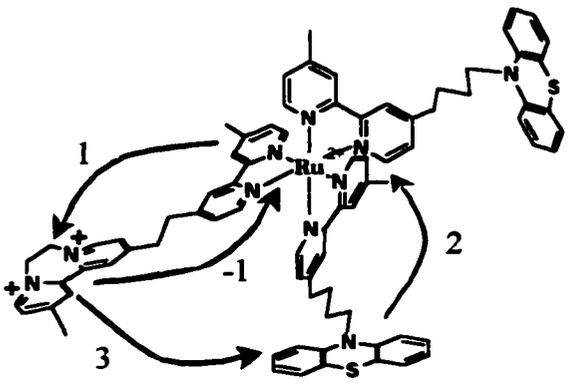

Figure 1.3: $Ru(44\text{-}PTZ)_2(423\text{-}DQ)^{4+}$ complex and electron transfer processes.

Without going into too much detail, the time-resolved optical spectroscopy of the $D\text{-}C^{2+}$, $C^{2+}\text{-}A^{2+}$, and $D\text{-}C^{2+}\text{-}A^{2+}$ [18-24] complexes have revealed the following processes (see Figures 1.3, 1.4):

Quenching by the C-A complexes is an order of magnitude faster than the quenching in the D-C complexes. In the $D\text{-}C^{2+}\text{-}A^{2+}$ complexes, it is assumed that all the quenching of the excited state is done by the acceptor.

Process 1: Quenching of the ^{3}MLCT state of the Ru(II)-complex by electron transfer to DQ^{2+} (Figure 1.2b) generates the CT state $Ru^{3+}\text{-}DQ^{+\bullet}$. The time constant of this process, ranging between 250 ps and 3000 ps, decreases with increasing *n* (decreasing driving force), which is consistent with the process being in the normal Marcus region.[20,22]

Process -1: Reverse electron transfer regenerates the Ru(II)-complex in its ground state. This process is always faster than process 1, so that only an lower limit of ca. $(80\ ps)^{-1}$ could be estimated for its rate constant (for the complex in Figure 1.3) from simple time

resolved spectrscopy.[20,22] It is important to note that direct detection of the CT state was not possible for either C^{2+}-A^{2+} diads or D-C^{2+}-A^{2+} triads, the reason being that:

Process 2, and the competing process -1 are both much faster than process 1. Consequently, the CS state ($D^{+\bullet}$-C^{2+}-$A^{+\bullet}$) of the triad appears at the same effective rate as the ^{3}MLCT state emission disappears.[20,22] Furthermore, the rates of emission decay are the same between analogous C^{2+}-A^{2+} and D-C^{2+}-A^{2+} complexes, indicating that the initial CT state is D-C^{3+}-$A^{+\bullet}$ irrespective of the presence or absence of donors in the complexes.[20,22,25]

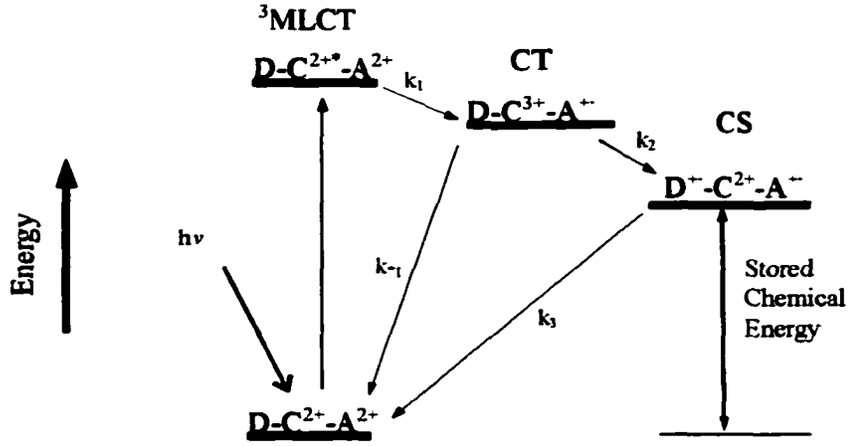

Figure 1.4: Energy diagram showing electron transfer processes in D-C^{2+}-A^{2+} triads.

Relative changes of the rate constant of process 2 as a function of the number of methylene units in the chain, *p*, have been estimated from the yield of the CS state.[25] For $p \geq 4$ the effective rate exhibits a moderate monotonic decrease with increasing *p* that can be assigned to the greater average distance between PTZ and Ru. Competing influences of changes in redox potential of PTZ and distance lead to non-systematic *p*-dependence

for $p<4$.[18]

Process 3: Finally, the CS state returns to the D-C^{2+}-A^{2+} ground state by electron transfer from DQ^{+} to PTZ^{+}- a process occurring on the time scale of some 100–300 ns for the whole range of values of *n* and *p* investigated.[25,26]

Quantum efficiency in forming the charge separated state (φ_{cs}) for the complex Ru(44-PTZ)$_2$(423-DQ)(PF$_6$)$_4$ was measured and originally reported as 0.26 ± 0.04.[25] Subsequently, a series of similar Ru(4*p*-PTZ)$_2$(4*mn*-DQ)$^{4+}$ complexes were investigated. From the data, a relative value for φ_{cs} from one complex to the next was obtained. These relative values were normalized to the above reported value. The quantum yields ranged from φ_{cs} = 0.13-0.43.[26]

Several years after the above experiments were performed, and after much of the work in Chapter 2 had been completed, we had reason to go back and recheck the calculations for the quantum efficiency for the Ru(44-PTZ)$_2$(423-DQ)(PF$_6$)$_4$ complex from the original data. While studying the magnetic field effects on the electron transfer processes in similar Ru(4*p*-PTZ)$_2$(4*mn*-DQ)$^{4+}$ complexes, it was found that the quantum yields for the charge separated state were much higher than expected based on the number that had been reported earlier. Using new data the quantum yield for the Ru(44-PTZ)$_2$(423-DQ)(PF$_6$)$_4$ complex was found to be φ_{cs} = 0.86 ± 0.08.[27] Recalculating the quantum yield from the data presented in the original Danielson, *et al.* paper showed an apparent error in the calculations. Using the data presented in that paper (Figure 1 in the Danielson, *et al.* paper), a rough quantum yield was recalculated to be φ_{cs} = 0.72. The

differences in the two numbers are most likely not due to experimental parameters, though the two experiments were performed in slightly different solvent systems (1,2-dichloroethane vs. dichloromethane).

Experimental

Instrumentation: Electrochemistry was performed either on an EG&G Princeton Applied Research model 173 potentiostat/galvanostat with a model 175 digital coulometer or on a Bio Analytical Systems 100B Electrochemical Workstation. All potentials were measured on a glassy carbon working electrode versus a saturated sodium calomel electrode with a platinum wire counter electrode in a 0.1 M $TBAPF_6$ or 0.1 M $LiClO_4$ solution in acetonitrile.

UV/Vis spectra were obtained from a Hewlett-Packard 8452A Diode Array Spectrometer using a 1 mm path length quartz cell unless otherwise noted. Emission spectra were obtained from a Perkin Elmer LS50B Luminescence Spectrometer using a 1 cm by 1 cm quartz fluorescence cell and averaged over 20 scans.

Time-resolved fluorescence experiments were performed on one or both of two instruments. Short lifetimes (< 100 ns) were obtained on an argon-ion-pumped mode-locked titanium sapphire laser system using the time-correlated single photon counting technique[28] (Figure 1.5).

A Coherent Innova 400 cw argon ion laser pumps a Coherent model 900 Mira Ti:sapphire laser operating at 865 nm. The mode-locked output of the Mira produces a train of 200 fs pulses at 76 MHz that are directed into a Coherent RegA model 9000 regenerative amplifier. The amplified output from the RegA consists of a train of pulses

with temporal pulse widths of 200 fs at a 250 kHz repetition rate and an average power of 700 mW. This output is then frequency doubled in a BBO crystal to produce light at 433 nm with an average power of about 65 mW. Residual light at 865 nm is separated from the excitation beam with a dielectric mirror.

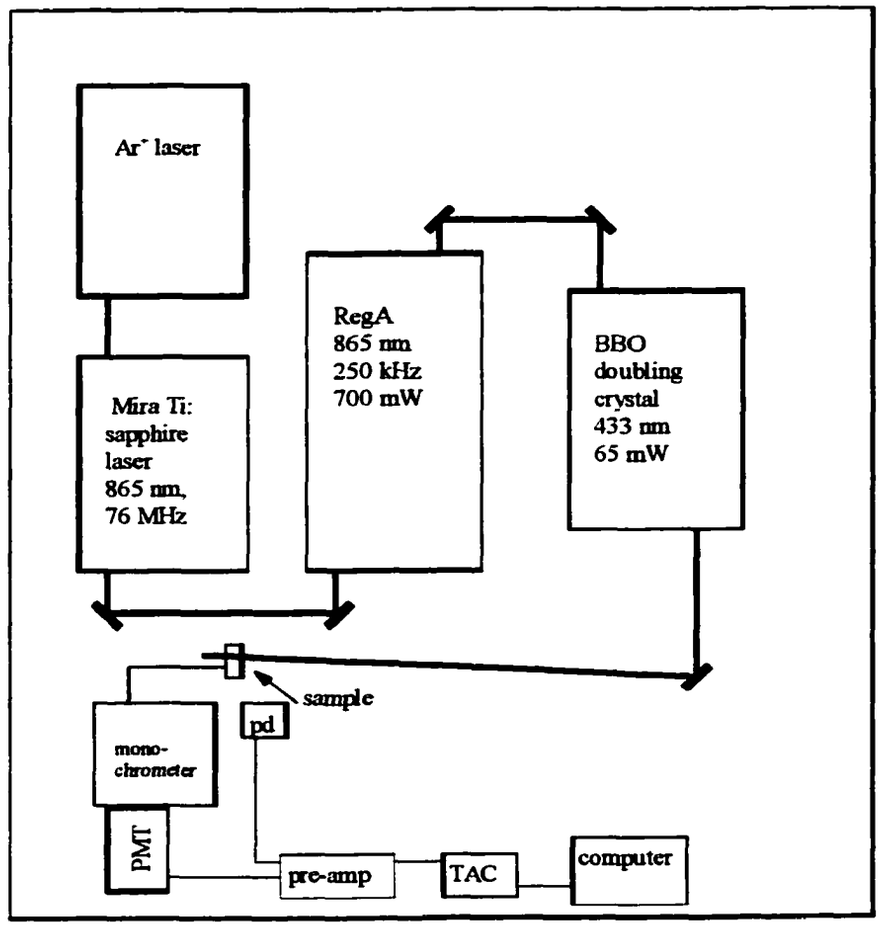

Figure 1.5: Ti:sapphire time resolved fluorescence schematic.

The excitation beam is focused onto a sample in a 1 mm cell. The beam crosses the cell at an angle of 10° with respect to its surface normal. Undispersed fluorescence is collected along the surface normal using a 4 cm focal length lens. The fluorescence beam is collimated and focused onto the entrance slit of an ISA Instruments model DHR320 f/5 monochromator with a 1800 grooves/mm grating set to pass 600nm light. Fluorescence

that exits the monochromator is detected by a Hamamatsu R3809U microchannel plate photomultiplier tube.

Anodic pulses from the PMT are amplified with an EG&G Ortec model 9327 1.1 GHz preamplifier/constant fraction discriminator. The resulting pulse is used as a start signal for a Tennelec TC864 time-to-amplitude converter. The stop signal is obtained by using a Thor DET210 fast photodiode to monitor the previously spatially separated Ti:sapphire laser fundamental beam. The stop pulses are also sent through an identical preamplifier/timing discriminator and into the TAC. The output signal from the TAC is fed into 8192 channels of a Tennelec PCA-multiport multichannel analyzer which produces a histogram of pulse height vs. time that is collected and stored with standard software (Oxford Instruments). To avoid pulse pile-up the fluorescence count rate is restricted to less than 5% of the excitation pulse rate. Curve fitting and analysis of the data was performed on Jandel SigmaPlot 4.1.

The overall instrument response function is measured by collecting scatter of the excitation laser light off of semi-transparent tape. The IRF typically has a temporal response of 35 ps.

Longer lifetimes (50-5000 ns) were measured on a Nd:YAG pumped dye laser using a photomultiplier coupled with a fast real-time oscilloscope (Figure 1.6). A Spectra-Physics LAB-190 Nd:YAG laser operating at 355 nm produces a train of ~8 ns pulses at 30Hz and 1.5 W of power. This output pumps Coumarin 450 dye in a Spectra-Physics PDL-3 dye laser. The average output from the dye laser is 50 mW at 450 nm.

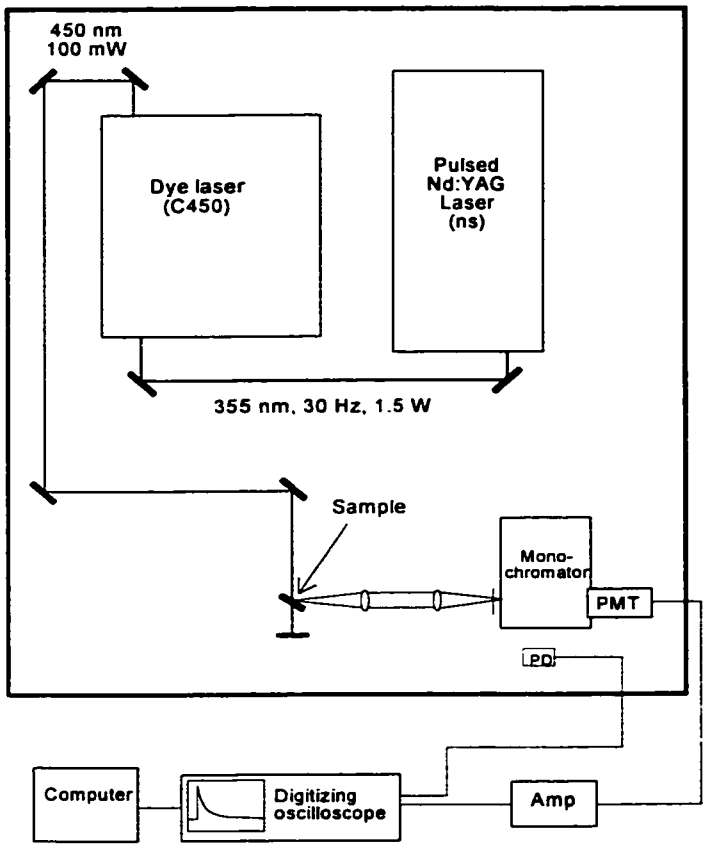

Figure 1.6: Nd:YAG/dye laser time resolved fluorescence schematic.

The excitation beam is directed onto a sample in a 1 mm pathlength cell. The beam crosses the cell at about 30° to the surface normal. Fluorescence is collected at 90° to the excitation beam, is collimated and then focused through an appropriate cut-off filter onto the entrance slit of a Jarrell Ash model 82-410 monochrometer set to pass 600 nm light. Fluorescence that exits the monochrometer is detected with a Hamamatsu model R2496 photomultiplier tube operated at ca. 500 V.

The output from the photomultiplier tube is sent to a Tektronix TDS 620B Digital Oscilloscope. A Thorlabs DET210 fast photodiode monitoring scattered 450 nm light is used to trigger the oscilloscope. An average of 1000 decay curves were collected for each sample to improve signal to noise. The output from the oscilloscope was saved to

disc in a binary format. Curve fitting and analysis was performed with Jandel SigmaPlot 4.1.

Transient absorbance measurements of the charge-separated state were performed with the dye laser as a pump beam and a Xe arc lamp providing the probe beam (see Figure 1.7).

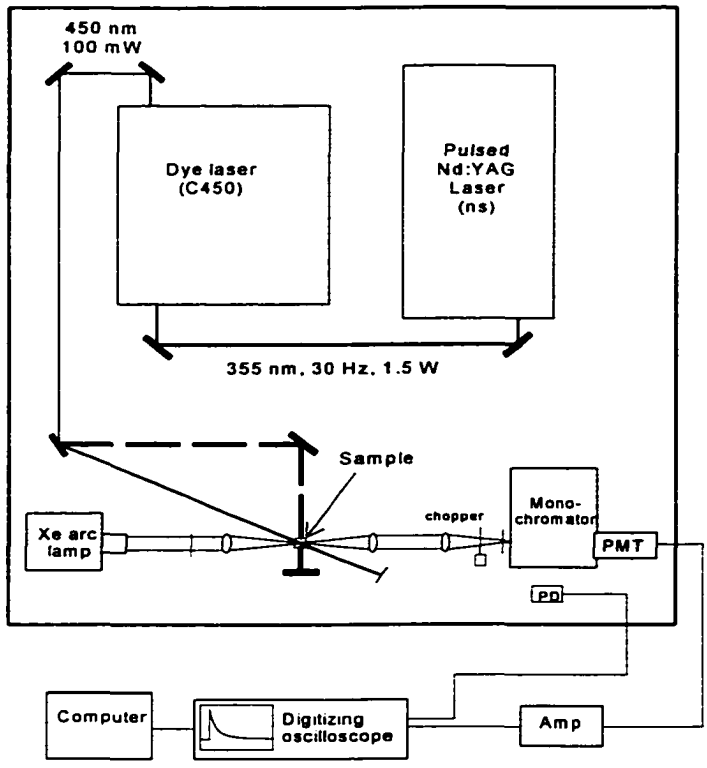

Figure 1.7: Nd:YAG/dye laser transient absorbance schematic. Shown are two configurations (see text).

The beam is focused onto the sample in a 1 cm x 1 cm cell at 20° to surface normal and passes through the sample into a beam dump (solid line, Figure 1.7). This is done to maximize the overlap between the pump beam and the probe beam which enters the sample at 90° to the cell surface. The probe beam is provided by an Oriel 66002 Xe arc lamp. The white light from the lamp is passed through two filters to remove wavelengths shorter than 300 nm and longer than 500 nm, then is focused on the cell.

Power of the probe beam at the cell is approximately 300 mW. The probe beam is collimated upon exiting the cell, then focused onto the entrance slit of a Jarrell Ash model 82-410 monochrometer. The monochrometer was set to 397 nm, where the reduced diquat has a strong absorbance and the ground state diquat as well as the ground state PTZ and oxidized PTZ have very small absorbances (see Figure 1.8).[25] Light that exits the monochrometer is detected with a Hamamatsu model R2496 photomultiplier tube operated at 500 V. The output from the photomultiplier tube is processed in the same way as outlined above for emission lifetimes.

An alternate configuration for the transient absorption experiment that was used in later experiments brings the pump beam into the sample at 90° to the probe beam (dashed line, Figure 1.7). A mirror was used to reflect the pump beam back through the sample. A chopper was added to reduce duty cycle on the PMT. The Ar^+ pump laser was triggered off the chopper.

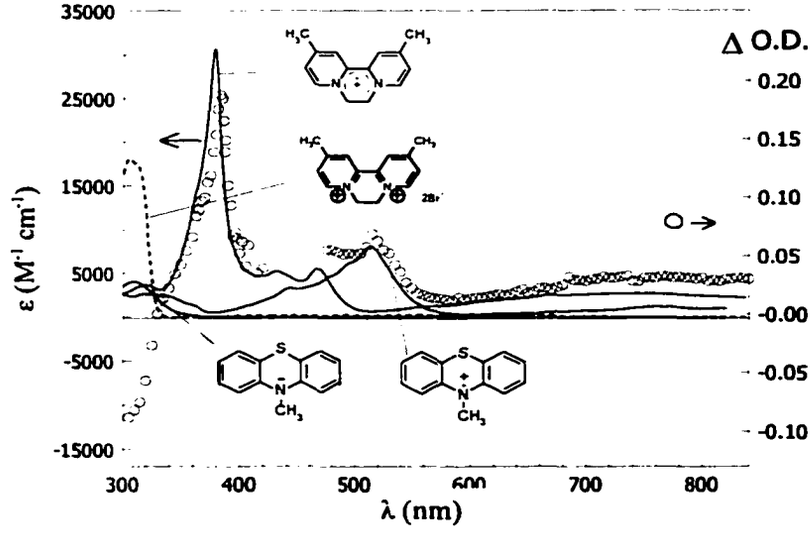

Figure 1.8: UV/Vis spectra of ground state and reduced diquaternary amine, ground state and oxidized N-methylphenothiazine, and transient absorbance (o) spectrum of $Ru(44\text{-}PTZ)_2(422\text{-}DQ)^{4+}$ in 1,2-DCE (excited at 450 nm).

Materials: All materials were used as received from there respective suppliers unless otherwise noted. All spectrochemical and electrochemical measurements were conducted with N_2-purged solutions prepared from Fisher Optima grade acetonitrile. Samples for lifetime measurements were further degassed by a series of 3 or more freeze-pump-thaw cycles to ensure removal any traces of residual oxygen. Samples for lifetime measurements were left under vacuum while samples for transient absorbance measurements were backfilled with N_2 to prevent boiling of the solution under experimental conditions. Final purity for ruthenium complexes was established by reaching a constant maximum in emitted light from emission spectra.

Due to the nature of the chemistry involved, there are several "generic" reactions involved in making many of the compounds (ie. the ruthenium complexes). What follows is a description of these reactions in general terms. To list the fine details of every one of these reactions is unnecessary. The compounds and any reactions that deviate from these generalized ones will be covered in their proper chapter. Also included here are products used as intermediates for other general reactions.

$Ru(DMSO)_4Cl_2$:[29] 1 g of $RuCl_3 \cdot xH_2O$ (42% Ru by weight, Johnson Matthey) was dissolved in 3 mL of DMSO (Fisher A.C.S. grade) and refluxed 90 minutes until solution developed a bright yellow color. *Note:* It is desirable to stop heating when the solution is at its lightest, otherwise a brown-orange side product is formed from over heating. The product was precipitated by addition acetone and filtered resulting in a dark yellow solid. The product was recrystallized from DMSO and precipitated by the addition of acetone as a pale yellow solid. Typical yield: ~90%.

$Ru(L)_2Cl_2$:[30] One equivalent of $Ru(DMSO)_4Cl_2$ was dissolved in a minimum of

DMF (dried over alumina) saturated with LiCl in a round bottom flask under N_2. Two equivalents of the appropriate bidentate ligand (L) were added and the reaction refluxed gently for 30 minutes or until a dark purple color predominates. The reaction is allowed to cool and the volume is doubled with H_2O and extracted with CH_2Cl_2. The volume is reduced by rotary evaporation and the product precipitated as a dark purple solid by the addition of diethyl ether. The product is separated from the main side product ($Ru(L)_3Cl_2$) by flash silica gel chromatography with 10% acetone in CH_2Cl_2 as the mobile phase. Further purification to remove $Ru(L)_2(H_2O)_xCl_{2-x}$ impurities was done as needed by flash silica gel chromatography with 88:10:2 CH_2Cl_2/EtOH/triethylamine as the mobile phase. Typical yield: ~85%.

$Ru(L)_2(L')(PF_6)_2$: One equivalent of $Ru(L)_2Cl_2$ was dissolved in a minimum of ethanol or methanol under N_2 and to this was added one equivalent of the appropriate bidentate ligand (L'). The reaction was refluxed gently until the dark purple color disappeared and was replaced by a bright orange color in 15-45 minutes, depending on the ligands. The reaction was cooled to room temperature and the volume doubled with H_2O. The product was precipitated with saturated aqueous NH_4PF_6 and filtered. Purification was done by flash silica gel chromatography with 50:40:10 acetonitrile/water/sat. KNO_3 (aq.). Final purity was determined by emission spectroscopy and/or TLC. Typical yield: 30-40%.

$Ru(L)_2$(4*p*-PTZ)$(PF_6)_2$: One equivalent of $Ru(L)_2Cl_2$ was dissolved in a minimum of ethylene glycol under N_2 in the absence of light and to this solution was added one equivalent of the appropriate linked phenothiazine-bipyridine ligand (**4*p*-PTZ**) dissolved in a minimum of ethylene glycol / 3,3-dimethyl-1,2-butane-di-ol mixture . The

reaction was heated to 110°C for 15-30 minutes until the dark purple color disappeared and was replaced by a bright orange color. The reaction was cooled to room temperature and the volume doubled with H_2O. The product was precipitated with saturated aqueous NH_4PF_6 and filtered. Purification was done by flash silica gel chromatography with 50:40:10 acetonitrile/water/sat. KNO_3 (aq.). Final purity was determined by emission spectroscopy and/or TLC. Typical yield: 30-40%.

$Ru(L)_3^{2+}$: Three equivalents of the appropriate bidentate polypyridyl ligand were dissolved in a minimum of MeOH, EtOH, ethylene glycol, or an ethylene glycol / 3,3-dimethyl-1,2-butane-di-ol mixture depending on solubility. One equivalent of $Ru(DMSO)_4Cl_2$ was added and the solution was heated gently until a bright orange color predominates. The reaction was cooled to room temperature and the volume doubled with H_2O. The product was precipitated with saturated aqueous NH_4PF_6 and filtered. Purification was done by flash silica gel chromatography with 50:40:10 acetonitrile/water/sat. KNO_3 (aq.). Final purity was determined by emission spectroscopy and/or TLC. Typical yield: 30-60%.

$Zn(L)_3(ClO_4)_2$: Approximately, one equivalent of $Zn(ClO_4)_2 \cdot XH_2O$ was dissolved in a minimum amount of hot acetone. To this was added ~3.5 equivalents of the appropriate bidentate ligand (**L**) and the reaction was stirred for five minutes then cooled to 0°C and the product precipitated out as a white solid. The product was recrystallized in acetone. Yield: ~95%.

$Ru(4p\text{-}PTZ)_2(4mn\text{-}DQ)(PF_6)_4$: One equivalent of $Ru(4n\text{-}PTZ)_2Cl_2$ was dissolved in a minimum of ethylene glycol and 3,3-dimethyl-1,2-butanediol under N_2 in the absence of light and heated to just under 120°C in an oil bath until the solution had

changed from a dark purple to a bright red color. The reaction was then cooled to just under 100°C and to it was added one equivalent of the appropriate diquat ligand (***4mn*-DQ**). The reaction was stirred until the red color was replaced by a bright orange color. The reaction was cooled to room temperature and the volume doubled with H_2O. The product was precipitated with saturated aqueous NH_4PF_6 and filtered. Purification was done by flash silica gel chromatography with 50:40:10 acetonitrile/water/sat. KNO_3 (aq.). Final purity was determined by emission spectroscopy and/or TLC. Typical yield: 20-30%.

4-Methyl-4'-[2-(4'-methyl-2,2'-bipyridin-4-yl)ethyl]-2,2'-bipyridine ("420"): 15.3g (0.0803 mol) of 4,4'-dimethyl-2,2'-bipyridine was dissolved in 600 mL dry THF. To this was added 1 eq. of lithiumdiisopropylamine [32 ml (0.0803 mol) of 2.5M n-butyllithium and 11.25 mL (0.0803 mol) of diisopropylamine (dried over alumina) combined in 50 mL dry THF under N_2 in a dry ice/acetone bath for 90 minutes] under N_2 in a dry ice/acetone bath and stirred for two hours. With a dropping funnel, 0.5 eq. I_2 in dry THF was added slowly and stirred until a pale yellow color persisted. The THF was removed by rotary evaporation and the yellow solid was dissolved in CH_2Cl_2 filtered through filter paper and extracted with H_2O. The organic layer was dried over anhydrous sodium sulfate then the solvent was removed by rotary evaporation resulting in a white solid. The desired product was separated from unreacted 4,4'-dimethyl-2,2'-bipyridine and polymer by flash silica gel chromatography (10% acetone in CH_2Cl_2). Yield: ~65%. ^1H NMR ($CDCl_3$) δ: Ar-CH_3 2.45 (s); Ar-CH_2- 3.1 (s); Ar 7.1-8.5 (m).

422-DQ^{2+}, 423-DQ^{2+}, 424-DQ^{2+}: ~0.5g of the 420 dimer and 1 eq. of the appropriate dibromoalkane were dissolved in 5-10 mL of o-dichlorobenzene. The

solution was degassed by 5 freeze-pump-thaw cycles and sealed under vacuum in a glass tube. The reaction was heated to 150° C for 3 days then cooled. The crude reaction mixture (including undissolved solids and solution) was dissolved/extracted into water and washed with diethyl ether. The product was precipitated with the addition of sat. $NH_4PF_{6\,(aq)}$. The light pink product was purified by silica gel chromatography (50:40:10 acetonitrile/water/sat. $KNO_{3\,(aq)}$). Typical yield: ~20%.

4-bromomethyl-4'-methyl-2,2'-bipyridine: 2.22g (0.012 mol) of 4,4'-dimethyl-2,2'-bipyridine (Reilly Tar; recrystallized from ethyl acetate) was dissolved in 100 mL CCl_4. 2.01g (0.012 mol) of N-bromosuccinamide (Aldrich) was added and the solution purged with N_2. AIBN (0.05g) was added. (*method 1*) The solution was brought to a gentle reflux under N_2. (*method 2*) The solution was stirred in front of a bright light source under N_2. The reaction was monitored by TLC (10% acetone in CH_2Cl_2) and was allowed to proceed until the appearance of 4,4'-bis(bromomethyl)-2,2'-bipyridine was noticed. The solution was filtered through filter paper and the solid washed with CCl_4. The eluent was washed twice with water and dried over anhydrous Na_2SO_4. The solvent was removed by rotary evaporation. The resulting brown solid contained the desired product, the di-brominated bipyridine and unreacted starting materials. The desired product was separated on flash silica gel by gradient elution chromatography (1-20% acetone in CH_2Cl_2). Yield: ~40%. ^1H NMR ($CDCl_3$) δ: $-CH_3$ 2.8 (s), $-CH_2-Br$ 3.8 (s), Ar 7.2-8.9 (m).

4-(Ω-bromo*alkyl*)-4'-methyl-2,2'-bipyridine: One equivalent of 4,4'-dimethyl-2,2'-bipyridine (Reilly Tar; recrystallized from ethyl acetate) was dissolved in a minimum of dry THF under N_2 in a dry ice acetone bath. One equivalent of lithium

diisopropylamine [1 eq. of 2.5M butyllithium and 1.1 eq. of diisopropylamine (dried over alumina) in a minimum of dry THF stirred for 90 minutes under N_2 in a dry ice/acetone bath] was added and the solution was stirred for 2 hours. When the solution had come to equilibrium, a seven fold excess of the appropriate α,Ω-dibromo-*n*-alkane was added and the solution was allowed to come to room temperature. (*Note:* The reaction does not proceed when 1,2-dibromoethane is used; 1,2-ditosylethane is used in its stead.) The solvent was removed by rotary evaporation. The solid was dissolved in CH_2Cl_2 and filtered through filter paper. The eluent was washed twice with water and dried over anhydrous Na_2SO_4. The solvent was removed by rotary evaporation. The resulting tan solid contained the desired product, the di-bromoalkylated bipyridine and unreacted starting materials. The desired product was separated by gradient elution flash silica gel chromatography (1-20% acetone in CH_2Cl_2). Typical yield: ~40%. ^1H NMR ($CDCl_3$) δ: $-(CH_2)_n-$ ~2-3.5, $-CH_3$ 2.8 (s), $-CH_2-Br$ 3.8 (t), Ar 7.2-8.9 (m).

4*p*-phenothiazine: Phenothiazine (Haver-Glover; recrystallized from benzene) was combined with 1 eq. of NaH (Acros Organics; 50% dispersion in oil) in dry THF at 0°C under N_2 and stirred for 45 minutes. The appropriate 4-(Ω-bromoalkyl)-2,2'-bipyridine in dry THF was added slowly. The solution was allowed to come to room temperature over two hours, then was quenched with H_2O. The product was extracted into CH_2Cl_2 and the solvent removed by rotary evaporation. The crude product was purified by flash silica gel chromatography (10% acetone in CH_2Cl_2). Typical yield: ~80%.

ENDNOTES

[1] Juris, A.; Balzani, V.; Barigelletti, F.; Campagna, S.; Belser, P.; von Zelewsky, A. *Coord. Chem. Rev.*, **1988**, *84*, 85.

[2] Kropf, M.; van Loyen, D.; Schwars, O.; Duerr, H. *J. Phys. Chem. (A)*, **1998**, *102(28)*, 5499.

[3] Nazeeruddin, M.K.; Kay, A.; Rodicio, J.; Humphrey-Baker, R.; Muller, E.; Liska, P.; Vlachopoulos, N; Graetzel, M. *J. Amer. Chem. Soc.*, **1993**, *115*, 6382.

[4] Kirch, M.; Lehn, J.-M.; Sauvage, J.-P. *Helv. Chim. Acta*, **1979**, *62*, 1345.

[5] Nickel, U.; Chen, Y.-H.; Schneider, S.; Silva, M; Burrows, H.; Formosinho, S. *J. Phys. Chem.*, **1994**, *98*, 2883.

[6] Kimura, E.; Bu, X.; Shionoya, M.; Wada, S.; Maruyama, S. *Inorg. Chem.*, **1992**, *31*, 4542.

[7] Kalayansunduram, K. *"Photochemistry of Polypyridine and Porphyrin Complexes"* Academic Press, San Diego, USA, **1992**.

[8] Yonemoto, E.; Saupe, G.; Schmehl, R.; Hubig, S.; Riley, R.; Iverson, B.; Mallouk, T. *J. Amer. Chem. Soc.*, **1994**, *116*, 4786.

[9] Marcus, R.A. *Discuss. Faraday Soc.*, **1960**, *29*, 21.

[10] Hush, N.S. *Trans. Faraday Soc.*, **1961**, *57*, 55.

[11] Sutin, N. *Topics in Current Chemistry*, **1990**, *156*, 441.

[12] Jortner, J.; Bixon, M.; Ratner, M. *Proc. Indian Acad. Sci.; Chem. Sci.*, **1997**, *109(6)*, 365.

[13] Bryant, G; Fergusson, J.E.; Powell, H. *Aust. J. Chem.*, **1971**, *24*, 257.

[14] DeArmond, M.; Carlin, C. *Coord. Chem. Rev.*, **1981**, *36*, 325.

[15] Cooley, L.F.; Berquist, P.; Kelley, D.F. *J. Amer. Chem. Soc.*, **1990**, *112*, 2612.

[16] Kober, E.M.; Meyer, T.J. *Inorg. Chem.*, **1982**, *21*, 3967.

[17] Stern, O.; Volmer, M. *Physik. Z.*, **1919**, *20*, 183.

[18] Larson, S.; Elliott, C.M.; Kelley, D.F. *Inorg. Chem.*, **1996**, *36*, 2070.

[19] Ryu, C.K.; Wang, R.; Schmehl, R.; Ferrere, S., Ludiwikov, M; Merkert, J.W.; Headford, C.E.L.; Elliott, C.M. *J. Amer. Chem. Soc.*, **1992**, *114*, 430.

[20] Cooley, L.F.; Larson, S.; Elliott, C.M. *J. Phys. Chem.*, **1991**, *95*, 10694.

[21] Schmehl, R.H.; Ryu, C.K.; Elliott, C.M.; Headford, C.E.L.; Ferrere, S. *ACS Adv. In Chem. Ser.*, **1990**, 211-223.

[22] Cooley, L.F., Headford, C.E.L.; Elliott, C.M., Kelley, D.F. *J. Amer. Chem. Soc.*, **1988**, *110*, 6673.

[23] Larson, S.L.; Elliott, C.M.; Kelley, D.F. *J. Phys. Chem.*, **1995**, *99*, 6530.

[24] Larson, S.L.; Cooley, L.F.; Elliott, C.M.; Kelley, D.F. *J. Amer. Chem. Soc.*, **1992**, *114*, 9504.
[25] Danielson, E.; Elliott, C.M.; Merkert, J.W.; Meyer, T.J. *J. Amer. Chem. Soc.*, **1987**, *109*, 2519.
[26] Larson, S.L. "Charge Transfer in Linked Donor-Chromophore-Acceptor Systems"; Ph.D. Thesis, Colorado State University, **1994**.
[27] Klumpp, T; Linsenmann, M.; Larson, S.L.; Limoges, B.R.; Bürssner, D.; Krissinel, E.B.; Elliott, C.M.; Steiner, U.E. *J. Amer. Chem. Soc.*, **1999**, *121*, 1076.
[28] O'Connor, D.V.; Phillips, D. "Time Correlated Single Photon Counting" Academic Press, London, **1984**.
[29] Evans, I.P.; Spencer, A.; Wilkinson, G. *J. Chem. Soc., Dalton Trans.*, **1973**, 204.
[30] Sullivan, B.P.; Salmon, D.J.; Meyer, T.J. *Inorg. Chem.*, **1978**, *17*, 3334.

Chapter 2:

New Donor Ligands for Ruthenium based D-C^{2+}-A^{2+} Complexes

When we originally believed the quantum yield for forming the charge separated state to range from 0.13-0.43 (see Chapter 1) for the D-C^{2+}-A^{2+} triads, we set out to improve it, i.e., produce more charge separated state from the excited state. Looking back at Figure 1.4, we know that k_2 and k_{-1} are both faster than k_1. We never see any build-up of the CT state. The relative rates of k_2 and k_{-1}, determine whether the CT state will go on to produce the CS state or back electron-transfer to the ground state. To improve the yield of the CS state one can either think of increasing k_2 or decreasing k_{-1}, or both.

One way in which k_2 might be increased in these triads is by increasing the driving force for the forward electron transfer in the charge separation step:

$$D - Ru^{3+} - A^{+\bullet} \rightarrow D^{+\bullet} - Ru^{2+} - A^{+\bullet}.$$

To simplify the experiments, we model the effects of driving force on the electron transfer with D-C complexes, where the electron transfer is:

$$D - Ru^{2+*} \rightarrow D^{+\bullet} - Ru^{1+}.$$

While the electron transfer occurs between the same donor and metal orbitals (an $n \rightarrow d$ transition) in both cases, there are some differences in the two electron transfer events. The $Ru^{3+/2+}$ reduction is about 0.44eV more energetically favorable than the $Ru^{2+*/1+}$ reduction.[1] The Ru^{2+*} also has an electron that is delocalized over its ligands on the time scale of the reductive quenching.

A limited driving force vs. ET rate study was conducted by S. Larson for his dissertation.[2] He attacked the problem by changing the nature of the remote, non-donor ligand, thus changing the $Ru^{2/1+}$ couple in equation 4a (Chapter 1). He concluded that the forward electron transfer follows normal Marcus behavior (i.e. increasing the driving force increased the rate) and that small changes in driving force (~100 mV) made significant changes in rate (about an order of magnitude).[2] The effect of changing the donor's driving force on the processes in the $D\text{-}C^{2+}\text{-}A^{2+}$ triads is not easily amenable to this approach. To investigate these effects, one would like to be able to vary the $D^{1+/0}$ couple in equation 4a. With the exception of the 41-PTZ,[3] the $PTZ^{1+/0}$ couple essentially constant and independent of the length of the alkyl chain or number of donor units associated with the complex.[2]

If one were to change the donor group to another moiety, a host of other non-trivial factors other than the $D^{1+/0}$ couple are affected. If the new donor is very different in structure, the solvation of the donor, the orbital which the electron comes from, and the interaction with the chromophore will all change. To make a comparison of driving forces meaningful, it is desirable that all these other factors influencing the electron transfer rate remain the same or are perturbed only slightly.

To correlate the effect of changing the donor's driving force in the D-C^{2+}-A^{2+} triads with existing data, new donor groups were synthesized based on the PTZ template. The original plan was to make linked ligands similar to the 4*p*-PTZ (fig. 1.2a) based on phenoxazine (POZ), phenoselenazine (PSZ), and tetramethylphenothiazine (tMe-PTZ) (see Figure 2.1).

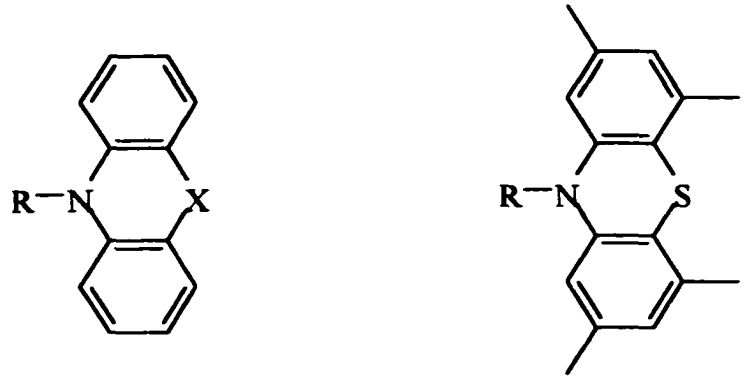

Figure 2.1: Phenothiazine type donors.

Two other donors were proposed to give greater driving forces, though they deviated from the 4*p*-PTZ design. One was based on a phenazine donor and the other on phenylene diamine (see Figure 2.2). Both of these ligands are tetradentate, which would make the D:C:A ratio 1:1:1 instead of 2:1:1 ratio at which the other triads had been studied.

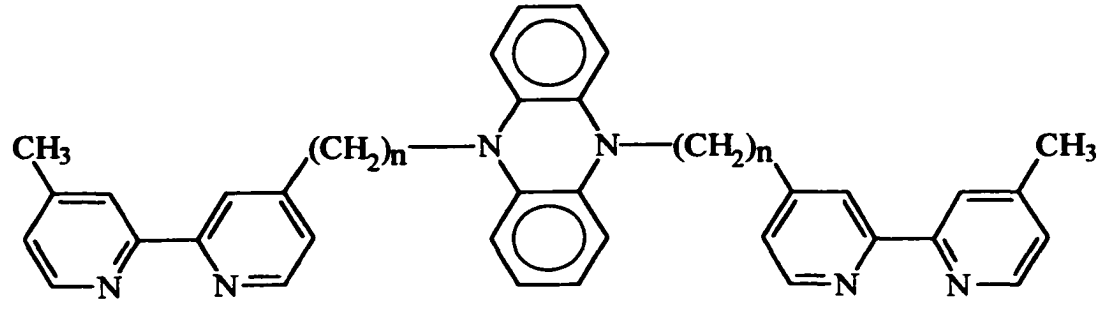

A)

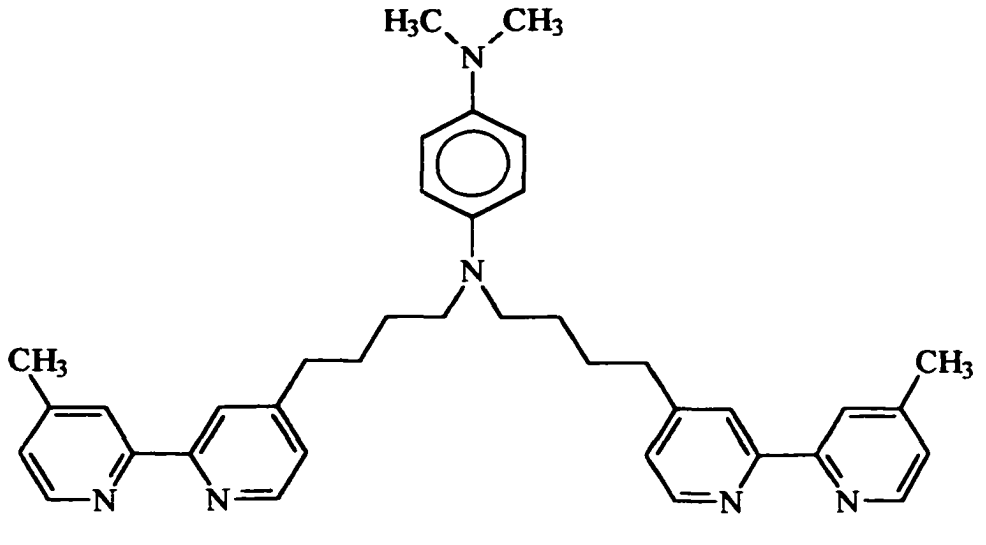

B)

Figure 2.2: Tetradentate donor ligands based on A) phenazine and B) *p*-phenylene diamine.

Experimental:

Se_2Cl_2:[4] 46.45g (0.42 mol) of SeO_2 was dissolved in 250 mL conc. HCl. 98.86g (1.25 mol) of Se metal was added and the solution was stirred until all the solid was dissolved. Conc. H_2SO_4 was added dropwise until the reaction stopped evolving HCl gas. The reaction was allowed to cool and the Se_2Cl_2 separated out as a red-brown liquid. The product was isolated with a separatory funnel and stored under N_2. The product was used without any further purification.

Phenoselenazine (PSZ):[5] 55.71g (0.33 mol) of diphenylamine (Aldrich, recrystallized from toluene) was dissolved in 250 mL of $CHCl_3$. 28 mL (0.334 mol) of Se_2Cl_2 in an additional 250 mL of $CHCl_3$ was added slowly over 1 hour. The reaction was refluxed for 6 hours and cooled to room temperature. The solvent was removed by rotary evaporation. The resulting solid was dissolved in 600 mL of acetic acid, filtered and precipitated by addition of with H_2O. The desired product was filtered and dried and then recrystallized in petroleum ether resulting in white crystals. Further purification was

achieved by flash silica gel chromatography (1:5 toluene in hexanes). Yield: ~ 85%. ^{1}H NMR (d_6-acetone) δ: -NH 4.2 (s), Ar 6.8-7.4 (m).

N-Methylphenoselenazine (Me-PSZ): 0.3480g (1.4×10^{-3} mol) of phenoselenazine was combined with 0.056g (1 eq.) of NaH (Acros Organics; 60% dispersion in oil) in 15 mL dry THF at 0°C under N_2 and stirred for 20 minutes. 90 μL (1.5×10^{-3} mol) of CH_3I diluted 1:10 (v/v) in dry THF was added slowly. The solution was allowed to come to room temperature over two hours, then was quenched with MeOH. The product was extracted into CH_2Cl_2 and the solvent removed by rotary evaporation. The crude product was recrystallized in petroleum ether resulting in white crystals. Yield: ~40%. ^{1}H NMR ($CDCl_3$) δ: N-CH_3 1.5 (s), Ar 6.8-7.0 (m).

44-phenoselenazine (44-PSZ): 0.50g (2.03×10^{-3} mol) of phenoselenazine was combined with 3 eq. of NaH (Acros Organics; 50% dispersion in oil) in dry THF at 0°C under N_2 and stirred for 2 hours. 0.3254g (1.066×10^{-3} mol) of 4-(4-bromobutyl)-4'-methyl-2,2'-bipyridine in dry THF was added slowly. The solution was allowed to come to room temperature slowly and then refluxed for an additional 12 hours. The reaction was quenched with H_2O and the product was extracted into CH_2Cl_2. the solvent was removed by rotary evaporation. The crude product was purified by flash silica gel chromatography (10% acetone in CH_2Cl_2). The final product was a tacky tan solid Yield approximately 40%. ^{1}H NMR ($CDCl_3$) δ: Ar-CH_2-**CH_2**-**CH_2**-CH_2-PSZ 1.8 (p); Ar_{bpy}-CH_3 2.4 (s); Ar-**CH_2**-CH_2-CH_2-**CH_2**-PTZ 2.6 (t), 3.4 (t); Ar_{ptz} 6.7-7.3 (m); Ar_{bpy} 7.2-8.5 (m).

1-amino-3,5-dimethylbenzene HCl salt: 3 mL of 1-amino-3,5-dimethylbenzene was dissolved in 5 mL of EtOH in 25 mL beaker. The volume was doubled with 6 M HCl. The EtOH was evaporated off on a hot plate and the product precipitated out as a

white solid. The solid was filtered over a glass frit and washed with three 15 mL 0.1 M HCl and dried. Yield: 3.6g.

Di-(3,5-dimethylphenyl)amine: 0.72g (4.6×10^{-3} mol) of 1-amino-3,5-dimethylbenzene·HCl and 0.57 mL (4.6×10^{-3} mol) 1-amino-3,5-dimethylbenzene were combined in an ampoule and sealed under vacuum. The tube was heated at 250°C for 24 hours then cooled to room temperature. The resulting solid was dissolved in CH_2Cl_2 and filtered. The organic solution was washed with 0.1M HCl and dried over anhydrous Na_2SO_4. The solvent was removed by rotary evaporation resulting in a dark brown oil. The product was purified by flash gel chromatography (1:1 toluene in hexanes) yielding a light tan solid. Yield: ~ 35%. ^{1}H NMR (d_6-benzene) δ: Ar-CH_3 2.35 (s), Ar 6.65 (s)-7.75 (s).

2,4,6,8-Tetramethylphenothiazine (tMe-PTZ): 6.54g (2.9×10^{-2} mol) of di-(3,5-dimethylphenyl)amine and 4.75g (0.15 mol) of sulfur were combined in a 100 mL round bottom flask. 0.10g of I_2 was added as a catalyst. The reaction was heated in an oil bath at 128°C for ten minutes, until product solidified, and cooled to room temperature. The resulting solid was dissolved in toluene and filtered. The desired product was purified by flash silica gel chromatography (1:5 toluene in hexanes) in the absence of light. Yield: ~ 40%. ^{1}H NMR (d_6-benzene) δ: Ar-CH_3 2.05 (s), 2.20 (s); -NH 5.05 (s); Ar 5.75 (s), 6.40 (s).

44-Tetramethylphenothiazine (44-tMe-PTZ): 0.5274g (2.03×10^{-3} mol) of 2,4,6,8-tetramethylphenothiazine was combined with 1 eq. of NaH (Acros Organics; 50% dispersion in oil) in dry THF at 0°C under N_2 and stirred for 30 minutes. 0.5169g (1.7×10^{-3} mol) of 4-(4-bromobutyl)-4'-methyl-2,2'-bipyridine in dry THF was added slowly. The

solution was allowed to come to room temperature over two hours, then was quenched with H_2O. The product was extracted into CH_2Cl_2 and the solvent removed by rotary evaporation. The crude product was purified by flash silica gel chromatography (1:1 toluene in hexanes) yielding a light tan powder. Yield: ~40%. ^1H NMR ($CDCl_3$) δ: Ar-CH_2-**CH_2**-**CH_2**-CH_2-PTZ 1.9 (p); Ar_{ptz}-CH_3 2.2 (s), 2.25 (s); Ar_{bpy}-CH_3 2.4 (s); Ar-**CH_2**-CH_2-CH_2-**CH_2**-PTZ 2.8 (t), 3.9 (t); Ar_{ptz} 6.7 (s); Ar_{bpy} 7.2-8.5 (m).

N-Methylphenoxazine (Me-POZ): 0.1497g (8.2×10^{-4} mol) of phenoxazine (97%, Aldrich) was combined with 0.033g (1 eq.) of NaH (Acros Organics; 50% dispersion in oil) in 15 mL dry THF at 0°C under N_2 and stirred for 45 minutes. 50 μL (8.0×10^{-4} mol) of CH_3I diluted 1:10 (v/v) in dry THF was added slowly. The solution was allowed to come to room temperature over two hours, then was quenched with H_2O. The product was extracted into CH_2Cl_2 and the solvent removed by rotary evaporation. The crude product was purified by flash silica gel chromatography with toluene as the mobile phase. The final product was an oily white solid. Yield: ~60%. ^1H NMR ($CDCl_3$) δ: N-CH_3 3.05 (s), Ar6.8-7.0 (m). *m/z*= 197.1.

44-Phenoxazine (44-POZ): 1.01g (5.54×10^{-1} mol) of phenoxazine (97%, Aldrich) was dissolved in 15 mL dry THF and stirred under N_2 at -78°C. To this was added 0.9 eq. (2.5 mL) of 2.0 M butyllithium in hexanes. The solution was allowed to come to equilibrium over 10 minutes then 0.600g (2.28×10^{-3} mol) of 4-(4-bromobutyl)-4'-methyl-2,2'-bipyridine in dry THF was added and the solution was stirred for an additional 10 minutes before being allowed to come to room temperature and stirred for an additional 30 minutes. The reaction was then quenched with H_2O, the product extracted into CH_2Cl_2 and the solvent removed by rotary evaporation. The crude product

was purified by flash silica gel chromatography with 1:5 toluene:hexanes as the mobile phase. The final product was an off-white powder. Yield: ~15%.

5,10-Dimethyl-5.10-dihydrophenazine (Me_2-PNZ): 3.6g (0.02 mol) of phenazine (Aldrich; recrystallized from ethyl acetate) was combined with 1.7g (0.04 mol) of K metal in 25 mL ethylene glycol dimethyl ether at 0°C under N_2 and stirred for 10.5 hrs. in the dark. CH_3I (10 eq.) diluted 1:1 (v/v) in glyme was added slowly. The solution was allowed to come to room temperature over two hours, then was quenched with EtOH to remove excess potassium. The volume was doubled with H_2O and the product extracted into CH_2Cl_2. The solvent was removed by rotary evaporation. The crude product was recrystallized in EtOH yielding and off white powder. Yield: 32%. ^1H NMR (d_6-acetone) δ: N-CH_3 3.1 (s), Ar 6.5-6.7 (m).

$Ru(44\text{-}tMe\text{-}PTZ)_3(PF_6)_2$ was prepared as in Chapter 1 for $Ru(L)_3^{2+}$.

Results:

Table 2.1 gives the 1+/0 redox couples vs. SSCE for the various donors.[6] Changing the chalcogen does not greatly affect the redox potential of the N-hydro-donors. Phenothiazine and phenoselenazine have essentially the same redox potential within experimental error while the phenoxazine is slightly harder to oxidize.

Methylating the nitrogen shifts the oxidation potentials to more positive values. The greatest effect is seen with phenoxazine, methylating causes an ~200 mV change in the redox potential. The effect decreases as we substitute down the group, ~80 mV for phenothiazine and ~10 mV for phenoselenazine. Substituting an N-alkylbipyridine for the methyl group has only a small effect on the redox potential except for the 44-POZ

Table 2.1: Oxidation Potentials of Various Donors

Compound	$E_{1/2}$ (mV)	Compound	$E_{1/2}$ (mV)	Compound	$E_{1/2}$ (mV)
POZ	630	44-PTZ	698	44-PSZ	649
N-Me-POZ	618	Tetramethyl-PTZ	451	DiMe-PNZ	393
44-POZ	605	44-tMe-PTZ	560	Phenylenediamine	88
PTZ	617	PSZ	625	TMPD	118
N-Me-PTZ	700	N-Me-PSZ	635		

which has an ~30 mV change. By changing the chalcogen in these donors we can vary the driving force by approximately 200 mV. While the geometry and the solvent shell are perturbed by the substitution, the changes are small and should not greatly effect the electron transfer. Moreover, since the reducing electron comes from essentially the same molecular orbital,[7] it can be inferred that the mechanism of electron donation is the same from donor to donor.

A fourth donor, 2,4,6,8-tetramethylphenothiazine (tMe-PTZ) (fig. 2.1), was synthesized to provide another driving force in the series. Both the N-hydro- and the 44-bpy ligand are substantially easier to oxidize than the phenothiazine equivalent. Structurally tMe-PTZ is similar to PTZ, and the reducing electron most likely comes from the same MO, yet the mechanism of electron donation into a metal-polypyridyl complex may not be strictly identical. This will be discussed in more detail later on.

Of these four donors, the phenoxazine was the only one not originally made into a donor-ligand. Later work discussed in Chapter 4 led us to renewed interest in this donor

ligand and it was synthesized and characterized and some preliminary work has been done, but is not present in this work. The N-MePOZ was synthesized for use in bi-molecular quenching experiments as is discussed in Chapter 4. The 44-PSZ ligand was prepared in sufficient quantities to obtain a usable NMR and to determine its electrochemistry (see Appendix A). No $D\text{-}C^{2+}$ or $D\text{-}C^{2+}\text{-}A^{2+}$ complexes were ever synthesized with 44-PSZ as the focus of the research shifted during scale up of the ligand (see Chapter 3). The ligand was neglected to the point that there was little usable compound left to do the electrochemistry shown in Appendix A. The N-MePSZ donor was also synthesized for use in bimolecular quenching experiments which will be discussed in Chapter 4.

The 44-tMe-PTZ ligand was used to make the homoleptic Ru(44-tMe-PTZ)$_3$(PF$_6$)$_2$ compound. The aromatic methyl groups make the 44-tMePTZ ligand 130 mV easier to oxidize than the corresponding 44-PTZ ligand (see Table 2.1). This change in potential directly translates into an increase in driving force for the electron transfer reaction by making the quantity in parentheses in equation 4a of Chapter 1 a smaller quantity. Furthermore, the emission onset energy for Ru(44-tMe-PTZ)$_3$(PF$_6$)$_2$[8] and Ru(44-PTZ)$_3$(PF$_6$)$_2$ are not identical,[2] with Ru(44-tMePTZ)$_3$(PF$_6$)$_2$ being ~20 nm blue shifted.[9] By plugging the relevant quantities into equation 4a of Chapter 1 we arrive at a driving force (ΔG) of ΔG = -0.100V for Ru(44-PTZ)$_3$(PF$_6$)$_2$[2] and ΔG= -0.325V for Ru(44-tMe-PTZ)$_3$(PF$_6$)$_2$. This results in a net 0.225V increase in driving force for Ru(44-tMe-PTZ)$_3$(PF$_6$)$_2$ over Ru(44-PTZ)$_3$(PF$_6$)$_2$. This increase in driving force is directly manifested in the electron transfer rate (see Table 2.2) where a nearly fourfold increase occurs when changing from 44-PTZ to 44-tMePTZ. We can infer that the electron

transfer is in the Marcus normal region[10] (i.e. an increase in driving force corresponds to an increase in electron transfer rate).

Table 2.2: Electron Transfer Rate Constants for D-C Complexes

Compound	k_{et} (s^{-1})	k_{et}/(#PTZ's) (s^{-1})
$Ru(dmb)_2(44\text{-}PTZ)^{2+}$	2.70E+06	2.70E+06
$Ru(44\text{-}PTZ)_3^{2+(11)}$	1.20E+07	3.90E+06
$Ru(44\text{-}tMePTZ)_3^{2+}$	4.19E+07	1.40E+07

The rate constant (k_{et}) for an electron transfer reaction is given by:

$$k_{et} = A\, e^{-\Delta G^{\ddagger}/RT} \qquad (6)$$

where A is a pre-exponential factor that varies with solvent and the perturbation caused by electron transfer[12] and $\Delta G^{\ddagger}/RT$ is the activation free energy for electron transfer. Marcus theory[13] gives the value of $\Delta G^{\ddagger}$ by:

$$\Delta G^{\ddagger} = \lambda/4\,(1 + \Delta G/\lambda)^2 \qquad (7)$$

where λ is the reorganizational energy upon electron transfer and ΔG is the reaction exothermicity.

Larson reported a value for $\lambda = 800 \pm 100$ meV for the electron transfer in C^{2+}-A^{2+} complexes in acetonitrile.[2] He used this value with good success when comparing electron transfer rates to driving force in D- C^{2+} complexes in acetonitrile.[2] This is not unreasonable as λ should vary little from complex to complex, making the error in the value of λ systematic. Using this value and electron transfer rate corrected for the

number of donor units[2] for $Ru(44\text{-}PTZ)_3(PF_6)_2$ one obtains a value for $A = 1.51 \times 10^9\ s^{-1}$. If one assumes for the moment that the pre-exponential factor A is the same for both D-C^{2+} complexes in acetonitrile, then the predicted electron transfer rate constant (corrected for the number of donor groups) for $Ru(44\text{-}tMe\text{-}PTZ)_3(PF_6)_2$ is $k_{et} = 9.71 \times 10^7\ s^{-1}$. This is nearly an order of magnitude faster than the experimental value of k_{et} (Table 2.2).

There are three possibilities to explain the data. One is that the assumption that the pre-exponential factor is the same for both D-C^{2+} complexes is wrong. The other two are that there is something in the electron transfer mechanism for these complexes that either hinders the electron transfer in $Ru(44\text{-}tMe\text{-}PTZ)_3(PF_6)_2$ or favors the electron transfer in $Ru(44\text{-}PTZ)_3(PF_6)_2$.

Unfortunately, in this comparison more than just the driving force is being changed. The reorganizational energy λ is customarily broken down into outer sphere and inner sphere components.[14]

$$\lambda = \lambda_o + \lambda_i \qquad (8).$$

The inner sphere reorganizational energy (λ_i) is associated with changes in nuclear positions and bond strengths within the D-C^{2+} unit upon electron transfer. Structurally the two complexes are nearly identical except for the twelve aromatic methyl groups on the three donors. We already know that these methyl groups play a part in the electron transfer by donating electron density into the π-system of the donor making it easier to oxidize. The addition of more nuclei and bonds to the PTZ unit can affect the equivalency of the λ_i terms.

The outer sphere component, sometimes referred to as the solvent reorganizational energy, can be calculated from a classical dielectric continuum treatment

assuming a hard sphere model of the reactants.[14]

$$\lambda_0 = (\Delta e)^2 \left(\frac{1}{2r_1} + \frac{1}{2r_2} - \frac{1}{d}\right)\left(\frac{1}{\epsilon_\infty} - \frac{1}{\epsilon_0}\right) \qquad (9)$$

In this expression, r_1 and r_2 are the radii of the two reactants, d is the electron transfer distance and ϵ_∞ and ϵ_0 are the high-frequency and static dielectric constants. Since the measurements were made in the same solvent, the solvent term in equation 9 is constant for the two complexes. Likewise, the radius of the chromophore is also constant. The electron comes from essentially the same donor orbital and goes to the same metal based orbital in both complexes. If one envisions an all trans alkyl link, then one would expect the electron transfer distance to be roughly equal in both cases.

The implied equality of the reorganizational energy for the electron transfer reactions could therefore be in error. The small differences in λ show up in the calculation of $\Delta G^{\ddagger}$ in equation 7. In our calculations we have used a value for λ obtained from an entirely different system. The differences also manifest themselves in the value of the pre-exponential factor.[2]

$$A \propto (1/\lambda)^{1/2} \qquad (10)$$

Calculating A for $Ru(44\text{-}tMe\text{-}PTZ)_3(PF_6)_2$ using the 0.8V value for λ gives us $A = 2.18 \times 10^8\ s^{-1}$. A also varies with other factors, such as electronic overlap and the solvent longitudinal relaxational time, depending on the initial assumptions and type of electron transfer (i.e. bimolecular or intramolecular).[15] Alone, these small perturbations to the reorganizational energy are enough to explain the discrepancy in the data.[16] A larger value for λ for $Ru(44\text{-}tMe\text{-}PTZ)_3(PF_6)_2$ gives a larger value for $\Delta G^{\ddagger}$ resulting in a smaller k_{et} as well as making the pre-exponential factor, A, a smaller value.

One cannot rule out, however, that there is something in the electron transfer mechanism for these complexes that either hinders the electron transfer for Ru(44-tMe-PTZ)$_3$(PF$_6$)$_2$ or favors the electron transfer for Ru(44-PTZ)$_3$(PF$_6$)$_2$. In Chapter 3 we propose that the π-system of the PTZ has the ability to form a charge-transfer complex with the π system of the bipyridine, in effect, forming a docking site for the donor in close proximity to the chromophore. If this charge-transfer effect plays a role in the electron transfer, it would affect the electron transfer distance, *d* in equation 9 and bring into question the assumption that *d* is constant across all of the complexes. Moreover, the charge-transfer interaction is controlled by van der Waals forces between the donor and the chromophore. The donor is tethered to the ligand by a flexible alkyl chain. In solution the chain can access many conformations which allow a range of donor-chromophore distances. Experimentally, there is a maximum distance at which the donor and the chromophore have sufficient electronic overlap for electron transfer to occur. The fraction of donors that reside within this distance at a given instant is a function of the alkyl chain length.[2] With no other interactions, this fraction should be the same for 44-PTZ and 44-tMe-PTZ, since they are both tethered by a four carbon alkyl chain. A charge-transfer interaction would increase the fraction of donors within the maximum distance at a given instant. The methyl groups on the 44-tMe-PTZ could be affecting the formation a charge-transfer interaction due to sterics, and thus this donor would not benefit from this interaction to the extent that the 44-PTZ would. This would manifest itself as a faster than predicted k_{et} for Ru(44-PTZ)$_3$(PF$_6$)$_2$.

Most likely the discrepancy in the data for k_{et} between Ru(44-PTZ)$_3$(PF$_6$)$_2$ and Ru(44-tMe-PTZ)$_3$(PF$_6$)$_2$ is a combination of the inaccuracy of the assumption that the

reorganizational energy and pre-exponential factor are the same for both complexes and the effects of the proposed charge-transfer interaction.

The second group of donors consisted of a bridging donor group attached to two different bipyridyl groups, making a tetradentate ligand. In the previously studied $D\text{-}C^{2+}\text{-}A^{2+}$ systems there were always two PTZ donors to one chromophore and one acceptor. Because such structures give rise to multiple isomers having different spatial relationships between the two donor and between the donors and the acceptors there was always a question as to which of the PTZ's was doing the donating. Likewise, such arrangements give rise to questions about the dynamics of the back electron transfer to the ground state. By having only one symmetrically disposed donor, all these questions are eliminated.

Two different donor groups were proposed. One was based on phenazine as a donor (fig. 2.2A) and the other on phenylenediamine (fig. 2.2B). The phenylenediamine group has a small positive redox potential (see Table 2.1), giving it a strong driving force for electron transfer. The *N,N,N',N'*-tetramethylphenylenediamine has been used in bimolecular quenching experiments[17] and the rates obtained for reductive quenching are comparable to the rates of oxidative quenching by the linked diquaternary amines studied in the $C^{2+}\text{-}A^{2+}$ complexes[18] (i.e. 0.1-1 ns^{-1}). This could change some of the processes elucidated in the first chapter about the previous $D\text{-}C^{2+}\text{-}A^{2+}$ complexes. For one, the donor might now compete with the acceptor in quenching the excited state chromophore (see Scheme 2.1).

The increase in driving force for the donor may favor the formation of the charge-separated (CS) state by making $k_{f,cs}$ (analogous to k_2 in Figure 1.4) faster in relation to

$k_{b,o}$ (k_{-1} in Figure 1.4). On the other hand, if the donor competes with the acceptor for the excited state and the electron transfers follow the left hand side of Scheme 2.1, the effect on the quantum yield of the CS state is uncertain. Intuitively, since $k_{f,r}$ is fast and $k'_{f,cs}$ should be fast (based on the fact that $k_{f,o}$ is fast and the $Ru^{2+/1+}$ couple is 0.44eV easier to

Scheme 2.1: Competing Pathways from the Excited State in D-C^{2+}-A^{2+} Triads

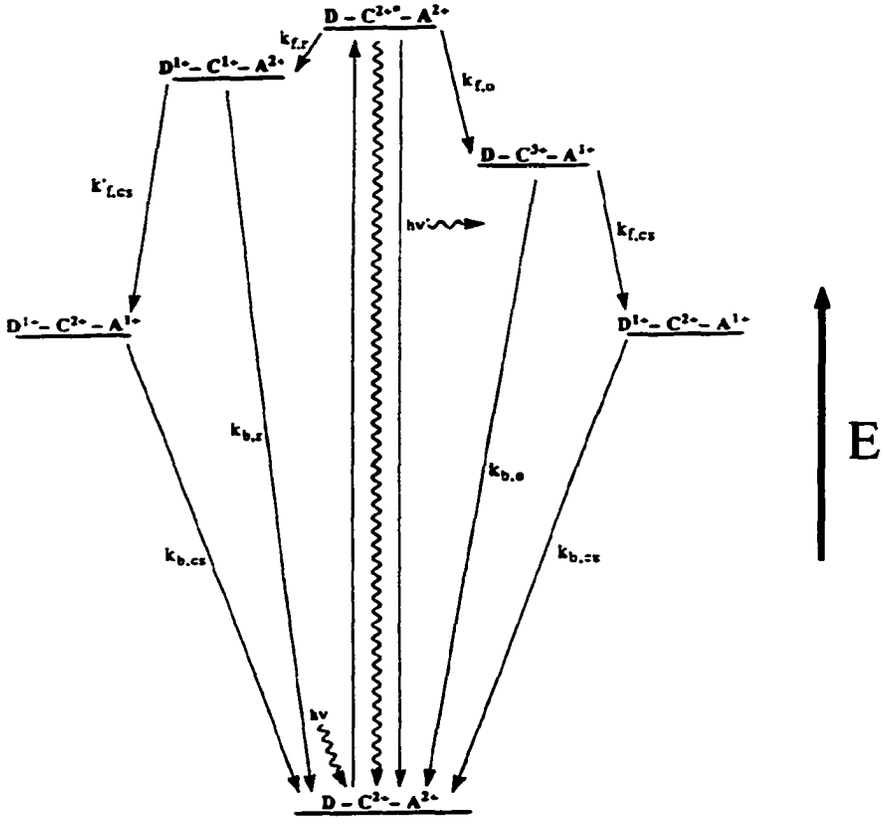

oxidize than the $Ru^{2+*/3+}$ couple),[1] one might expect a high quantum yield. The quantum yield for the CS state in this pathway is based on the relative rates of $k'_{f,cs}$ and $k_{b,r}$. Without adequate knowledge of $k_{b,r}$ in this system, there is no way to hypothesize on the quantum yield. In theory, by increasing the driving force to the point that the donor competes with the acceptor for the initial electron transfer, we could be taking a step in the wrong direction towards increasing our quantum yield.

Unfortunately, the ease of oxidation of phenylenediamine groups compounds the already difficult job of asymmetrically substituting identical functional groups. Phenylenediamine is so easily oxidizable that silica gel chromatography tends to oxidize it on the column. One can actually observe the color changes as it moves down the column until it finally degrades so much that it stops eluting. Phenylenediamine obtained commercially (Aldrich, 90%) comes as a purple/black solid. It must be sublimed to give relatively pure white needles. This solid degrades within days even when stored under N_2 in the dark at 0°C.

A wide variety of conditions and strategies were used to try to synthesize the proposed ligand. None met with success. A tetradentate ligand based on phenazine showed more promise. Being slightly harder to oxidize than phenylenediamine makes it much easier to work with. Both phenazine and *N,N'*-dihydro-dimethylphenazine are stable over long periods of time and give reversible electrochemistry when cycled through the 1+/0 couple (see appendix A). Due to the low yields during alkylation, the *N,N'*-(4-bromo-n-butyl)phenazine was proposed as the intermediate to the tetradentate ligand (as opposed to the 4-methyl-4'-(4-bromo-n-butyl)-2,2'-bipyridine which was the standard route for making donor ligands).

While work on this ligand proceeded, the error in the initial values for the quantum yield of the D-C^{2+}-A^{2+} triads was exposed (see Chapter 1). In light of this information, work on new donors was shelved for work presented in Chapter 3. The focus of the research switched from "How do we improve the quantum yield of these D-C^{2+}-A^{2+} triads?" to "Why is the quantum yield for the triads we have so large?".

ENDNOTES

[1] Kalayansunduram, K. *"Photochemistry of Polypyridine and Porphyrin Complexes"* Academic Press, San Diego, USA, **1992**.

[2] Larson, S.L. "Charge Transfer in Linked Donor-Chromophore-Acceptor Systems"; Ph.D. Thesis, Colorado State University, **1994**.

[3] Ibid., p. 94. The coordinated 41-PTZ is ~150 mV harder to oxidize than the rest of the 4*p*-PTZ series.

[4] Lentner, T. *J. Amer. Chem. Soc.*, **1925**, *37*, 2342.

[5] Podolesov, B.D.; Jordanovska, N.B. *Croatica Chimica Acta*, **1970**, *42*, 61.

[6] *See appendix A for the cyclic voltammograms of the donors.*

[7] Chin, M.F.; Gilbert, B.C.; Hanson, P. *J. Chem. Soc. (B)*, **1970**, 1700.

[8] *See appendix B.*

[9] Due to the quenching by the tMe-PTZ, the emission from the $Ru(44\text{-}tMe\text{-}PTZ)_3^{2+}$ chromophore is very weak (*see appendix B*). There is a peak in the spectrum at 525 nm that arises from the acetonitrile. Since there is considerable overlap between the two peaks, the measured 20 nm blue shift when comparing $Ru(44\text{-}tMe\text{-}PTZ)_3^{2+}$ to $Ru(44\text{-}PTZ)_3^{2+}$ is subject to some error as the overlap effects the shape of the emission peak. A 2 nm error in the measurement of the emission onset energy corresponds to ~10 mV in ΔG. The error in this measurement therefore effects the magnitude of the difference in the driving force and not the qualitative result.

[10] Cooley, L.F.; Larson, S.; Elliott, C.M. *J. Phys. Chem.*, **1991**, *95*, 10694.

[11] Larson, S.L. "Charge Transfer in Linked Donor-Chromophore-Acceptor Systems"; Ph.D. Thesis, Colorado State University, **1994**, Table 5.6.

[12] Sutin, N. *Topics in Current Chemistry*, Springer-Verlag, Berlin, **1990**, *156*, 441.

[13] Marcus, R. A *J. Chem. Phys.*, **1956**, *24*, 979.

[14] Marcus, R.A. *Discuss. Faraday Soc.*, **1960**, *29*, 21.

[15] Marcus, R.A., *Reviews of Modern Physics*, **1993**, *65*, 599.

[16] If one assumes λ= 800 meV and calculates for the constant A using the data for the $Ru(44\text{-}PTZ)_3^{2+}$ data, then uses this value to back calculate λ using the $Ru(44\text{-}tMePTZ)_3^{2+}$ data, one finds that λ must change by a factor of 2 to be consistent with the data. However, there are reasonable values of λ that would be consistent with our data.

[17] Anderson, C.P.; Salmon, D.J.; Meyer, T.J. *J. Amer. Chem. Soc.*, **1977**, *99*, 1980.

[18] Cooley, L.F., Headford, C.E.L.; Elliott, C.M., Kelley, D.F. *J. Amer. Chem. Soc.*, **1988**, *110*, 6673.

Chapter 3:

Charge-Transfer Interactions Between Rutheniumtrisbipyridine-type Chromophores and Phenothiazine

As mentioned in Chapter 1, while studying the magnetic field effects on electron transfer in the D-C^{2+}-A^{2+} triads, it was found that the quantum yield for forming the charge-separated state was $\varphi_{cs}= 0.86 \pm 0.08$ for $Ru(44\text{-}PTZ)_2(423\text{-}DQ)^{4+}$, three times the previously reported value of $\varphi_{cs}= 0.26 \pm 0.04$. With such a large value for the quantum yield, research was discontinued on donors with greater driving forces, the purpose of which was to increase yield to the CS state. The question then became, what is causing such high quantum yields in these D-C^{2+}-A^{2+} triads and can we manipulate the system to favor the formation of the charge separated state and/or hinder the recombination to the ground state?

Careful analysis of the UV-Vis spectra of the D-C^{2+}, C^{2+}-A^{2+} and D-C^{2+}-A^{2+} complexes mentioned in Chapter 1 revealed an interesting pattern. For the C^{2+}-A^{2+} complexes one could in effect, build the UV-Vis spectrum for an individual C^{2+}-A^{2+}

complex from the appropriately weighted UV-Vis spectra of the component parts (i.e. $Ru(dmb)_3^{2+}$ and the appropriate diquat ligand). The two spectra would be virtually identical. For the phenothiazine containing $D\text{-}C^{2+}$ and $D\text{-}C^{2+}\text{-}A^{2+}$ complexes, a similar treatment always shows an additional unaccounted for absorbance on the MLCT band (see Figure 3.1). The additional absorbance is most obvious on the low energy side of the MLCT band.

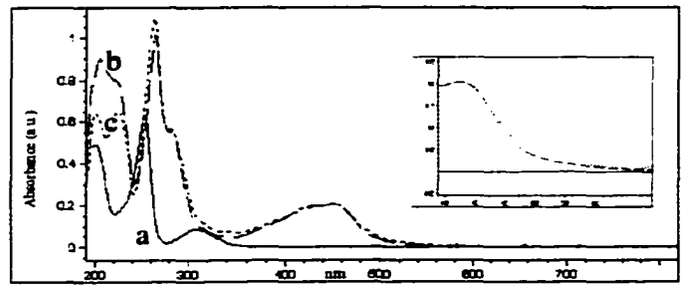

Figure 3.1: Absorbance spectra of a) Me-PTZ, b) $Ru(phen)_2(47\text{-}PTZ)^{2+}$, and c) $Ru(phen)_2(dmb)^{2+}$.

A charge-transfer (CT) interaction between the π system of the phenothiazine donor and the π system of one of the ligands was hypothesized as a likely cause of the additional absorbance. A polar acetonitrile solution, as well as the alkyl chain tether to keep the two species from diffusing apart, could favor the formation of a CT interaction. As mentioned in Chapter 2, a charge transfer interaction puts the donor in close proximity to the chromophore. This in turn affects the electron transfer distance, *d*, in equation 9 of Chapter 2 (when compared to an extended conformation) and should provide good electronic overlap between the donor and the chromophore.

The first order of business is to show that we are indeed observing a CT interaction between the phenothiazine donor and one of the chromophore's ligands. The

second is to determine what effect, if any, that the CT interaction has on the electron transfer in D-C complexes (and in Chapter 4, D-C^{2+}-A^{2+} complexes).

Previous members of the Elliott group had amassed quite a bit of data on D-C^{2+}, C^{2+}-A^{2+} and D-C^{2+}-A^{2+} complexes. This data was reviewed in the light of the CT interaction hypothesis with the assumption that the interaction does affect the electron transfer in these complexes. While the conclusions are speculative, they were intriguing enough to encourage further research.

In his dissertation, Dr. Larson showed that the quenching rate in $Ru(dmb)_2(4p\text{-}PTZ)^{2+}$ (see Figure 1.2a) complexes is independent of the chain length, *p*, when $p>4$ in acetonitrile.[1] (Electron transfer rates should fall off exponentially with distance.)[2] This was originally attributed to a maximum electron transfer distance at which quenching could occur.[1] As noted in Chapter 2, a flexible alkyl chain linkage leads to a wide variety of conformers that give a statistical range of D-C distances in room temperature solution. A longer chain length, *p*, means the PTZ unit is within that maximum electron transfer distance for a smaller fraction of the time, which should fall off roughly linearly as the chain gets longer. This was seen in 1,2-dichloroethane (DCE) (see Figure 3.2). Acetonitrile, it was proposed, did not solvate the alkyl chain well, leaving it to fold back and interact with itself, leading to shortened D-C distances and a virtual independence on chain length for quenching.[1]

The same arguments of solvent interactions are also consistent with a CT interaction. Polar acetonitrile facilitates the formation of a CT interaction, which reduces the range of D-C distances and thus the quenching rate is not dependant on the chain length.

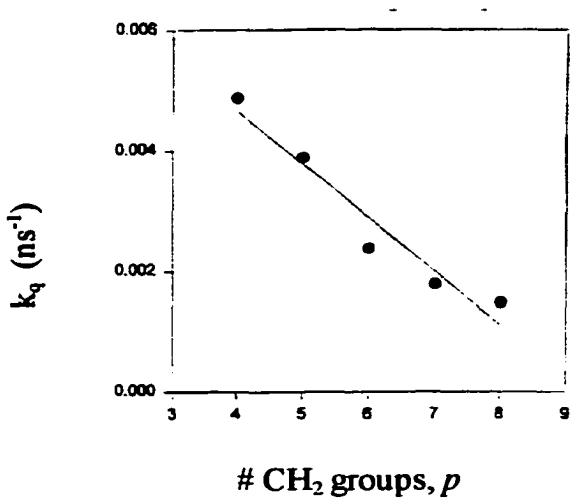

Figure 3.2: Dependence of alkyl chain length, p, on quenching rate in Ru(dmb)$_2$(4p-PTZ) complexes in 1.2-dichloroethane.[3]

The fairly non-polar DCE should not promote CT formation, and either the CT interaction does not form, does not predominate, or is not the dominant factor in the electron transfer in DCE, as a significant fraction of the PTZ units diffuse beyond a maximum distance as p increases. While Larson's data for the linked complexes is consistent with this picture of solvent interaction, recent data from J.Weber[4] on related bimolecular systems suggest the opposite solvent dependency.

As mentioned above, the conclusions drawn from the existing data are interesting but speculative. There is nothing in the data that suggests that the original conclusions drawn from them are necessarily incorrect. With this in mind we set out to prove the hypothesis that a CT interaction is forming and that it plays a significant role in the electron transfer processes in D-C^{2+} and D-C^{2+}-A^{2+} complexes.

To accomplish our objectives, we proposed to look for physical evidence of the proposed CT interaction. The CT interaction should manifest itself in both the UV/Vis

spectra and NMR spectra. We also proposed to look at the effect of ligand substitution in D-C^{2+} and D + C^{2+} systems. By varying the size of the π system and/or sterics of the ligand (see Figure 3.3), we hoped to affect the proposed CT interaction. We then looked for changes in the electron transfer rate with changes in the CT interaction.

Experimental:

5-nitro-1,10-phenanthroline:[5] 20.0g (0.101 mol) of 1,10-phenanthroline hydrate was dissolved in 100 mL fuming sulfuric acid (20% v/v; Fischer) and heated to 100°C. 30 mL of fuming nitric acid (72% v/v; Fischer) was added dropwise keeping the temperature less than 110°C. The reaction was refluxed at 110°C for an 30 minutes. Another 50 mL of fuming nitric acid was added over 30 minutes and the reaction refluxed for 1.5 hours. The solution was cooled to room temperature, poured over ice and neutralized with $NaOH_{(aq)}$, precipitating out the product as a solid. The solid was filtered, then dissolved in CH_2Cl_2 and extracted with H_2O. The organic solvent was removed by rotary evaporation and the remaining solid was recrystallized in MeOH yielding fine white crystals. This product contained some (<5%) 1,10-phenanthroline-5,6-quinone as a side product. As this was the desired end product, the 5-nitro-1,10-phenanthroline was used without further purification. Yield: ~70%. ^{1}H NMR ($CDCl_3$) δ: C_2, C_8 7.85 (2t's), C_7 8.45 (d), C_6 8.52 (s), C_3 9.05 (d), C_9 9.33 (d), C_1 9.38 (d).

5-amino-1,10-phenanthroline:[6] 11g (0.05 mol) of crude 5-nitro-1,10-phenanthroline and 34g (3 eq.) of $SnCl_2$ were dissolved in 250 mL EtOH and refluxed 4 hours. The cloudy, pale yellow solution was then cooled to room temperature and approximately 1/3 of the solvent was removed by rotary evaporation. The solution was

then made slightly basic by the addition of $NaOH_{(aq)}$.[7] The resulting white precipitate was filtered over a glass frit and dried under vacuum leaving a hard, claylike solid. The solid showed no side products by thin layer chromatography (10% acetone in CH_2Cl_2) and was used without further purification. Yield: ~95%, determined by thin-layer chromatography. ^1H NMR ($CDCl_3$) δ: C_6 6.9 (s), C_8 7.3 (t), C_2 7.4 (t), C_7 8.2 (d), C_3 8.3 (d), C_9 9.0 (d), C_1 9.2 (d).

1,10-phenanthroline-5,6-quinone (phen-quinone):[8] 12g (0.06 mol) of crude 5-amino-1,10-phenanthroline was dissolved in 80 mL fuming sulfuric acid (20% v/v; Fischer) at 0°C. 50 mL of fuming nitric acid (72% v/v; Fischer) was added over 1 hour with stirring. The reaction was then refluxed for 2 hours, then cooled to room temperature. The cloudy, light green solution was then poured over ice and its pH adjusted to ~6 with $NaOH_{(aq)}$. The product was extracted into CH_2Cl_2 and the solvent removed by rotary evaporation. The product was recrystallized in MeOH resulting in a pale orange powder. Yield: ~85%. ^1H NMR ($CDCl_3$) δ: C_2, C_8 7.55 (dt); C_3, C_7 8.45 (dd); C_1, C_9 9.08 (dd).

Dipyrido[3,2-*a* : 2',3'-*c*]phenazine (dppz):[8] 50mg (2.4×10^{-4} mol) of phen-quinone was dissolved in 2 mL hot EtOH. To this was added 30mg (2.7×10^{-4} mol) of *o*-phenylenediamine (Aldrich, recrystallized in ethyl acetate) dissolved in 2 mL of hot EtOH. To the hot solution was added ~ 1 mL of H_2O until the solution turned cloudy. The solution was cooled to 0°C and the product precipitated as a light tan solid. The product was filtered, dried and recrystallized in EtOH. Yield: 100%, determined by thin-layer chromatography. ^1H NMR ($CDCl_3$) δ: C_1, C_4 8.05 (dd); C_{11}, C_{12} 8.15 (dd); C_2, C_7 8.45 (dt); C_{10}, C_{13} 9.60 (dd); C_3, C_6 9.95 (dd). UV/Vis λ_{max}= 378 nm.

Benzo[3,2-*a*]-dipyrido[2,1-*e* : 1',2'-*g*] phenazine (bbppz): This compound was synthesized by a modification of the dppz synthesis (*vide supra*). 0.1788g (8.5×10^{-4} mol) of phen-quinone was dissolved in 5 mL hot EtOH. To this was added 0.1383g (8.6×10^{-4} mol) of 2,3-diaminonapthalene (Aldrich) dissolved in 5 mL of hot EtOH. The reaction was refluxed for 15 minutres. The solvent was removed by rotary evaporation until the solution turned cloudy. The solution was cooled to 0°C and the product precipitated out as an orange solid. The product was filtered, washed with diethyl ether, and dried. Yield: 100%, determined by thin-layer chromatography. $m/z^+ = 333.2$ UV/Vis $\lambda_{max} = 408$ nm.

Dibenzo[3,2-*a* : 2',3'-*c*]-dipyrido[2,1-*e* : 1',2'-*g*] phenazine (ddp): This compound was synthesized by a modification of the dppz synthesis (*vide supra*). 50mg (2.4×10^{-4} mol) of phen-quinone was dissolved in 2 mL hot EtOH. To this was added 50mg (2.4×10^{-4} mol) of 9,10-diaminophenanthrene (Aldrich) dissolved in 2 mL of hot EtOH. To the hot solution was added ~ 1 mL of H_2O until the solution turned cloudy. The solution was cooled to 0°C and the product precipitated out as a light orange solid. The product was filtered, washed with EtOH, and dried. Yield: 100%, determined by thin-layer chromatography. $m/z^+ = 382.1$ UV/Vis $\lambda_{max} = 418$ nm.

2,3-Diaminophenazine:[9,10] 0.4826g (4.5×10^{-3} mol) of *o*-phenylenediamine and 1.134g (4.5×10^{-3} mol) of I_2 were combined in 15 mL of EtOH and refluxed for 2 hours. The solution was cooled to room temperature and the solvent reduced to ½ volume by rotary evaporation. Saturated $AgNO_{3(aq)}$ was added to precipitate excess iodide and the solution was decanted. NH_4OH was added until the solution was basic and the product was extracted into CH_2Cl_2. The organic solvent was removed by rotary evaporation. The

remaining solid was recrystallized in EtOH producing yellow-tan needles. Yield: 35%. ^{1}H NMR (d_6-acetone) δ: -NH_2 5.6 (s), $C_{1,4}$ 7.1 (s), $C_{7,8}$ 7.55 (dd), $C_{6,9}$ 7.95 (dd).

Dipyridodiphenazine (dpdpz): This compound was synthesized by a modification of the dppz synthesis (*vide supra*). 0.1311g (6.2 x 10^{-4} mol) of 2,3-diaminophenazine was dissolved in 5 mL hot EtOH. To this was added 0.1532g (7.3 x 10^{-4} mol) of phen-quinone dissolved in 5 mL of hot EtOH. The reaction was refluxed for 1.5 hours until a cloudy, red-maroon color persisted. To the hot solution was added ~ 5 mL of H_2O. The solution was cooled to 0°C and the product precipitated out. Yield: 100%, determined by thin-layer chromatography. m/z^+ = 384.2 UV/Vis λ_{max}= 682 nm.

Bis-isoquinoline (i-biq): This ligand was prepared by the method described by Rosevear and Sasse[11] for the synthesis of terpyridines. 22.5g (0.17 mol) of iso-quinoline (Aldrich) and 1g of Pd on carbon (10 wt.%, Aldrich) were combined in a round bottom flask and heated in an oil bath at 160°C for 24 hours. An additional 1g of Pd on carbon was added and the reaction was heated for another 24 hours, then cooled to room temperature. The residue was dissolved in hot 3:2 toluene/acetone and filtered. The filtrate was cooled and the product precipitated out. The solid was filtered and washed with diethyl ether. The product was recrystallized in toluene/acetone. Yield: ~ 70%. m/z^{+H}= 257.1 ^{1}H NMR ($CDCl_3$) δ: $C_{5,5',6,6'}$ 7.6-7.8 (m); $C_{4,4',7,7'}$ 8.05 (t); $C_{8,8'}$ 8.95 (s); $C_{3,3'}$ 9.4 (s).

Neopentyltosylate: 2.51g (2.85 x 10^{-2} mol) of neopentyl alcohol (Aldrich) was combined with 5.41g (2.84 x 10^{-2} mol) of p-toluenesulfonyl chloride (Aldrich) in 4 mL pyridine. The reaction was gently refluxed for 15 minutes then cooled to room temperature. 30 mL of H_2O was added and the product extracted into CH_2Cl_2. The

organic layer was dried over Na_2SO_4 and the solvent removed by rotary evaporation. Excess neopentyl alcohol was removed under vacuum at 50°C leaving the pure product as an oil (d: ~0.85) Yield: ~95% yield. ^1H NMR ($CDCl_3$) δ: -C-$(CH_3)_3$ 0.9 (s), -O-CH_2-C- 2.45 (s), Ar-CH_3 3.65 (s), Ar 7.34-7.76 (dd).

N-Neopentylphenothiazine (np-PTZ): 0.99g (4.97×10^{-3} mol) of phenothiazine (Haver-Glover; recrystallized from benzene) was combined with 0.198g (~1 eq.) of NaH (Acros Organics; 50% dispersion in oil) in 25 mL dry THF under N_2 and stirred for 45 minutes at 0°C. 1.00 mL (1.36×10^{-3} mol) of neopentyltosylate was added slowly and the solution gently refluxed for 2 hours. The reaction was quenched with 50 mL H_2O and extracted into CH_2Cl_2. The organic layer was dried over Na_2SO_4 and the solvent removed by rotary evaporation. The crude product was purified by flash silica gel chromatography (1:5 diethyl ether:CH_2Cl_2). Approximate yield: 20%. ^1H NMR ($CDCl_3$) δ: -C-$(CH_3)_3$ 0.9 (s), -N-CH_2-C- 4.0 (s), Ar 6.9-7.1 (m). m/z^+ 269.1.

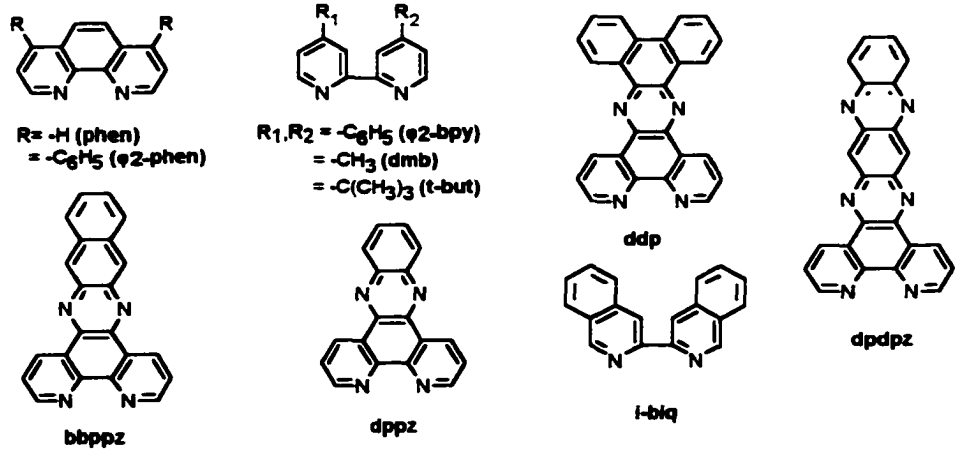

Figure 3.3: Polypyridyl ligands mentioned in Chapters 3 and 4.

The following compounds were synthesized by the general method outlined in Chapter 1 for $Ru(L)_2Cl_2$ (see Figure 3.3 for the structures and abbreviations of the ligands used): **$Ru(dmb)_2Cl_2$**; **$Ru(phen)_2Cl_2$** [phen = 1,10-phenanthroline]; **$Ru(dppz)_2Cl_2$**; **$Ru(\varphi_2\text{-bpy})_2Cl_2$** [$\varphi_2$-bpy = 4,4'-diphenyl-2,2-bipyridine]: **$Ru(\varphi_2\text{-phen})_2Cl_2$** [$\varphi_2$-phen = 4,7-diphenyl-1,10-phenanthroline]; **$Ru(t\text{-but})_2Cl_2$** [t-but = 4,4'-di-*t*-butyl-2,2'-bipyridine]; **$Ru(i\text{-biq})_2Cl_2$**; **$Ru(ddp)_2Cl_2$** [see fig.3.3]; **$Ru(bbppz)_2Cl_2$** [see fig. 3.3]; **$Ru(PQ)_2Cl_2$** [PQ = 1,10-phenanthroline-5,6-quinone].

The following compounds were synthesized by the general method outlined in Chapter 1 for $Ru(L)_3^{2+}$: **$Ru(dmb)_3^{2+}$**; **$Ru(phen)_3^{2+}$**; **$Ru(\varphi_2\text{-bpy})_3^{2+}$**; **$Ru(\varphi_2\text{-phen})_3^{2+}$**; **$Ru(t\text{-but})_3^{2+}$**; **$Ru(i\text{-biq})_3^{2+}$**; **$Ru(ddp)_3^{2+}$**; **$Ru(bbppz)_3^{2+}$**.

The following compounds were synthesized by the general method outlined in Chapter 1 for $Ru(L)_2(L')(PF_6)_2$: **$Ru(phen)_2(dmb)(PF_6)_2$**; **$Ru(dppz)_2(dmb)(PF_6)_2$**; **$Ru(\varphi_2\text{-bpy})_2(dmb)(PF_6)_2$**; **$Ru(\varphi_2\text{-phen})_2(dmb)(PF_6)_2$**; **$Ru(t\text{-but})_2(dmb)(PF_6)_2$**; **$Ru(i\text{-biq})_2(dmb)(PF_6)_2$**; **$Ru(ddp)_2(dmb)(PF_6)_2$**; **$Ru(bbppz)_2(dmb)(PF_6)_2$**; **$Ru(PQ)_2(dmb)(PF_6)_2$**.

The following compounds were synthesized by the general method outlined in Chapter 1 for $Ru(L)_2(4p\text{-PTZ})(PF_6)_2$: **$Ru(dmb)_2(47\text{-PTZ})(PF_6)_2$**; **$Ru(phen)_2(47\text{-PTZ})(PF_6)_2$**; **$Ru(dppz)_2(47\text{-PTZ})(PF_6)_2$**; **$Ru(\varphi_2\text{-bpy})_2(47\text{-PTZ})(PF_6)_2$**; **$Ru(\varphi_2\text{-phen})_2(47\text{-PTZ})(PF_6)_2$**; **$Ru(t\text{-but})_2(47\text{-PTZ})(PF_6)_2$**; **$Ru(i\text{-biq})_2(47\text{-PTZ})(PF_6)_2$**; **$Ru(ddp)_2(47\text{-PTZ})(PF_6)_2$**; **$Ru(bbppz)_2(47\text{-PTZ})(PF_6)_2$**.

The following compounds were synthesized by the general method outlined in Chapter 1 for $Zn(L)_3(ClO_4)_2$: **$Zn(phen)_3(ClO_4)_2$**; **$Zn(dppz)_3(ClO_4)_2$**; **$Zn(\varphi_2\text{-bpy})_3(ClO_4)_2$**; **$Zn(\varphi_2\text{-phen})_3(ClO_4)_2$**.

Results: UV-Vis Measurements of the CT Interaction

The optical transition in the UV-Vis spectra resulting from the proposed CT interaction is weak and in a region of the spectrum where the Ru(II) complex itself absorbs strongly. We therefore chose to look for evidence of a similar interaction in a surrogate complex; one with less spectral interference in the region of interest. Initially we chose $Zn(phen)_3^{2+}$. Zn^{2+} lacks the metal-based redox chemistry of Ru^{2+} and the complexes have no MLCT band. However, since the most likely mode of CT interaction would be the donation of charge density from the π-system of the PTZ into the π^*-system of one of the bound phen ligands, and since the first ligand based reduction of $Zn(phen)_3^{2+}$and $Ru(phen)_3^{2+}$ are at very similar potentials, we concluded that the difference in metal-base redox chemistry was probably largely irrelevant.

Upon mixing equal volumes of a 0.010 M solution of $Zn(phen)_3^{2+}$ and a 0.150 M solution of N-Me-PTZ in acetonitrile the solution develops a perceptible yellow color. If the volume of this solution is slowly reduced on a rotary evaporator, the color intensifies and becomes a bright lemon yellow color just before the solvent is completely gone. The film left on the sides of the flask is, likewise, bright lemon yellow. When this film is re-dissolved in a large amount of acetonitrile the color disappears and when the solvent is again removed the color reappears. Figure 3.4c shows a Uv/Vis spectrum of the solution prepared as described above. Also included are the spectra of the individual solutions of

$Zn(phen)_3(ClO_4)_2$ (3.4a) and N-Me-PTZ (3.4b) scaled to reflect their dilution upon mixing.

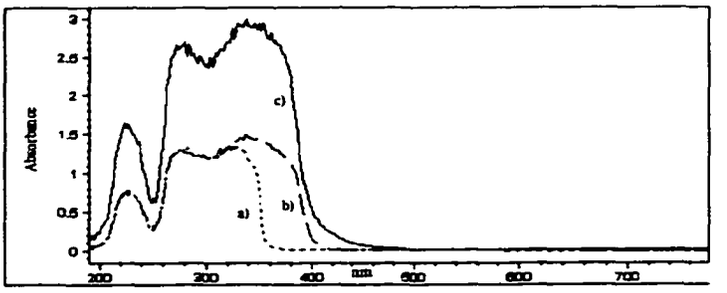

Figure 3.4: Uv/Vis spectra of a) $Zn(phen)_3^{2+}$. b) N-Me-PTZ. and c) N-Me-PTZ + $Zn(phen)_3^{2+}$ in acetonitrile.

Figure 3.5 is a difference spectra between curves 3.4b and 3.4c. There is clearly a new absorption in the mixture which begins around 500 nm and which increases in intensity to at least 390 nm, where the absorbtion from the $Zn(phen)_3(ClO_4)_2$ becomes too intense for measurement. This behavior strongly suggests the existence of a weak ground-state charge-transfer interaction between $Zn(phen)_3^{2+}$ and N-Me-PTZ.

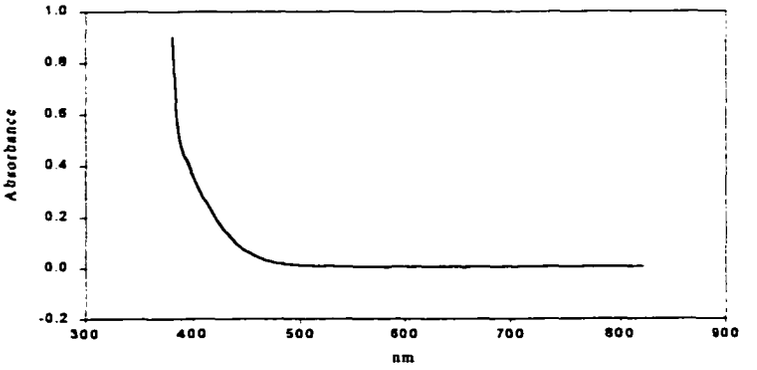

Figure 3.5: Difference spectra between $Zn(phen)_3^{2+}$ + N-Me-PTZ (fig.3.4c) and N-Me-PTZ (fig. 3.4b).

With the idea that a more extended ligand π-system would favor the CT formation, the dppz ligand was synthesized. The $Zn(dppz)_3^{2+}$ complex exhibits the same

behavior as the $Zn(phen)_3^{2+}$ complex with N-Me-PTZ. Based on these results, a series of ligands (the bbppz, ddp, dpdpz and dpdpz ligands (see Figure 3.3)) were all synthesized in a similar manner to the dppz, essentially a double Schiff base reaction between 1,10-phenanthroline-5,6-quinone and the appropriate ortho-diamine.

Later, for reasons which will be discussed below, we moved away from the dppz type ligands to other multi-ring ligands. The $Zn(\varphi_2\text{-bpy})_3(ClO_4)_2$ and $Zn(\varphi_2\text{-phen})_3(ClO_4)_2$ complexes were made and solutions were prepared in a similar manner to the $Zn(phen)_3^{2+}$ complex. Both ligands show a similar CT absorbtion as the phen ligand.

The "extra" absorbance noted for the covalently linked $RuL_2(4p\text{-PTZ})^{2+}$ systems is much more difficult to measure because of the interference from the MLCT band. Figure 3.6 shows difference spectra (obtained on a Varian Cary 500 Scan UV/Vis/N-IR) of $\sim 10^{-5}$M solutions of $Ru(phen)_2(47\text{-PTZ})(PF_6)_2$ and $Ru(phen)_2(dmb)(PF_6)_2$. By scaling one spectra and subtracting it from the other, we obtain a series of traces which only differ in the scaling factor (the scaling factor varies approximately 15% in Figure 3.6).

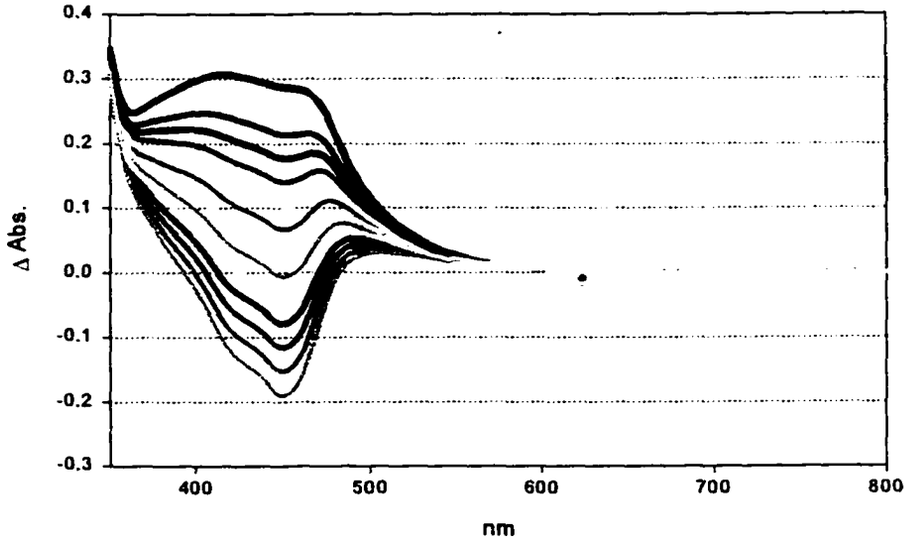

Figure 3.6: Difference spectra between $Ru(phen)_2(47\text{-PTZ})^{2+}$ and $Ru(phen)_2(dmb)^{2+}$.

If there was not a CT interaction providing additional absorbance, then the trace that intersects 0.0 at 452 nm should be virtually identical to the N-Me-PTZ spectra (i.e. no absorbance between 400-800 nm). Figure 3.6 shows that there is no scaling factor which eliminates the absorbance over this range. Furthermore, there is no trace that gives a smooth, featureless curve as we saw in Figure 3.5 with the $Zn(phen)_3^{2+}$ - N-Me-PTZ system. This implies that the CT interaction perturbs the MLCT spectrum of the chromophore. This is not unexpected as both the CT interaction and the MLCT spectrum involve the ligand π orbitals.

The CT interaction is most evident on the low energy side of the MLCT, though it most likely extends through the maximum of the MLCT. It tails down to at least 600 nm. It should be noted that the difference spectra for all the linked complexes show similar additional absorption; even where L has sterically bulky groups (such as t-butyl). This has led us to believe that it might be true that the linked PTZ ligand (fig. 1.2a) folds back and interacts with the bipyridine to which it is attached.

Spectral evidence for a similar charge transfer interaction between unlinked $Ru(phen)_2(dmb)^{2+}$ and N-Me-PTZ also exists. These spectra are very similar in shape to those for the linked systems. Figure 3.7 is a spectral titration performed with 10^{-4} M $Ru(phen)_2(dmb)^{2+}$ and N-Me-PTZ in 10 mL acetonitrile in a 1 mm cell with a 20 mL sidearm reservoir. Solid N-Me-PTZ was added to the sidearm and dissolved. The acetonitrile was purged before hand with N_2, but no further efforts were made to prevent oxygen from entering the system. One can clearly see an absorbance growing in over the entire spectral range shown. It should be noted that the curves converge at zero between 700 and 800 nm. At N-Me-PTZ concentrations over 0.1 M, which is near the saturation

point of N-Me-PTZ in acetonitrile (~240 mM), the spectra become erratic and no longer increase in a uniform fashion. This non-uniformity at high N-Me-PTZ concentrations was also noticed in the bimolecular quenching experiments and experiments done on the D/C-A complexes in Chapter 4. It is almost certainly a result of the nearly saturated N-Me-PTZ solution,[12] whether it is PTZ/PTZ interactions or solvent effects has not been resolved.

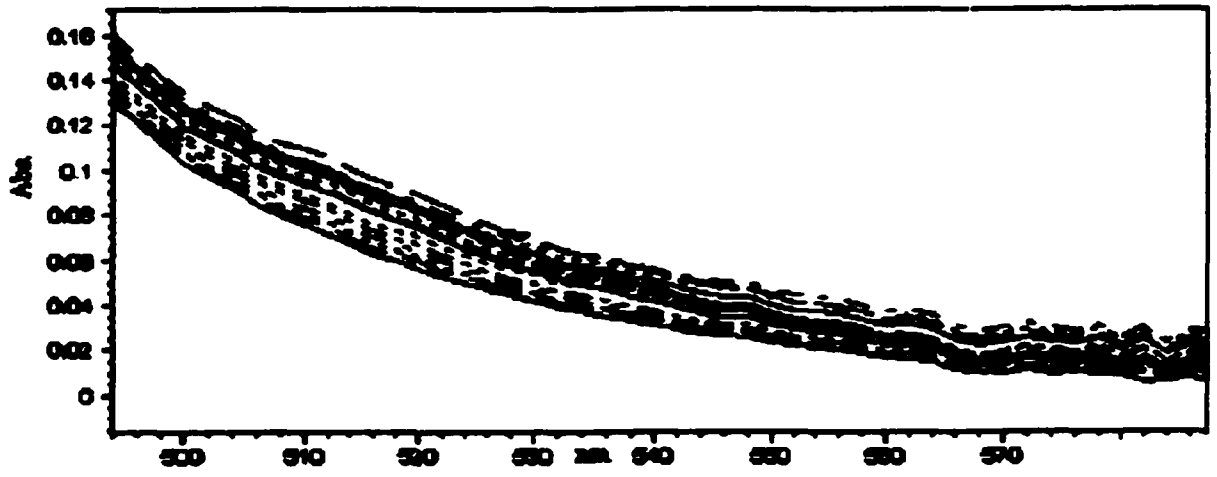

Figure 3.7: Spectral titration of 10^{-4} M $Ru(phen)_2(dmb)^{2+}$ with N-Me-PTZ. The bottom, solid curve is spectrum with no quencher. The top curve has a 150 mM N-Me-PTZ concentration.

Figure 3.8 is a graph of the change in absorbance at 515 nm versus the concentration of N-Me-PTZ. The slope of the line gives us:

$$m = \varepsilon_{ct,515} \cdot b \cdot K_{eq}[Ru] \quad (10).$$

Accounting for the path length and concentration of the chromophore gives us $\varepsilon_{ct,515} \cdot K_{eq} = 1.03 \times 10^5 / M^2 \cdot cm$. The value of K_{eq} is expected to be small. Since [N-Me-PTZ] » [Ru], if K_{eq} were large, the CT interaction would be saturated, and the spectra would not change upon addition of more N-Me-PTZ. Data presented in Chapter 4, with the

assumptions outlined there, give us a K_{eq} value of K_{eq}= 7 $\underline{M}^{-1}$. Based on this, the molar extinction coefficient for the CT interaction is relatively large (10^{-4} $\underline{M}^{-1}cm^{-1}$).

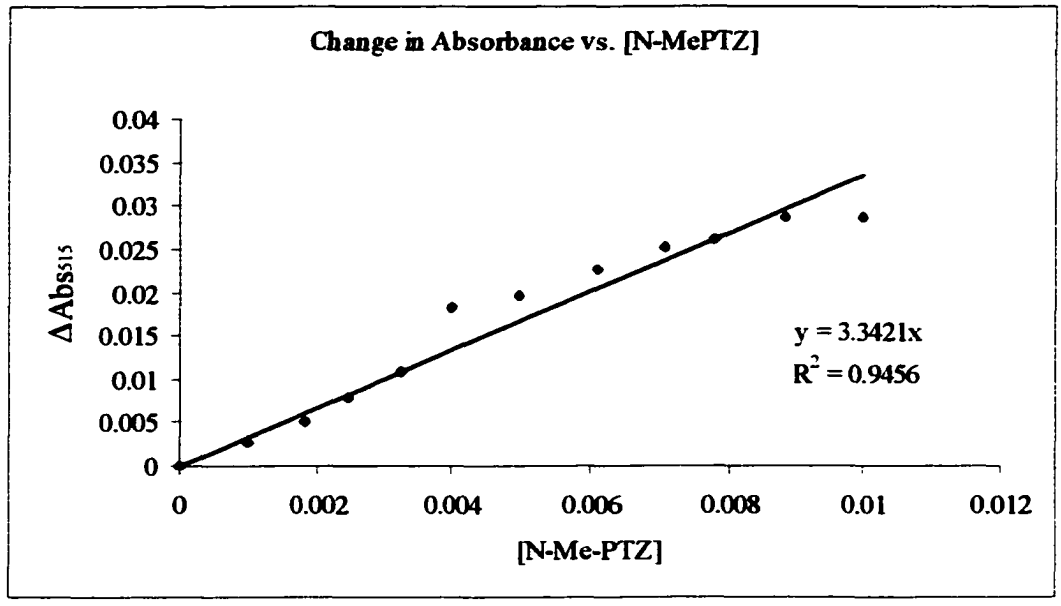

Figure 3.8: Change in absorbance at 515 nm of 10^{-4} $\underline{M}$ $Ru(phen)_2(dmb)^{2+}$ with varying concentrations of N-Me-PTZ.

NMR Measurements of the CT Interaction

One of the next places we looked for influences from the proposed CT was in the NMR spectra of the linked complexes. A sample of $Ru(phen)_2(47\text{-}PTZ)(PF_6)_2$ in d_6-acetonitrile was given to Dr. Chris Ritner for analysis. A 500 MHz Bruker NMR was used to perform 2D N.O.E experiments. The signal-to-noise for the spectra suffer because of the limit of solubility of the complex in acetonitrile. There is also considerable overlap of the signals from the phen ligands, the bipyridyl ligand and the PTZ. Furthermore, the configuration of the phen ligands around the metal center, as well as the CT interaction, give rise to many proton-proton interactions in the spectra. Another complication is that the protons on the ligands and those on the PTZ seem to

have different relaxation times, most likely due to different tumbling rates for the smaller donor and the larger chromophore.

With all of these caveats, what could be gleaned from the spectra was that there is an interaction between the protons of the PTZ and the protons on one of the phenanthrolines. The strongest interactions are between $H_{3,4}$ on the PTZ (those furthest from the N-S axis) and $H_{5,6}$ on the phenanthroline (those on the middle ring)

One can also look at the chemical shift in ligand protons with and without donor present in a 1D NMR experiment. Slightly higher concentrations of complex and less complicated spectra can be generated by the symmetrical $Ru(phen)_3^{2+}$ complex. A 5.3 x 10^{-4} M solution of $Ru(phen)_3(PF_6)_2$ was analyzed on a 400 MHz Varian NMR. Successive additions of solid N-Me-PTZ cause an upfield shift as well as a broadening in the phenanthroline ring protons (see Figure 3.9). This shift is up to 20 Hz for some protons at the solubility limit of the N-Me-PTZ in d_6-acetonitrile (~0.24 M). This is consistent with addition of electron density from a complexed N-Me-PTZ to the ring. The peaks with the largest shifts were those associated with $H_{5,6}$ and $H_{2,9}$ (those *ortho* to the nitrogens). The N-Me-PTZ ring and methyl protons also show an upfield shift and broadening (the full spectra and region expansions can be found in Appendix B). This is consistent with our hypothesis, though at these concentrations, some contribution to the peak shift and broadening in N-Me-PTZ is most likely due to π-π interactions between N-Me-PTZ molecules.

Since the N-Me-PTZ is not constrained by a tether to the chromophore, it is free to associate with the chromophore in any arrangement, the least sterically hindered of which is with the middle ring of the phen ligand. The $H_{3,8}$ protons are the least affected

and $H_{4,7}$ are intermediate between $H_{3,8}$ and $H_{5,6}$. We assume that the proposed CT interaction is with the outer-middle part of the phen ligand and that the large shift of $H_{2,9}$ is due to induction into the ring.

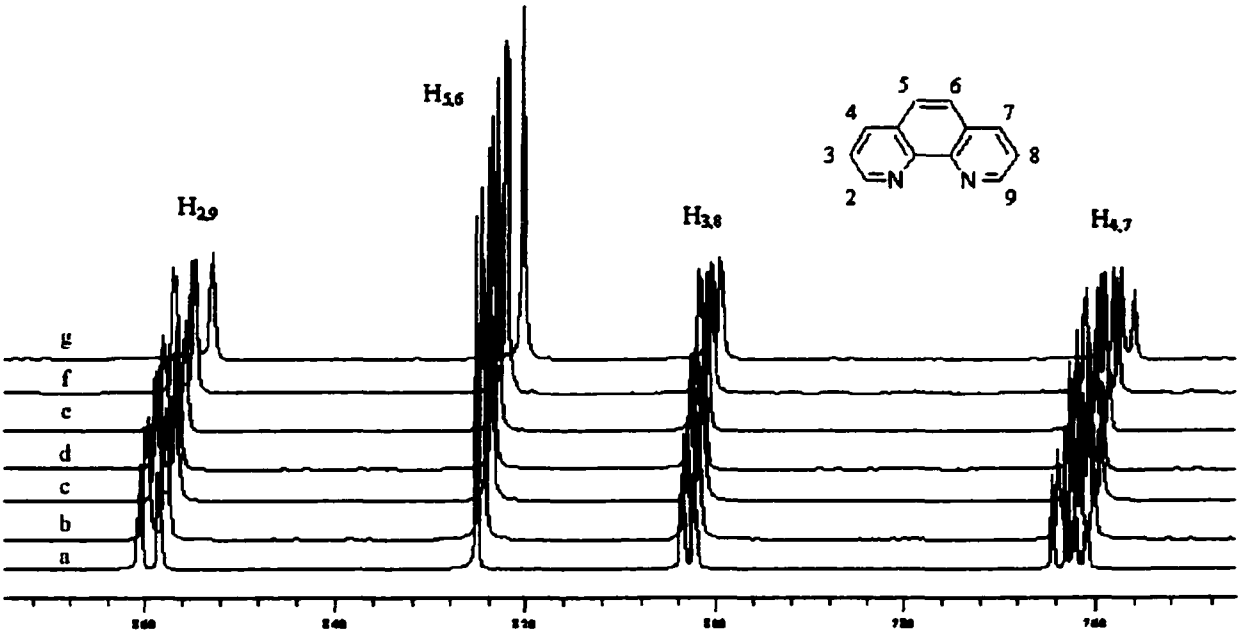

Figure 3.9: NMR spectra of 10^{-4} M $Ru(phen)_3^{2+}$ + x mM N-Me-PTZ in d_6-acetonitrile: a) 0 mM; b) 27 mM; c) 54 mM; d) 74 mM; e) 98 mM; f) 144 mM; g) 239 mM.

The equilibrium constant for the formation of the CT interaction is expected to be temperature dependent, so the most concentrated sample from the above experiment (fig. 3.9; g) was analyzed at various temperatures on a Varian 300 MHz NMR. Figure 3.10 shows an expansion of the phenanthroline ring protons at room temperature and -30°C. (For the full spectra and spectra of some intermediate temperatures, see Appendix B.) There is an obvious upfield shift and a broadening of the peaks. The $H_{5,6}$ protons on the phenanthroline shift an additional 10.5 Hz with the drop in temperature, making the total shift ~30 Hz with the addition of the N-Me-PTZ and the change in temperature.

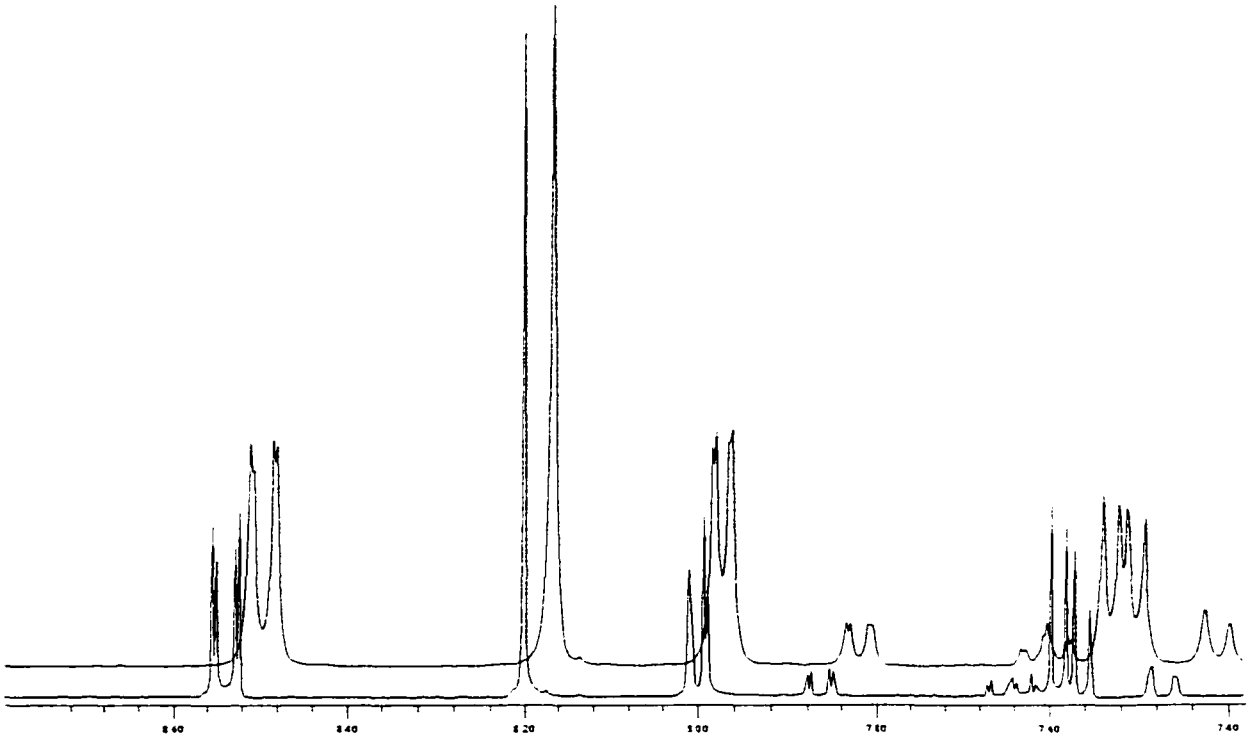

Figure 3.10: NMR spectra of 10^{-4} M $Ru(phen)_3^{2+}$ + 239 mM N-Me-PTZ in d_6-acetonitrile at 25°C (bottom trace) and -30°C (top trace).

Some of the broadening that we see may be due to T_2 relaxation. At -30°C we are not near enough to the freezing point of d_6-acetonitrile (~45°C) for this to normally be a problem, though some contribution to the broadening cannot be ruled out. The ring and methyl protons of the N-Me-PTZ also shift and broaden. As mentioned above, this sample is near the solubility limit of the N-Me-PTZ, and for similar reasons as outlined above, some of the shift and broadening is most likely due to π-stacking between N-Me-PTZ molecules. At these temperatures one might worry about precipitation of N-Me-PTZ. Upon ejection of the sample from the instrument, no precipitation of the N-Me-PTZ or ruthenium complex was observed.

All of the NMR data is consistent with a CT interaction between a PTZ donor and a ligand on the chromophore. Quantitatively, an equilibrium constant for the CT interaction between $Ru(phen)_3^{2+}$ and N-Me-PTZ could have been obtained if the corresponding experiment were performed (i.e. the [N-Me-PTZ] were kept constant and the change in chemical shift with the change in $[Ru(phen)_3^{2+}]$ were measured). However, solubility limits $Ru(phen)_3^{2+}$ and poor signal to noise at lower concentrations of the complex dissuaded us from carrying out these experiments.

Fluorescence Measurements on the CT Interaction

One would expect to observe manifestations of the CT interaction in the rate of electron transfer quenching. As mentioned in Chapter 2, this rate is distance dependent. A CT interaction should decrease the average donor to chromophore distance (assuming the CT interaction is in dynamic equilibrium). More importantly, a CT interaction implies a significant degree of orbital overlap. Adopting a conventional transition-state model for a thermally activated electron transfer, the pre-exponential factor A in equation 6 from Chapter 2 can be expanded:

$$k_{et} = \nu_{eff} \kappa_{el} \Gamma_n e^{-\Delta G^{\ddagger}/RT} \quad (11)$$

where ν_{eff} is the effective frequency for motion along the reaction coordinate, κ_{el} is the electronic transmission factor, and Γ_n is the nuclear tunneling factor.[13] In the non-adiabatic limit

$$\kappa_{el} = 2 \left| H_{if} \right|^2 \pi^{3/2} / h\nu_{eff}[k_b T\lambda]^{1/2} \quad (12)$$

where H_{if} is the transfer integral and λ is the reorganizational energy. Equation 12 also gives us the relationship of λ to the pre-exponential factor which was discussed with equation 7 of Chapter 2.

$$H_{if} \equiv \langle \psi_i \left| H_{el} \right| \psi_f \rangle \equiv \int \psi_i^* H_{el} \psi_f d\tau \quad (13)$$

H_{if} therefore reflects the degree of electronic overlap between the donor and acceptor orbitals in an electron transfer reaction.[14] In the strongly coupled, non-adiabatic limit, H_{if} is large and $\kappa_{el} \approx 1$. As mentioned above, the very nature of the proposed CT interaction, i.e. electron density being shared between the π-system of the donor and the π^* of a ligand, implies an existing electronic overlap between orbitals on the donor and the acceptor (the chromophore).

By making conditions favorable for the CT interaction (i.e. more ring systems on the ligands to provide better docking for the PTZ), we can in theory increase the electronic overlap and/or the equilibrium constant for the formation of the CT interaction.

The original course of action was to make a series of ligands based on the dppz synthesis template and make complexes of the type $Ru(L)_2(47\text{-}PTZ)^{2+}$. The ligands chosen for this series were dmb, phen, dppz, bbppz, dpp, and dpdpz (see Figure 3.3). The PQ (1,10-phenantholine-5,6-quinone) ligand was also considered, but it has electrochemistry making it unsuitable for quenching studies. The dppz, bbppz, dpp and dpdpz ligands seemed to be an ideal choice for our purposes. The dppz, bbppz, and dpp ligands have a node in the LUMO at the phenazine nitrogens.[15] As a consequence, an electron deposited in the π^* level of these ligands (as happens when a photon is absorbed at the MLCT band) does not interact strongly with the whole ligand.[16] So from the metal's point of view, each of the three different phenazine based ligands are essentially equivalent to each other. (Small differences in the emission spectra give the complexes of these ligands slightly different driving forces.)

A drawback which comes into play throughout is the fact that, due to the extended π system, these ligands have a lower π^* energy level than the ligand to which the donor is attached (which is essentially a dmb ligand as far as the Ru^{2+} is concerned). It was mentioned in Chapter 1 that the $Ru(bpy)_3^{2+*}$ electron can be considered to be localized on one ligand at short time scales and delocalized over all three at longer times. By asymmetrically substituting the chromophore with ligands having different π^* levels, one affects the time that the excited electron resides on a particular ligand.[17] Thus the excited electron may be predominantly localized on the ligand with which the PTZ is hopefully interacting with. (Assuming that the CT interaction is weak enough that it does not perturb the energy of the ligand π^* orbital in a way that forces the electron entirely onto the other ligands, or that the PTZ is not folding back and interacting with the ligand to which it is attached.) The proximity of the excited electron to the donor may or may not influence the rate of electron transfer in these systems.

As mentioned in Chapter 1, the purity of the metal complexes were determined by the emission spectra. Not surprisingly, emission spectra are highly sensitive to impurities. Complexes that appear to be clean by TLC and NMR can still have impurities that are evident from the emission spectra. In practice, what is done for a particular complex is a UV/Vis spectra and an emission spectra of a sample are taken so we can relate concentration to the amount of light emitted. The complex is then chromatographed and/or recrystallized and another set of spectra are then taken. By removing any impurities that quench the excited state (which would affect lifetime measurements on which electron transfer rates are based) we should get more emitted light for a given concentration of a complex. Successive iterations of the purification

process are performed until the emitted light becomes constant at a maximum value for each complex.[18] Generally, one would repeat the purification process 6-10 times, though occasionally 20+ times, to obtain sufficiently pure complex.

One might be concerned with complexes having a linked PTZ group that we are removing from our sample desired product (clean complex with a linked donor) and promoting impurities which fluoresce more (i.e. complex with no quencher or on which the quencher has degraded). This is unlikely for several reasons. Complexes with no quencher are fairly easy to separate by chromatography and tend to show up on TLC plates as a very bright fluorescent band. Complexes with degraded PTZ linked to them (degradation occurs even with careful handling) are even easier to separate by chromatography as the degraded complex tends to stick at the origin in the solvent system we employ (see Chapter 1). Furthermore, as mentioned in the chapter endnotes [12], the degradation products of N-alkyl-PTZ's seem to be better quenchers of the excited state than the original donor.

When the ligand (L) was dmb, phen, or dppz, for the $Ru(L)_2(dmb)^{2+}$ and $Ru(L)_2(47\text{-}PTZ)^{2+}$ complexes, the sample eventually reached a satisfactory purity for further study. The rest of the series, bbppz, dpp, and dpdpz, refused to yield clean complexes despite many efforts at removing the impurities. This is mostly due to solubility problems with the larger ligands. While the dppz ligand is soluble in a few solvents, among them ethanol, methanol and DMF; the bbppz and dpp ligand (which are one and two fused rings larger respectively) are only soluble in strong acids. This made characterization of the ligands difficult. We were able to obtain mass spectra of the ligands. When the ligands are attached to ruthenium, the complexes are moderately

soluble in acetonitrile, which allowed us to obtain proton NMR spectra. The reactions to form the complexes give low yields and highly impure products. The complexes tend to streak badly during chromatography and recrystallization does not seem to remove the trace impurities that significantly affect the emission spectra.[19]

As no headway was being made with these ligands, it was deemed prudent to modify the ligand series to include the φ_2-bpy, φ_2-phen, i-biq, and later t-but ligands (see Figure 3.3). The complexes made from these ligands were made in sufficiently pure form for further study. The ligand series now included dmb, phen, dppz, φ_2-bpy, φ_2-phen, and i-biq. Representative emission spectra of the various complexes can be found in Appendix C.

At the time that these complexes were originally prepared there were not in-house capabilities available to do accurate emission lifetime measurements on the timescales that would cover all of our complexes (tens of nanoseconds to several microseconds). We looked at the emission data for the various D- C^{2+} complexes made from our ligand series. Quenching reduces the total amount of emitted light for a given concentration of chromophore. Thus the decrease in the area under the curve between the emission spectrum of the parent (unquenched) complex and the emission spectrum of the D-C^{2+} complex should be proportional to the electron transfer rate. We wanted to see if these decreases correlated with the increase in the size of the π-system of the ligand. As the emission spectra are used to determine final purity of the metal complexes, this seemed to be a sensible check on our hypothesis. The data from these experiments is in Table 3.1.

Table 3.1: Percent Emitted Light Between $Ru(L)_2(dmb)^{2+}$ and $Ru(L)_2(47\text{-}PTZ)^{2+}$ for a Series of Ligands (L).

Ligand	PTZ_{em}/dmb_{em}
dmb	93%
phen	33%
i-biq	91%
dppz	33%
φ_2-bpy	19%
φ_2-phen	18%

The first thing that stands out from the table is that the i-biq ligand does not follow the general trend. This could be the result of one or more reasons. When the heteroleptic $Ru(i\text{-}biq)_3^{2+}$ complex is made, it has a slightly different shape to its MLCT band and its emission spectrum is significantly blue shifted and of different shape when compared to similar complexes composed of other ligands (see Figure 3.11 and Appendix C).

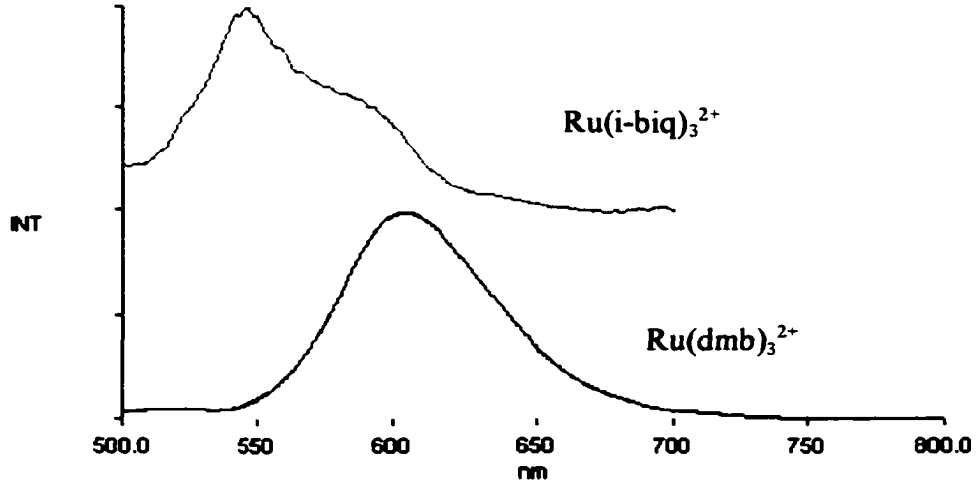

Figure 3.11: Emission spectra of $Ru(i\text{-}biq)_3^{2+}$ and $Ru(dmb)_3^{2+}$.

This is due to a high π^* energy level on the ligand.[20] When the $Ru(i\text{-}biq)_2(L)^{2+}$ complex is made, it has been shown that the electron is largely localized on the non- i-biq ligand and that the emission also comes solely from that ligand.[21] It may be that the high π^* energy level impedes or diminishes the ability of the PTZ to form a CT interaction in the linked complex. The excited electron, essentially localized on bipyridine to which the PTZ is attached, may prevent the PTZ from folding back on itself as mentioned above, or it may impede the electron transfer mechanism from the donor to the chromophore.

The other five ligands are grouped a bit. Qualitatively, it appears that increasing the π-system of the remote ligands increases the amount of quenching by the 47-PTZ donor. Unfortunately, the fluorimetry data did not allow us to obtain electron transfer rates. As mentioned in chapter endnote [18], even with signal averaging of many scans, the reproducibility of the emission spectra was only ±5%. Include deviations in the UV/Vis spectra (used to determine the concentration of a sample) and the error in the presented data is substantial (~ ±7%).

The other bit of information that is obtained from the emission spectra are the emission onset energies (E_{em} equations 4a-b; Chapter1). These combined with electrochemical data give the driving force for the reductive quenching of the ^{3}MLCT state of the complex by an N-alkyl PTZ moiety. The data is listed is Table 3.2 in the first column. These values are, effectively, the same whether the quenching process is intramolecular (i.e., covalently linked PTZ) or bimolecular, regardless of the nature of the alkyl chain. Based on these values, the quenching in each case is very modestly energetically favorable; and the range in driving forces is narrow (~200 mV).

Table 3.2: Driving Forces, Emission Rate Constants and Electron Transfer Rate Constants for Donor/Chromophore Complexes

Complex	Driving Force (V)[a]	k_{em} (1/s)[b]	k_q intramolecular (1/s)[b]	k_q bimolecular Me-PTZ (1/Ms)[b,d]	k_q bimolecular np-PTZ (1/Ms)[b,e]
$Ru(t\text{-}but)_3$		$1.09\pm0.01 \times 10^6$		$2.6\pm0.1 \times 10^5$	$6.6\pm0.1 \times 10^5$
$Ru(t\text{-}but)_2(47\text{-}PTZ)^{2+}$	-0.10		$2.41\pm0.06 \times 10^6$		
$Ru(dmb)_3^{2+}$		$1.16\pm0.01 \times 10^6$		$3.5\pm0.1 \times 10^5$	$6.6\pm0.1 \times 10^5$
$Ru(dmb)_2(47\text{-}PTZ)^{2+}$	-0.11		$2.53\pm0.04 \times 10^6$		
$Ru(phen)_2(dmb)^{2+}$		$1.15\pm0.01 \times 10^6$		$5.34\pm0.01 \times 10^6$	$1.60\pm0.01 \times 10^6$
$Ru(phen)_2(47\text{-}PTZ)^{2+}$	-0.32		$1.11\pm0.05 \times 10^7$		
$Ru(dppz)_2(dmb)^{2+}$		$1.17\pm0.01 \times 10^6$		$1.150\pm0.001 \times 10^7$	$1.17\pm0.01 \times 10^6$
$Ru(dppz)_2(47\text{-}PTZ)^{2+}$	-0.19		$1.6\pm0.1 \times 10^6$		
$Ru(\varphi\text{-}bpy)_2(dmb)^{2+}$		$7.1\pm0.1 \times 10^5$		$4.32\pm0.01 \times 10^6$	$1.21\pm0.01 \times 10^6$
$Ru(\varphi\text{-}bpy)_2(47\text{-}PTZ)^{2+}$	-0.20		$1.02\pm0.05 \times 10^7$		
$Ru(\varphi\text{-}phen)_2(dmb)^{2+}$		$2.2\pm0.3 \times 10^5$		$1.89\pm0.04 \times 10^6$	$2.14\pm0.04 \times 10^6$
$Ru(\varphi\text{-}phen)_2(47\text{-}PTZ)^{2+}$	-0.26		$3.7\pm0.3 \times 10^7$ [c]		

[a] Calculated from eqs. 4a-b, Chapter 1.

[b] Data collected on Nd:YAG pumped dye laser (see Instrumentation, Chapter 1) except where noted. Experimental conditions are outlined in the respective section.

[c] Data collected on Ar^+ pumped Ti sapphire laser (see Instrumentation, Chapter 1).

[d] 2.9 mM N-Me-PTZ

[e] 3.3 mM np-PTZ

Lifetime Measurements of the Linked Complexes

The samples were prepared as outlined in Chapter 1. The samples were made to have an absorbance of approximately 0.1 at the maximum of the MLCT band. This gives a concentration of $\sim 10^{-6}$ M of the complex. Since we are primarily interested in the shape of the decay of the emission curve, the absolute concentration of the complexes is not critical for these experiments. Initially we started collecting data on an argon ion pumped mode-locked titanium sapphire laser system. As mentioned in the Instrumentation section of Chapter 1, this system is optimized for short lifetimes. By adding in all the electronic delays and fifty meters of coaxial cable, we were able to reach 120 ps/channel or about 160 ns full scale for the time window that we could observe. This small time window meant for complexes with very long lifetimes, such as $Ru(\varphi_2\text{-phen})_2(dmb)^{2+}$ which has an emission lifetime of ~4 μs, only a fraction of the lifetime is represented by the data. As a consequence, only the data for the $Ru(\varphi_2\text{-phen})_2(47\text{-PTZ})^{2+}$ complex collected on this instrument was used for Table 3.2. It's emission lifetime (28 ns) is on the same order as the pulse width (~8 ns) of the Nd:YAG pumped dye laser system (see Instrumentation; Chapter1) that was used to collect the rest of the data. For complexes and bimolecular quenching systems in which the chromophore exhibited an emission lifetime in the 100-500 ns range there was good correlation between the data obtained from both instruments (±5-10%), with the error increasing with lengthening lifetimes. The fits for the data were typically much better for the Nd:YAG system (r^2= 0.999-0.9999+ vs. 0.97-0.99+). Typical lifetime data from the Nd:YAG system is shown in Figure 3.12.

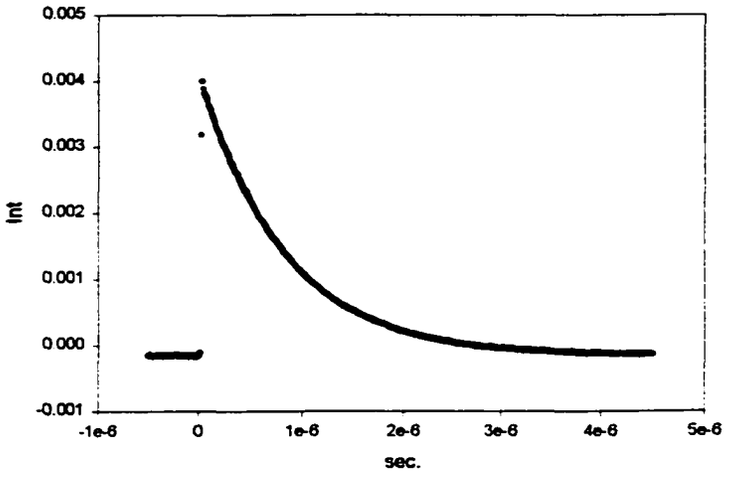

Figure 3.12: Emission lifetime data from $Ru(phen)_2(dmb)^{2+}$ in acetonitrile.

Table 3.2 is arranged with the complexes with the most sterically hindered ligands for the CT interaction being on top, while those with the most rings are on the bottom. The third column gives the intramolecular quenching rates for the various complexes. The range of rates covered is fairly narrow, slightly more than an order of magnitude. For the most part, the quenching rates followed as predicted. Ligands that promote the CT interaction increased the quenching rate of the D-C complexes. The notable exception of the dppz ligand will be discussed below.

To get an idea of the effect of changes in the driving force on the electron transfer rate, values of –0.100, -0.200, and –0.300 eV (roughly corresponding to the driving forces in Table 3.2) were substituted in for ΔG in equation 7 of Chapter 2. The value then obtained for $\Delta G^{\ddagger}$ was substituted into equation 6 of Chapter 2. These equations are reproduced below.

$$k_{et} = A\, e^{-\Delta G^{\ddagger}/RT} \qquad (6)$$

$$\Delta G^{\ddagger} = \lambda/4\,(1 + \Delta G/\lambda)^2 \qquad (7)$$

For this exercise, we need to make the all inclusive assumption that the change in driving force is the only thing affecting the electron transfer rate; i.e. the reorganizational energy, λ, and the pre-exponential factor, A, are the same for all complexes, and there is no CT interaction. Again, as we did in Chapter 2, we substitute in a value of λ= 0.800 eV. For the input values of ΔG = –0.100; -0.200; and –0.300 eV, we get $k_q = 2.6\text{x}10^{-3}\cdot A$; $1.3\text{x}10^{-2}\cdot A$; and $4.8\text{x}10^{-2}\cdot A$ respectively. In theory, with everything else being equal, we should see a five-fold increase in the electron transfer rate on increasing the driving force from 100 to 200 meV and a nearly four-fold additional increase when going from 200 to 300 meV.

The data in column three of Table 3.2 cannot be explained in terms of changing driving force alone. The trends in the data, bypassing the dppz ligand for the moment, seem to be a combination of the changes in the driving force coupled with changes in the CT interaction. This would explain, for example, why $Ru(\varphi_2\text{-phen})_2(47\text{-PTZ})^{2+}$, which has ~60meV less driving force, has a four-fold faster quenching rate than $Ru(phen)_2(47\text{-PTZ})^{2+}$.

Bimolecular Quenching Experiments

From the $Zn(L)_3^{2+}$ experiments and NMR experiments, we had evidence that the PTZ did not need to be linked to the chromophore for a CT interaction to take place. To allow comparisons with the linked donors, N-Me-PTZ was used in one set of bimolecular quenching experiments, and N-neopentylphenothiazine (np-PTZ) was used in another. The neopentyl group could sterically hinder the CT formation, though it is not impossible

to imagine configurations in which the CT complex could form despite the neopentyl group.

To make comparisons meaningful, all chromophore concentrations were prepared to have an absorbance of approximately 0.100 (±5%) at the maximum of the MLCT band. PTZ concentrations were kept at ~$3x10^{-3}$ M for all experiments.[22] With a 1 mm cell, this puts the chromophore concentration in the 10^{-6} M range. Only a fraction of the chromophores are excited during a given laser pulse. This means [PTZ] » [Ru^{2+*}].

Column four in Table 3.2 lists the pseudo-first order rate constants for the bimolecular quenching with N-Me-PTZ. Column five list the pseudo-first order rate constants for the bimolecular quenching with np-PTZ. The N-Me-PTZ's rates cover nearly two orders of magnitude while the np-PTZ's rates span only a half an order.

Taken by itself, the data in column four follow the predicted trend. Ligands that promote the CT interaction have a faster bimolecular quenching rate. As with the linked complexes, the trends in the data most likely are a combination of changes in the driving force coupled with changes in the CT interaction. The φ_2-phen appears to be an anomaly in the trend. There is a drop off in the electron transfer rate of nearly an order of magnitude from the dppz ligand. One might suspect that it is the dppz ligand that is out of line with the rest of the ligands, as it was for the linked complexes, and this may well be true. Even disregarding the dppz ligand in the trend, the φ_2-phen ligand is still out of line, having a quenching rate of half that of the phen and φ_2-bpy ligands. Based on the rate for the more sterically hindered np-PTZ, it would seem that the N-Me-PTZ is equally hindered in forming a CT interaction with the φ_2-phen ligand.

The rates for the np-PTZ nearly parallel the driving forces, implying that the driving force is the dominant factor in the difference in rates. It is interesting to note that the rates for the two complexes whose ligands have alkyl groups doubled when the donor was switched from Me-PTZ to np-PTZ. Possibly the alkyl group on the np-PTZ and the ligand are interacting with each other in the polar acetonitrile solution. This would have a similar effect as the CT interaction, though with different coupling between the donor and the chromophore.

There are several possibilities for why the dppz ligand's rates don't follow the trends. As mentioned above, the dppz ligand has a node in the LUMO at the phenazine nitrogens.[23] For the linked complex, a seven carbon tether may constrain the donor to a CT interaction that has poor electronic overlap with the ligand. The N-Me-PTZ, free to move in relation to the chromophore, may form a CT interaction with good electronic overlap to the chromophore, while the np-PTZ is sterically hindered. Another possibility is residual water as a contaminant. The dppz ligand makes complexes whose excited state is quenched by water. In fact the $Ru(bpy)_2(dppz)^{2+}$ complex shows no room temperature luminescence in aqueous solutions.[24] Prior to use all samples were chromatographed and/or recrystallized, both procedures put the complex in contact with water. They were then dried at room temperature, under vacuum for a minimum of 4, but typically for 12+ hours. The acetonitrile (Fischer Gold Label; $\leq 0.01\%$ H_2O) was kept under N_2 and sealed from atmospheric moisture. Other than this, no other measures were used to keep water from the complex. On the other hand, if residual water was causing an order of magnitude change in observed electron transfer rates, one would expect to get highly variable results for each of the three experiments (linked, bimolecular with Me-

PTZ and np-PTZ). This is not the case. Furthermore, as mentioned above, we were able to get consistent emission spectra for the dppz complexes.

In an effort to better understand the data in Table 3.2, Stern-Volmer plots were generated for the quenching of $[Ru(phen)_2(DMB)]^{2+*}$ by N-Me-PTZ and by np-PTZ and the quenching of $[Ru(4,4'\text{-t-butyl-}2,2'\text{-bipyridine})_3]^{2+*}$ by N-Me-PTZ. These data are presented in Figure 3.13 where the Y-axis is the pseudo-first-order quenching rate and the X-axis is the concentration of the respective PTZ quencher. All the data show normal Stern-Volmer behavior, extrapolated through zero, the slope is equal to the quenching rate constant. The data clearly show that as the CT interaction is hindered by bulky alkyl groups, the rate constants drop off considerably.

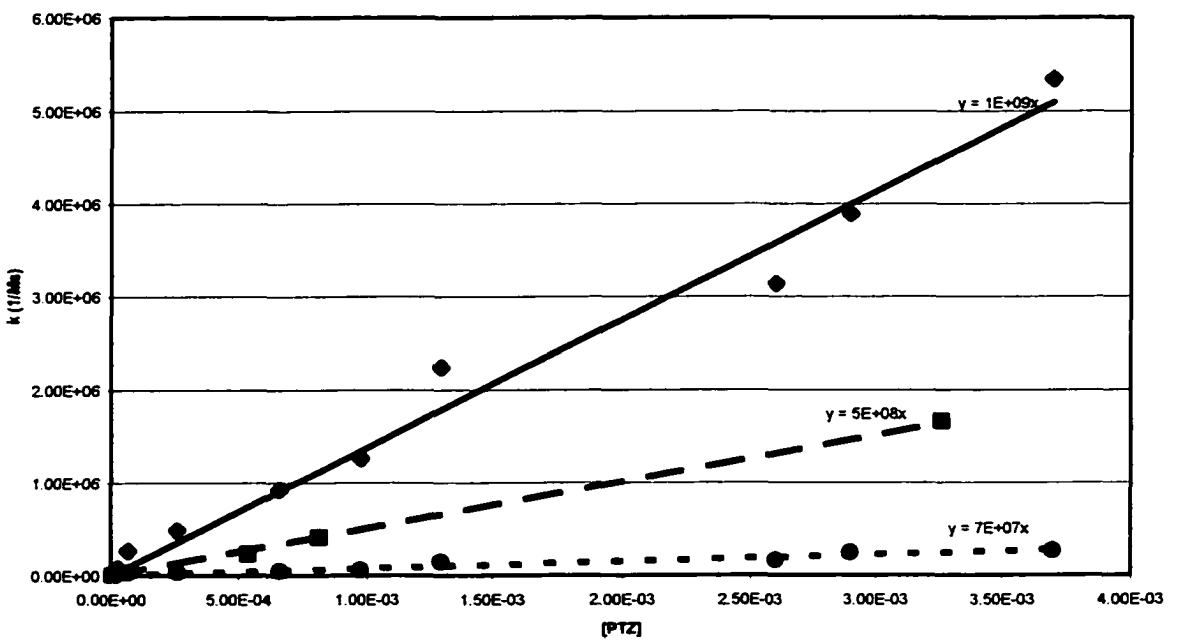

Figure 3.13: Pseudo-first order quenching rates versus concentration for (♦) $Ru(phen)_2(dmb)^{2+}$ + N-Me-PTZ; (■) $Ru(phen)_2(dmb)^{2+}$ + np-PTZ; (●)$Ru(t\text{-but})_2(dmb)^{2+}$ + N-Me-PTZ in acetonitrile.

For the experiments represented by the data in Figure 3.13, all the PTZ concentrations were kept below 5 mM to cover the range of concentrations that we had been working at. This also avoids solubility problems with the PTZ's in acetonitrile. Higher concentrations of N-Me-PTZ can easily reached in 1,2-dichloroethane (DCE). While many factors change when switching solvents in these systems (i.e. solvent polarity, unquenched emission lifetime, pseudo-first order rates, etc.), work done by J. Weber in our group has shown that many of the experiments outlined in Chapter 4 that were performed in acetonitrile give similar results when performed in DCE. In particular, the data shown in Figure 4.7, when compared to the analogous data in DCE, show a similar plateau at higher concentrations and can be fit to the same equation presented with that figure.[25] In addition, the problems encountered with the data at higher concentrations in acetonitrile (noisy, irreproducible data), were non-existent in DCE.

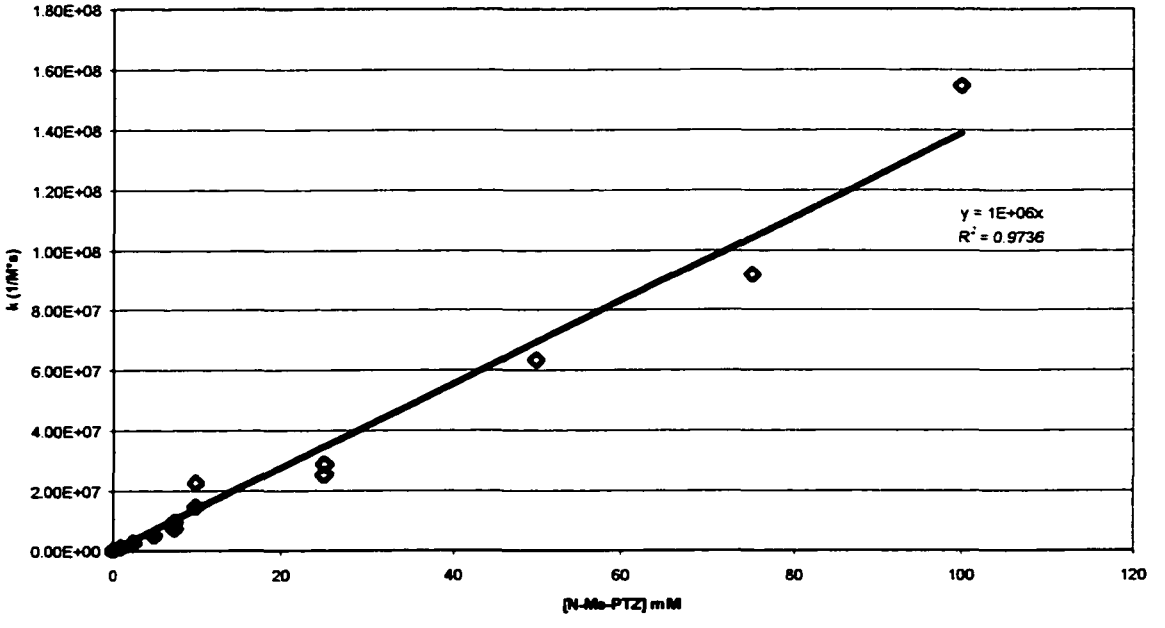

Figure 3.14: Pseudo-first order quenching rates versus concentration for $Ru(phen)_2(dmb)^{2+}$ + N-Me-PTZ in 1,2-DCE. Data from (♦) Nd:YAG/dye laser and (◊) Ti-sapphire laser.

Figure 3.14 shows a Stern-Volmer plot for $Ru(phen)_2(dmb)^{2+}$ + N-Me-PTZ in DCE. Because the emission lifetimes for the quenched chromophore span such a large range(~5-500 ns), it was necessary to collect data on both instruments that were described in Chapter 1. The solid data points were collected on the Nd:YAG/dye laser system (having less quenching, gives longer emission lifetimes) and the hollow points were collected on the Ti-sapphire system. The plot shows normal Stern-Volmer behavior even at high concentrations. Based on these results and the results obtained by J. Weber, we have no reason to believe that the bimolecular quenching in acetonitrile deviates from normal Stern-Volmer behavior at higher concentrations. The first order quenching rate obtained from the slope is three orders of magnitude slower in DCE than acetonitrile.

Conclusions

The NMR and spectroscopy experiments show fairly conclusively that a weak ground state CT interaction exists between phenothiazine type donors and the ligands on $Ru(bpy)_3^{2+}$ chromophores. Efforts to vary this interaction through ligand and donor modifications and study the effects on $D\text{-}C^{2+}$ diads gave mixed results. This appears to be a result of several competing factors (the CT interaction, driving force and possibly solvent effects) that all affect the observable data, i.e. the emission lifetimes.

There is some correlation between the early fluorescence data and the emission lifetime data. In general, sterically hindered ligands like dmb and t-but had slower quenching rates (had less overall quenching of the chromophore) than ligands with large π systems (i.e. φ_2-phen). If one ratios the emission lifetimes of the $D\text{-}C^{2+}$ linked

complexes and the parent chromophores, one should obtain a ratio that is proportional to reduction of emitted light in each system. When we compare the numbers from the fluorescence data (Table 3.1) and the emission lifetime data (Table 3.2, $[1/k_q+1/k_{em}]/[1/k_{em}]$), we find that there is a high correlation in the numbers. The ligands follow the exact same trend, but with the fluorescence data being ~3x the value obtained from the emission lifetime. The errors associated with the reproducibility of fluorescence data[18] make it suspect, and the large difference in numbers when compared to the emission lifetime data raises more doubts about the data. The dppz ligand is the only anomaly, its emission lifetime numbers being slightly larger than the ratio obtained in the fluorescence experiments. If we compare the data for the bimolecular quenching with N-Me-PTZ (Table 3.2) to the fluorescence data, we find no direct correlation in the data. This may be due to a difference in the quenching in linked complexes versus bi-molecular quenching. Such a difference might shed light on the opposing solvent dependencies seen by Larson and Weber (*vide supra*).

What the CT interaction means in terms of the $D\text{-}C^{2+}\text{-}A^{2+}$ complexes is the subject of Chapter 4. The $D\text{-}C^{2+}\text{-}A^{2+}$ complexes have very high quantum yields to the charge-separated state, around 80%.[26] It was mentioned in Chapter 1 that process 2 (see Figure 1.3) competes with the back electron transfer process, 1', in these $D\text{-}C^{2+}\text{-}A^{2+}$ complexes. Process 1' has a lower limit for its rate of about $(80\ ps)^{-1}$.[27,28] A CT interaction with the ground state, or a strong interaction with the excited state or charge-transfer state would provide an explanation of these high quantum yields.

ENDNOTES

[1] Larson, S.L. "Charge Transfer in Linked Donor-Chromophore-Acceptor Systems"; Ph.D. Thesis, Colorado State University, **1994**.

[2] Marcus, R.A. *J. Chem. Phys.*, **1956**, *24*, 966.

[3] *Figure reproduced from*: Larson, S.L. "Charge Transfer in Linked Donor-Chromophore-Acceptor Systems"; Ph.D. Thesis, Colorado State University, **1994**, p. 101.

[4] Unpublished results.

[5] Amouyal, E.; Homsi, A.; Chambron, J-C.; Sauvage, J-P. *J. Chem. Soc., Dalton Trans.*, **1990**, 1841.

[6] Koft, E.; Case, F.H. *J. Chem. Soc., Dalton Trans.*, **1962**, *27*, 865.

[7] The literature preparation includes a liquid/liquid extraction into diethyl ether at this point to separate the compound from precipitated SnO_2, a step accidently omitted by the author. The yield is based on the organic components of the precipitate.

[8] Dickeson, J.E.; Summers, L.A. *Aust. J. Chem.*, **1970**, *23*, 1023.

[9] Knoevenagel, E. *J. Prakt. Chem.*, **1914**, *89*, 25.

[10] Tarch, P.T.; Chu, V.P.; Whitten, D. *Anal. Biochem.*, **1987**, *165*, 230.

[11] Rosevear, P.E.; Sasse, W.H.F. *J. Heterocycl. Chem.*, **1971**, *8*, 483.

[12] Another possibility in this case is that the N-Me-PTZ is degrading in solution. It was noticed that N-Me-PTZ tends to degrade in oxygenated solutions of acetonitrile at room temperature. Solutions could be kept for three or four days at 0°C, but after 24 hours at room temperature they show evidence of degradation. Furthermore, the degradation products experimentally seem to be better quenchers of the Ru^{2+*} than the N-Me-PTZ. This caused some erratic results when we first attempted to look at N-Me-PTZ concentrations in bi-molecular quenching experiments. Especially since low N-Me-PTZ concentrations were made from higher N-Me-PTZ concentrations that had sat in solution for a day or two.

[13] Newton, M.D. *Chem. Rev.*, **1991**, *91*, 767.

[14] For an overview of the role of the transfer integral in electron-transfer kinetics see ref. [12].

[15] Pan, D.; Phillips, D.L. *J. Phys. Chem. A*, **1999**, *103*, 4737. The dpdpz ligand may also have this node.

[16] Bolger, J.; Gourdon, A; Ishow, E.; Lannay, J-P. *Inorg. Chem.*, **1996**, *35*, 2937.

[17] Turro, C.; Bossman, S.H.; Leroi, G.E.; Barton, J.K.; Turro, N.J. *Inorg. Chem.*, **1994**, *33*, 1344.

[18] Due to instrument limitations, the reproducibility for a single sample was ± 5%.

[19] Similar problems were encountered by other researchers working with a tetradentate ligand made in a similar manner to the dppz type ligands. *See* Bolger, J.; Gourdon, A; Ishow, E.; Lannay, J-P. *Inorg. Chem.*, **1996**, *35*, 2937.

[20] Barigelletti, F.; Juris, A.; Balzani, V.; Belser, P.; von Zelewsky, A. *Inorg. Chem.*, **1983**, *22*, 3335.

[21] Juris, A.; Barigelletti, F.; Balzani, V.; Belser, P.; von Zelewsky, A. *Inorg. Chem.*, **1985**, *24*, 202.

[22] The exact concentrations were 2.92 mM N-Me-PTZ and 3.26 mM np-PTZ.

[23] Pan, D.; Phillips, D.L. *J. Phys. Chem. A*, **1999**, *103*, 4737. The dpdpz ligand may also have this node.

[24] Hartshorn, R.M.; Barton, J.K. *J. Amer. Chem. Soc.*, **1992**, *114*, 5919.

[25] Weber, J. *Unpuplished results.*

[26] Klumpp, T.; Linsenmann, M.; Larson, S.L.; Limoges, B.R.; Bürssner, D.; Krissinel, E.; Elliott, C.M.; Steiner, U.E. *J. Amer. Chem. Soc.*, **1999**, *121*, 1076.

[27] Cooley, L.F.; Larson, S.; Elliott, C.M. *J. Phys. Chem.*, **1991**, *95*, 10694.

[28] Cooley, L.F., Headford, C.E.L.; Elliott, C.M., Kelley, D.F. *J. Amer. Chem. Soc.*, **1988**, *110*, 6673.

Chapter 4:

Charge-Transfer Interactions Between C^{2+}-A^{2+} Diads and N-Methylphenothiazine

Background and Motivation:

As mentioned in Chapter 1, while studying the magnetic field effects on D-C^{2+}-A^{2+} triads,[1] we had occasion to recalculate the quantum yield of the charge separated state (φ_{cs}) which had previously been reported for $Ru(44\text{-}PTZ)_2(423\text{-}DQ)^{4+}$ as $\varphi_{cs} = 0.26 \pm 0.04$.[2] Data obtained during the MFE experiments showed quantum yields of 0.86 ± 0.08.[3]

It was also mentioned in Chapter 1 that process 2 (see Figure 4.1) competes with the back electron transfer process, -1, for the CT state (not to be confused with the CT interaction). Process -1 has an lower limit for its rate of about 1.25×10^{10} s^{-1}.[4] The forward process, 1, occurs with near unit efficiency.[5] The quantum yield from the MLCT state can therefore be expressed in terms of the rate constants for the two competing pathways from the CT state:

$$\varphi_{cs} = k_2 / (k_{-1} + k_2) \qquad (14).$$

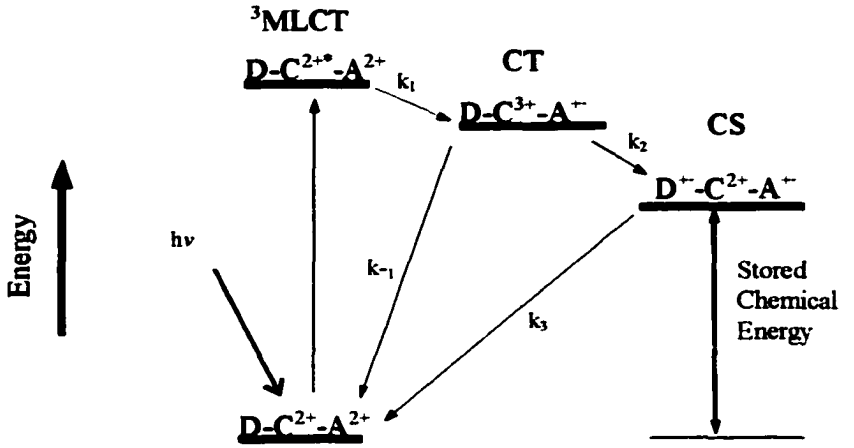

Figure 4.1: Energy diagram showing electron transfer processes in $D\text{-}C^{2+}\text{-}A^{2+}$ triads.

Rearranging and solving for k_2 gives us:

$$k_2 = \varphi_{cs}k_1 / (1 - \varphi_{cs}) \qquad (15).$$

Putting in our values for k_1 and φ_{cs} gives us a lower value of approximately 8×10^{10} s^{-1} for k_2. This is an order of magnitude faster than our fastest intramolecular quenching rates for $D\text{-}C^{2+}$ complexes presented in Chapter 3. As was mentioned in the background section to that Chapter, there are differences in driving force and environment between the PTZ $\rightarrow$ Ru^{2+*} electron transfer and the PTZ $\rightarrow$ Ru^{3+} electron transfer. These differences, especially in the light of the proposed CT interaction, are most likely large enough to account for increased rate of electron transfer from the PTZ donor. The calculated rate is therefore not unreasonable in its magnitude based on the work outlined in Chapter 3.

In this complex the donor is linked to the chromophore by an alkyl chain. We proposed to investigate similar systems to the linked $D\text{-}C^{2+}\text{-}A^{2+}$ triads where we have a linked $C^{2+}\text{-}A^{2+}$ diad and unlinked donor (denoted hereafter as $D + C^{2+}\text{-}A^{2+}$). In theory,

this turns process 2 leading to the CS state into a simple bimolecular process, which has a diffusion limiting rate which is determined by the viscosity of the solvent. The reaction is pseudo-first order for our system because $[D]>[C^{2+}\text{-}A^{2+}]>>[C^{3+}\text{-}A^{+\bullet}]$. By looking at the concentration dependence of the donor on the formation of the CS state, we hoped to find evidence of the CT interaction playing a crucial role in this step.

In a bimolecular system like we proposed to study, one can also think of changing the diffusion limited rate by changing the viscosity of the solution. In practice we achieved this by dissolving polymers in our solvent to change the viscosity by several orders of magnitude and monitoring the affect on the formation of the CS state.

Materials: N-Me-PTZ was prepared as above. To simplify synthesis of the $C^{2+}\text{-}A^{2+}$ complex, a methyl-viologen type acceptor ligand was employed in place of the diquats that had been used previously. The $C^{2+}\text{-}A^{2+}$ complex used throughout the remainder of this chapter is shown in Figure 4.2. The bpy-MV^{2+} ligand is considerably easier to synthesize than the diquat ligands, so we were able to obtain larger quantities of the $C^{2+}\text{-}A^{2+}$ complex in less time than if we had stayed with the diquat acceptors.

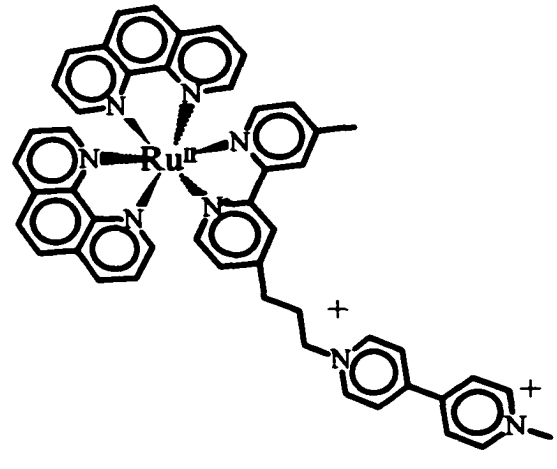

Figure 4.2: $Ru(phen)_2(bpy\text{-}MV)^{4+}$

This complex was prepared in sufficient purity and donated by J. Weber following the method of Mallouk, *et al.*[6] The back electron transfer rate for the Mallouk complex (corresponding to k_t in Figure 4.1) is 6.5×10^9 s^{-1}.[6] This is very close to the lower-limit value calculated for the diquat ligand and we made the blanket assumption that the bpy-MV^{2+} ligand behaves in an identical manner to the diquat ligand (i.e. the initial electron transfer is from the excited chromophore to the acceptor, there is no build up of the CT state, etc.). Some of these assumptions have been confirmed experimentally by J. Weber.

Poly(methylmethacrylate) (avg. M_w= 996,000) and poly(styrene) (avg. M_w= 280,000) were obtained from Aldrich and used without further purification.

Methods: The transient absorbance experiments (see Chapter 1 for experimental conditions and set-up) and data work-up were done in collaboration with Dr. Valerie MacKenzie.

The formation of the CS state was monitored by transient absorbance of the reduced viologen at 397 nm. This is a wavelength where neither the ground state viologen, the ground state N-Me-PTZ nor the oxidized N-Me-PTZ has much absorbance (see Figure 1.8). There is some absorbance by the chromophore at this wavelength, but the change in absorbance at this wavelength due to photo-bleaching of the chromophore is small. Moreover, after the initial quenching (which is fast on the time scale of the experiment) the change in absorbance due to photo-bleaching should be zero.

To obtain data on the relative amounts of the CS state being formed, we measure the initial change in absorbance ($\Delta A_{t=0}$) at 397 nm (see Figure 4.3 for a representative spectra). We can use this method if several assumptions hold true. One is that all the measured change is due to the reduced viologen in the CS state. We assume this to be true because, as mentioned in Chapter 1, with C^{2+}-A^{2+} complexes alone, we never see any change in the absorbance at 397 nm due to the reduced viologen on the timescale of our experiments. This means that we never observe the reduced viologen from the CT state in these experiments (which is how we know that k_{-1} is faster than k_1 in the above energy diagram).

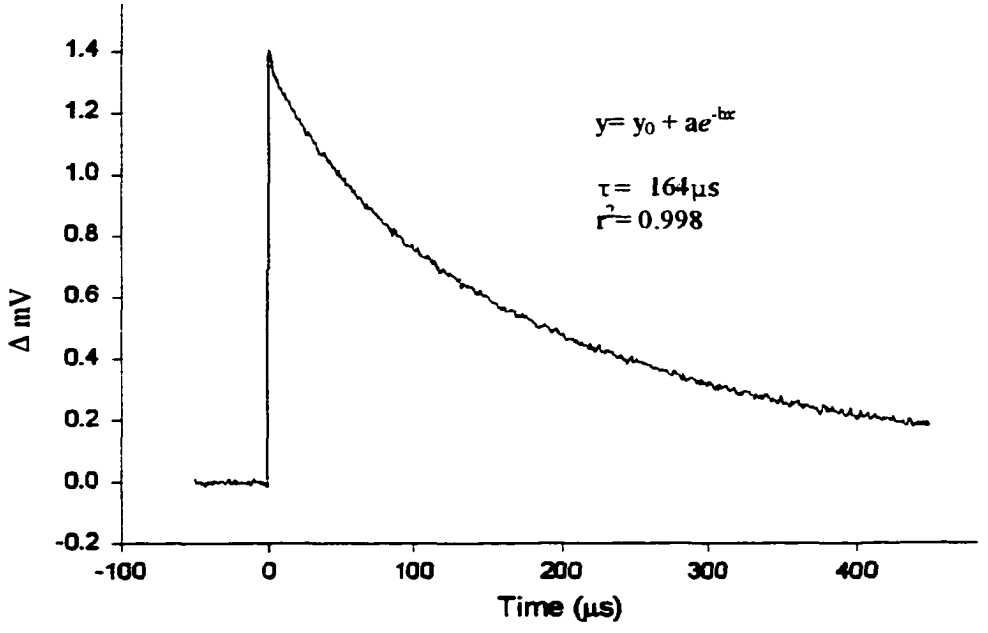

Figure 4.3: Transient absorbance at 397 nm of 10^{-5} M $Ru(phen)_2(bpy\text{-}MV)^{4+}$ and 125 mM N-Me-PTZ in acetonitrile pumped with 450 nm light.

Another assumption is that all the available CT state is depleted by the two competing processes within the rise time of our experiment (the time elapsed between the initial pulse and the maximum signal). The rise time in our experiments was typically less than 4 ns. This means $k_{-1} + (k_2[\text{N-Me-PTZ}]) >> (4\text{ ns})^{-1}$. As the number given above for k_{-1} for Mallouk's complex suggests, this relation is most likely correct. A third assumption is that the spin forbidden back electron transfer from the CS state to the ground state is slower than the rise time (i.e. $k_{3,obs} < (4\text{ ns})^{-1}$). The back electron transfer in these systems is sensitive to many parameters. The lifetimes obtained by fitting the decay in the transient absorbance spectra give us k_3 for a given sample. Since

$$\frac{\partial[CS]}{\partial t} = -k_3[CS][D^+] \qquad \textbf{(16)}$$

the lifetime of the CS state is dependant on the concentrations of the oxidized donor and the CS state complex (ground state chromophore-reduced acceptor complex) which are both dependant on initial C^{2+}-A^{2+} and D concentrations, photo intensity of the pump beam and cross-sectional overlap of the pump and probe beams. In all cases however, the experimental lifetime is on the order of microseconds, so reduction of the initial concentration of the CS state by efficient recombination to the ground state is not a major concern.

The measured parameter, $\Delta A_{t=0}$, is also sensitive to the initial C^{2+}-A^{2+} and D concentrations, intensity of the pump beam and cross-sectional overlap of the pump and probe beams. Since one of the relationships that we wish to examine is how $\Delta A_{t=0}$ varies with [D], it is crucial that all the other variables remain constant. To minimize error, all the data for each sample for a particular experiment was collected on the same day. Once data for the initial samples were collected, the PMT voltage, slits, and lens alignment

were all left untouched for the remainder of the samples. The Nd:YAG laser was left on and the beam was blocked before entering the dye laser (see Figure 1.7) between samples.

The samples were prepared by making the appropriate concentration of N-Me-PTZ in acetonitrile and adding approximately 4 mL of this solution to a cell. A few microliters of a concentrated solution of the C^{2+}-A^{2+} complex in acetonitrile was added to the cell. More of each solution was added until the UV/Vis absorbance at 450 nm was $Abs._{450}= 0.200 \pm 0.005$. The extra absorbance at this wavelength due to the CT interaction was not factored in as its contribution to the overall absorbance is small and its impact on the concentration of the C^{2+}-A^{2+} complex is within the instrumental error of the instrumentation. The dilution of the N-Me-PTZ by the C^{2+}-A^{2+} complex solution is negligible and was not accounted for in the calculations. The samples were then subjected to the freeze-pump-thaw (f-p-t) cycles as outlined in Chapter 1. Sample preparation was done under low light conditions until the f-p-t cycle at which point no further care was taken to keep them from ambient light. Due to a limited number of the appropriate sized degassable side-arm cells used for the samples, we collected data on about three samples per hour, most of the time spent in sample preparation involving the f-p-t cycles.

Typically ten data sets of 1000 scans were taken for each sample. The sample was removed from the cell holder and shaken lightly to thoroughly mix the contents between each data set collected. All ten data sets were collected within 5-10 minutes.

Results: Figure 4.4 shows a typical result for a single sample. Shown are the first, last and average of 10 data sets. All three curves have been normalized at the maximum pmt voltage. There is clearly a change in the decay of the curves between the first and last data sets collected. There is also a slight change in $\Delta A_{t=0}$, the quantity that we are most concerned with. This was clearly due to degradation of the sample.

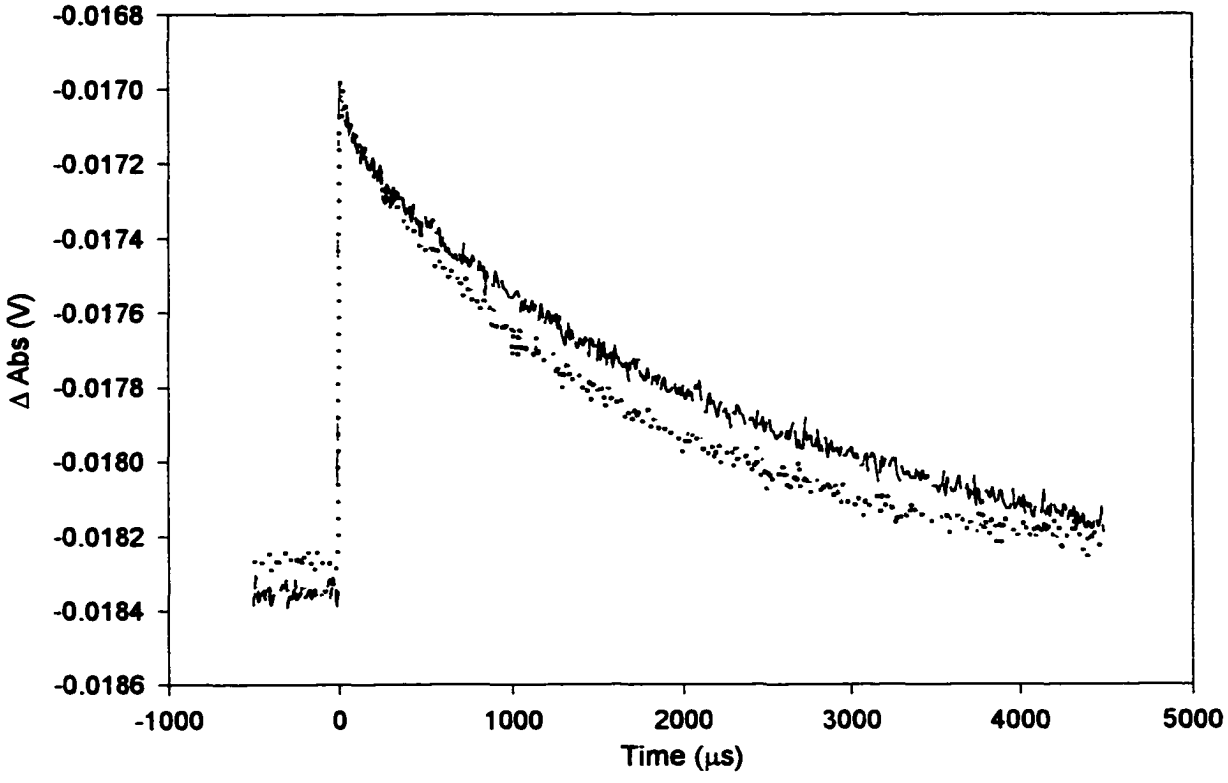

Figure 4.4: Transient absorbance spectras of $Ru(phen)_2(bpy\text{-}MV)^{3+}$ + 100 mM N-Me-PTZ. Shown are the first data set (dashed curve); tenth data set (dotted curve); and average of the 10 data set (solid curve).

Before measurements were taken, the solution in the cell had a bight yellow-orange color to the naked eye. After the measurements, the solution had a orange-brown tint. Figure 4.5 shows UV/Vis spectra before and after measurements. There is clearly a difference

between the two spectra. The base-line shift over the region of 650-800 nm is due to instrumentation. The change in shape of the MLCT band between 450-550 nm is real.

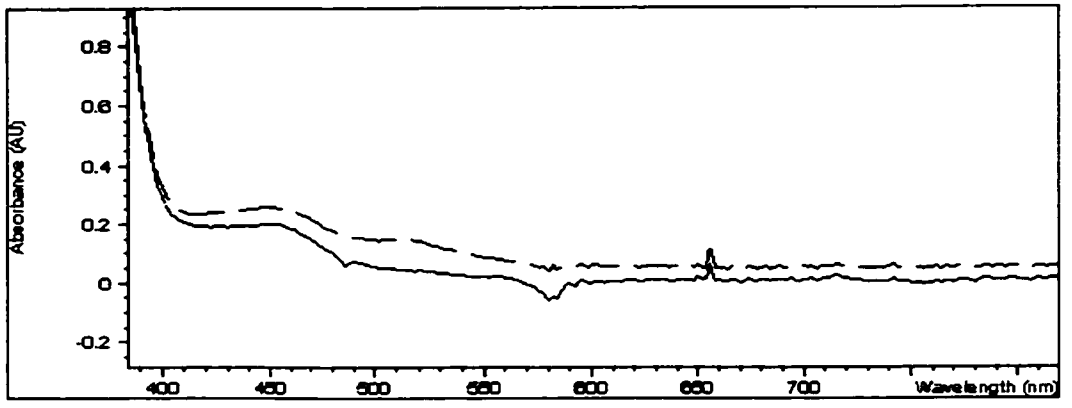

Figure 4.5: Uncorrected UV/Vis spectra of $Ru(phen)_2(bpy\text{-}MV)^{4+}$ + 100 mM N-Me-PTZ before transient absorbance spectroscopy (solid curve) and after transient absorbance spectroscopy (dashed curve).

The degradation of the sample is caused by UV light being absorbed by the N-Me-PTZ. The rate of degradation is dependent on the concentration of N-Me-PTZ in solution, with higher concentrations degrading faster. This is not too surprising as at the higher concentrations, the N-Me-PTZ solution is nearly opaque to UV light, and the Xe lamp used as a probe source in the experiment provides a high intensity of these wavelengths. In the concentration study presented below, no efforts were made to minimize this degradation. In later experiments, including the viscosity study presented below, various cut off filters were employed to minimize excess UV light from the sample. Despite our best efforts, photo-degradation of the $D + C^{2+}\text{-}A^{2+}$ system continues to plague our results.

Two other bits of data support the hypothesis that the degradation is caused by UV light absorption by the N-Me-PTZ. One is that a sample of saturated solution of N-

Me-PTZ in acetonitrile placed in the beam path of the Xe lamp eventually develops a pink-brown color. The second is that $D + C^{2+}\text{-}A^{2+}$ samples that are left in their cells under ambient light continue to exhibit further degradation, presumably caused by UV light from the fluorescent lighting.

Figure 4.6 shows a plot of $\Delta A_{t=0}$ vs. [N-Me-PTZ]. Plotted are the values obtained from the first data set, the last data set and the average over all the data sets for a given sample at a given concentration. One can see the concentration dependence of the photo-degradation clearly in the data. Once the [N-Me-PTZ] > 100 mM the data becomes very erratic. This is analogous to what we saw with the bimolecular quenching experiments in Chapter 3.

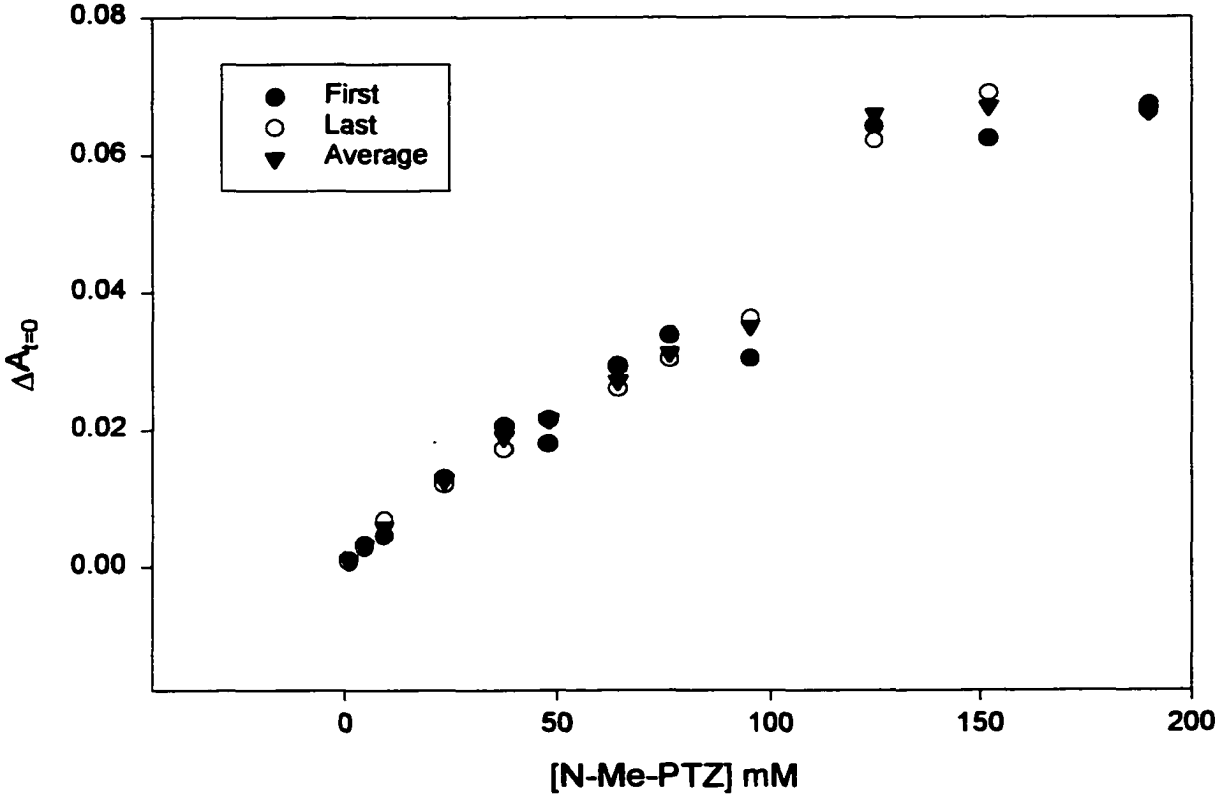

Figure 4.6: Plot of $\Delta A_{t=0}$ vs. [PTZ] for 10^{-5} M $Ru(phen)_2(bpy\text{-}MV)^{4+}$ + x mM N-Me-PTZ in acetonitrile.

If we omit the data from the higher concentrations, and fit the averaged data to the equation:

$$y = A\left(\frac{bx}{1+bx}\right), \qquad (17)$$

we obtain the results in Figure 4.7.

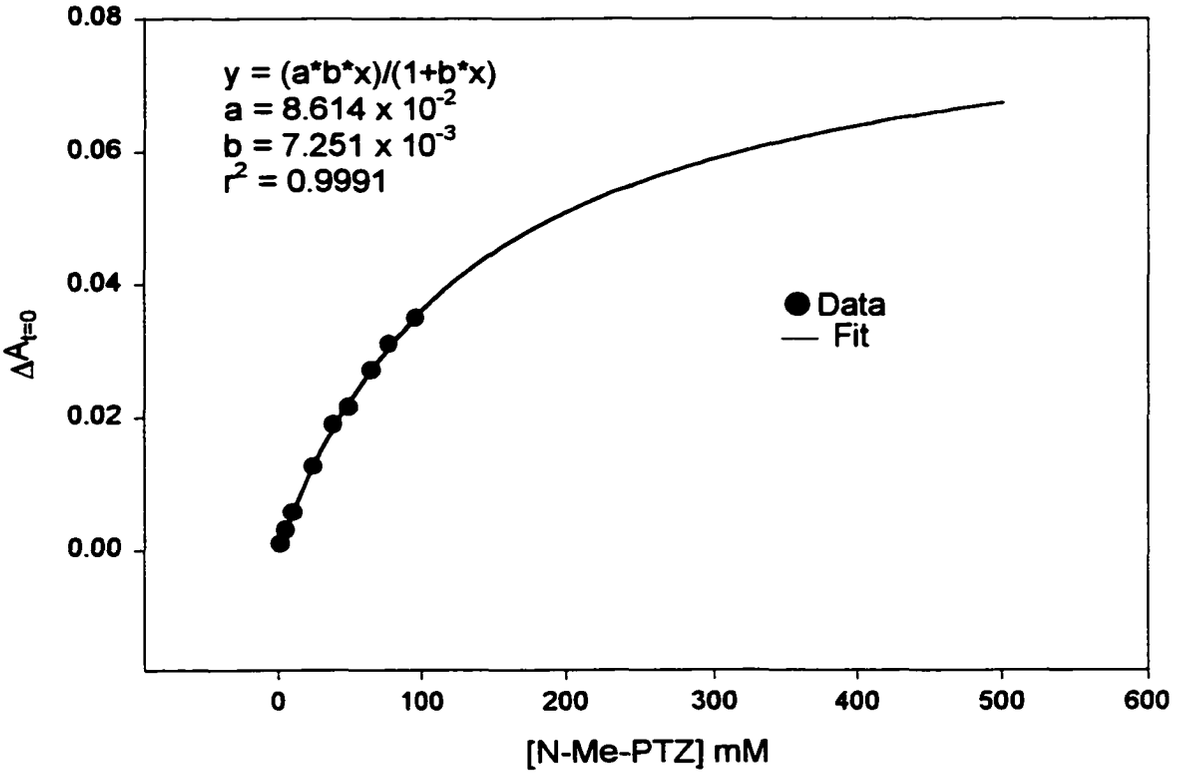

Figure 4.7: Fit of averaged data from Figure 4.6 for [N-Me-PTZ] ≤ 100 mM.

In our system, there are two limiting cases which each give the relation of $\Delta A_{t=0}$ to N-Me-PTZ concentration in the form of equation 17. At one limit, if one assumes that there is no CT interaction, then the reduction of the chromophore by the donor is a simple bimolecular electron transfer process. The energy diagram for such a system, shown in

Figure 4.8, is analogous to the energy diagram for the D-C^{2+}-A^{2+} triad shown in Figure 4.1. The rate constant to the CS state, k_2, is now pseudo-first order as [D] >> [C^{2+}-A^{2+}].

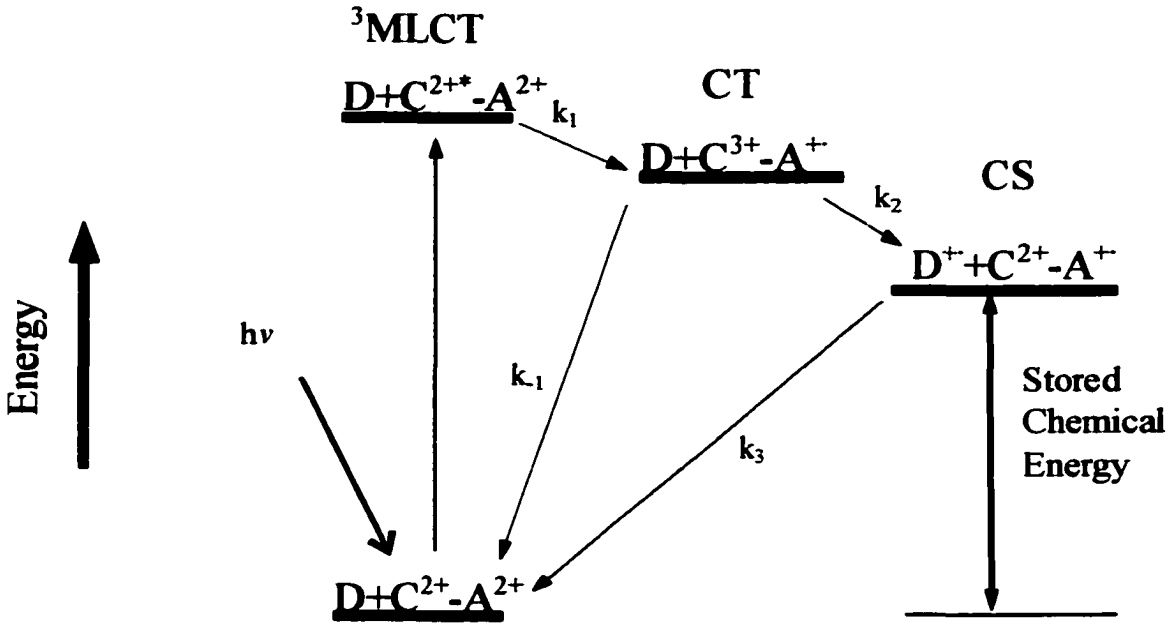

Figure 4.8: Energy diagram of a donor plus chromophore-acceptor (D + C^{2+}-A^{2+}) bimolecular system.

As mentioned above, one of the assumptions we make when dealing with the kinetics of these systems is that $k_2 > k_1 >> k_3$. This means in our systems at t=0[7]

$$\Delta A_{t=0} \propto [CS] \qquad (18).$$

The concentration of the CS state is given by

$$[CS] = k_2[D][CT] \qquad (19).$$

The change in the concentration of the CT state with time is given by

$$\frac{d[CT]}{dt} = k_1[MLCT] - k_{-1}[CT] - k_2[D][CT] \qquad (20).$$

At t = 0, the concentration of the CT state is zero, in other words $\frac{d[CT]}{dt} = 0$.

Substituting this into equation 20 and solving for [CT] gives us

$$[\mathrm{CT}] = \frac{k_1[MLCT]}{k_{-1} + k_2[D]} \qquad (21).$$

Substituting this into equation 19 and rearranging gives us

$$[\mathrm{CS}] = \frac{\left(\frac{k_2}{k_{-1}}\right)[D]}{1 + \left(\frac{k_2}{k_{-1}}\right)[D]} k_1[MLCT] \qquad (22).$$

The concentration of the MLCT is given by

$$[\mathrm{MLCT}] = \varepsilon[C^{2+}\text{-}A^{2+}]_i \qquad (23).$$

where $[C^{2+}\text{-}A^{2+}]_i$ is the initial chromophore concentration and ε is a constant that includes the molar absorbtivity, intensity at the pump wavelength, the volume of the overlap of the pump and probe beams and the pmt voltage. Substituting equation 23 into equation 22 and dividing by the initial concentration of the chromophore gives us the overall quantum yield from the ground state to the CS state

$$\Phi = [\mathrm{CS}]/[C^{2+}\text{-}A^{2+}]_i = \frac{\left(\frac{k_2}{k_{-1}}\right)[D]}{1 + \left(\frac{k_2}{k_{-1}}\right)[D]} k_1\varepsilon \qquad (24).$$

This is in the same form as equation 17 where **b** = $\left(\frac{k_2}{k_{-1}}\right)$ and **a** contains k_1, ε and a scaling factor dependant on instrumental conditions.

The other limiting case occurs if only C^{2+}-A^{2+} complexes that have a donor in a CT interaction in the ground state (denoted as D/ C^{2+}-A^{2+}) can reach the CS state. The energy diagram for such a case is shown in Figure 4.9.

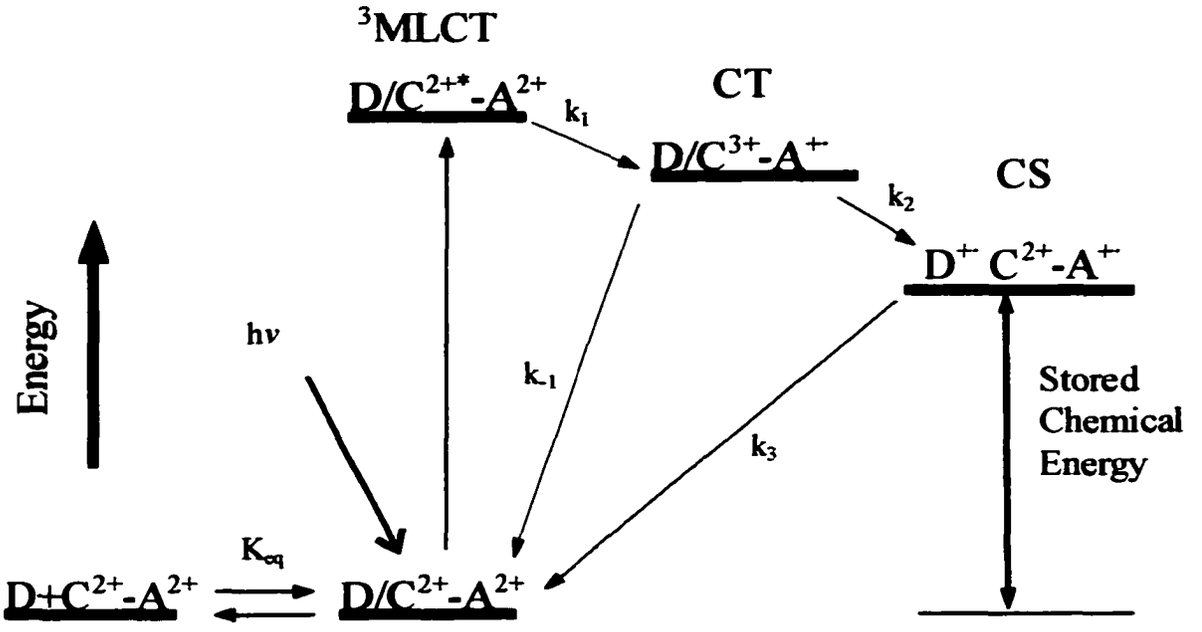

Figure 4.9: Energy diagram of a ground state CT interaction donor/chromophore-acceptor (D/C^{2+}-A^{2+}) bimolecular system as described in the text.

The two major differences in this scheme are the ground state interaction and that we no longer have a bimolecular electron transfer to get to the CS state.

$$[CS] = k_2[CT] \qquad (25).$$

Using the same reasoning as above, we can solve for equation 22 in the ground state interaction case and obtain equation 26

$$[CS] = \frac{\left(\frac{k_2}{k_{-1}}\right)}{1+\left(\frac{k_2}{k_{-1}}\right)} k_1[MLCT] \qquad (26).$$

The proportion of the MLCT state that is in the ground state interaction and can therefore go on to the CS state is given by

$$\frac{[MLCT]}{[C^{2+} - A^{2+}]_i} = \frac{\varepsilon[D/C^{2+} - A^{2+}]}{\varepsilon[D/C^{2+} - A^{2+}] + \varepsilon[C^{2+} - A^{2+}]_i} \qquad (27).$$

Canceling out the ε's (assuming them to be equal) and substituting in the equilibrium relation

$$[D/C^{2+}\text{-}A^{2+}] = K_{eq}[D][C^{2+}\text{-}A^{2+}]_i \qquad (28)$$

to equation 27 and reducing terms gives us

$$\frac{[MLCT]}{[C^{2+} - A^{2+}]_i} = \frac{K_{eq}[D]}{1 + K_{eq}[D]} \qquad (29).$$

Dividing both sides of equation 26 by $[C^{2+}\text{-}A^{2+}]_i$ and substituting in equation 29 gives us a final overall quantum yield of

$$\Phi = [CS]/[C^{2+}\text{-}A^{2+}]_i = \frac{\left(\frac{k_2}{k_{-1}}\right)}{1 + \left(\frac{k_2}{k_{-1}}\right)} k_1 \cdot \frac{K_{eq}[D]}{1 + K_{eq}[D]} \qquad (30).$$

This is also in the same form as equation 17, where **b** is now equal to K_{eq} and **a** contains a host of rate constants as well as instrumental factors.

When corrected for pathlength of the cell the value obtained from the fit of the data in Figure 4.7 is **b** = 7.251 $\underline{M}^{-1}$ (or $\underline{M}^{-2}$). Mallouk, *et al*,[6] reported a value of $k_{-1} = 6.5 \times 10^9\ s^{-1}$ for the $Ru(bpy)_2(bpy\text{-}MV)^{4+}$ complex. If **b** = $\left(\frac{k_2}{k_{-1}}\right)$ as in the simple bimolecular case, then $k_2 = 4.7 \times 10^{10}\ \underline{M}^{-1}s^{-1}$. The diffusion controlled limit in a particular solvent is given by

$$k_{diff} = \frac{8RT}{3\eta} \qquad (31),$$

where η is the viscosity of the solvent.[8] For acetonitrile at 30°C $k_{diff} = 2.0 \times 10^{10}\ \underline{M}^{-1}s^{-1}$. Thus a simple bimolecular electron transfer mechanism results in a calculated value of k_2 that is at least 2.3 times faster than diffusion controlled.

In the scenario where the CT interaction is the only path to the CS state, **b** = K_{eq} = 7.251 $\underline{M}^{-1}$. As we have seen earlier, this value is consistent with data obtained from our D-C^{2+} experiments.

It should be noted that an exiplex formation, i.e. the N-Me-PTZ forming a π-π interaction with the CT state, also gives us an equation in the same form as equation 17

$$\Phi = [CS]/[C^{2+}\text{-}A^{2+}]_i = \frac{\left(\frac{k_2}{k_{-1}}\right)K_{eq}[D]}{1+\left(\frac{k_2}{k_{-1}}\right)K_{eq}[D]}k_1\varepsilon \qquad (32).$$

An exiplex formation is not an unreasonable mechanism. The neutral N-Me-PTZ is not hindered electrostatically from complexing to a ligand on a Ru^{3+} chromophore any more than a ligand on a Ru^{2+} chromophore. Furthermore, all the energetics of the system that favor a π-π interaction in the ground state are equivalent or possibly even more favored in the CT state. In this case **b** = $\left(\frac{k_2}{k_{-1}}\right)K_{eq}$. Based on the diffusion limited rate arguments used above, we can rule the exiplex formation out as the sole mechanism to reach the CS state. However, some contribution to the shape of the curve in Figure 4.7 may be due to this mechanism.[9]

In an effort to slow down diffusion of the two species, to further rule out the simple bimolecular electron transfer process, a high molecular weight polymer was incorporated into the solvent. Originally we used an acetonitrile-polymethylmethacrylate (Acn/PMMA) solvent system. Difficulties degassing the solvent caused us to switch solvent systems to 1,2-dichloroethane-polystyerene (DCE/PS) as the high viscosity solvent and DCE as the low viscosity solvent. The overall change in viscosity was over three orders of magnitude.[10] Figure 4.10 shows the transient absorbance of ten averaged

specta at 397 nm for a 10^{-5} M C^{2+}-A^{2+} complex plus 50 mM N-Me-PTZ in the two solvents.

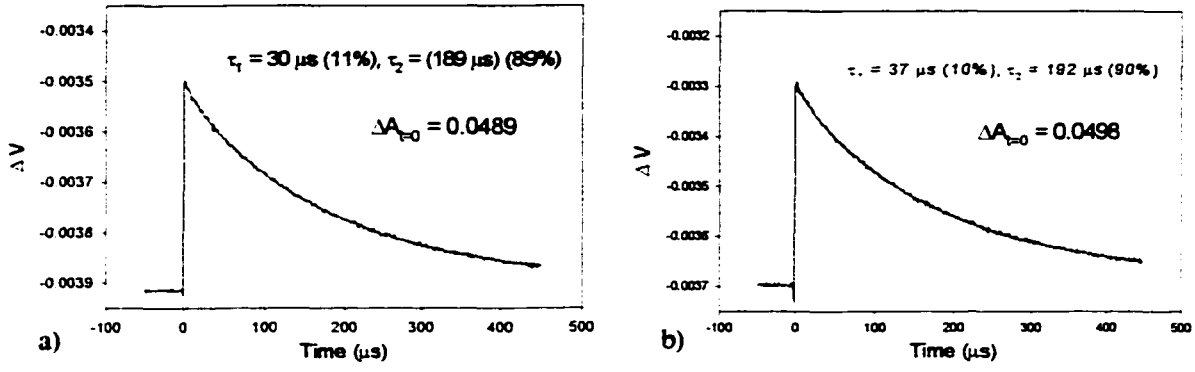

Figure 4.10: Ru(phen)$_2$(bpy-MV)$^{4+}$ + 50 mM N-Me-PTZ in a) DCE and b) DCE/PS.

What can be seen in these two decays is that the initial concentration of the CS state (given by $\Delta A_{t=0}$) does not change with the huge change in viscosity. Taken together with the above data, these results rule out CS state formation by bimolecular diffusional processes. There is a wide range of lifetimes that are observed for the spectra that were averaged to make Figure 4.10. The long component varied from ~180-210 μs in each of the two solutions. There were no trends in the way the lifetimes varied. Some of this variation was due to sample degradation over the ten sets of 1000 scans. The fact that the lifetimes for the averaged spectra are nearly identical seems to be a coincidence. Neither spectra return to the baseline after nearly 0.5 s which suggests that a small fraction of the N-Me-PTZ does diffuse away from the chromophore during the timescale of the experiment.

Scheme 4.1 gives a cartoon of the most likely route to the CS state in the D-C^{2+}-A^{2+} triads based on the results we obtained from the bimolecular systems.

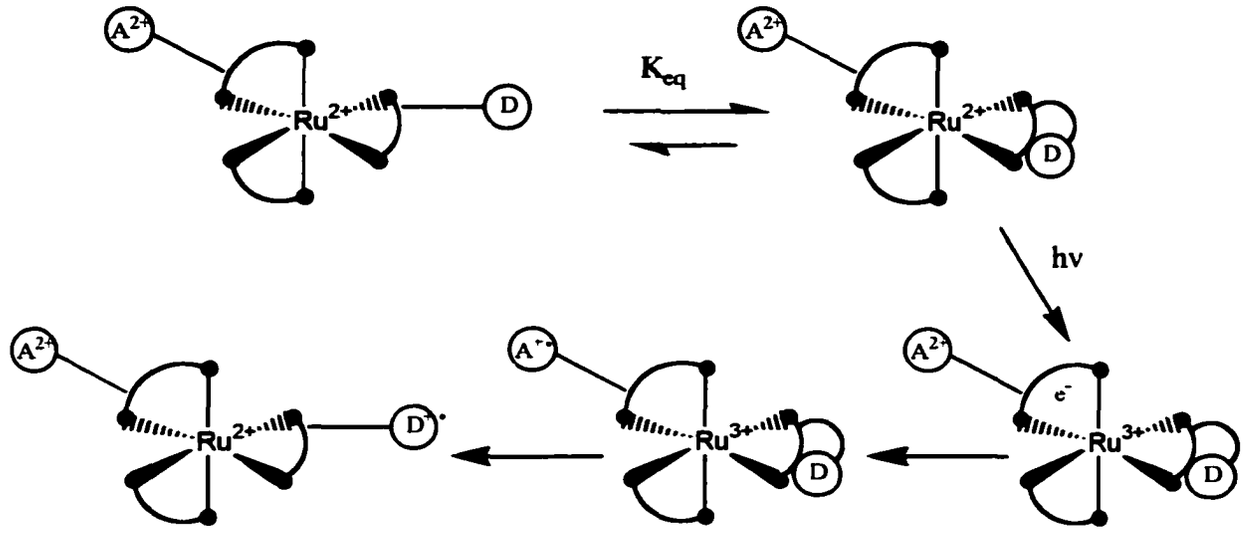

Scheme 4.1: Intramolecular charge transfer interaction followed by photoinduced charge separated state formation.

Several things are implied by this scheme. One is that the PTZ is associating with the ligand to which it is attached. For shorter alkyl chain lengths (less than 4 methylene units), sterics dictate this type of association. For longer chains it is possible, as we saw in Chapter 3, for the donor to interact with the remote ligands. The scheme also shows the photo-excited electron to be localized on a ligand other than the one involved in the CT interaction. As mentioned in Chapter 3, the nature of the CT interaction raises the energy of the π^* orbital of the ligand making it unfavorable for the excited electron to reside on that ligand. In the last step for the formation of the CS state, the oxidized donor now no longer has an interaction with the chromophore, and due to the positive charge on all three subunits, electrostatics will drive them away from each other.

Also implied in the scheme as well as Figure 4.9 is that the CS state is formed only from chromophores that have the CT interaction in the ground state when they are photoexcited. We know from earlier work that for the C^{2+}-A^{2+} complexes, the MLCT state is oxicdatively quenched by these acceptors with near unit efficiency.[5] Any loss in

quantum efficiency to the CS state from the MLCT state arises from the back electron transfer to the ground state competing for the CT state (k_{-1} competing with k_2). We also know that the equilibration rate for the D/C^{2+} charge transfer interaction must be slow on the time scale of the second electron transfer to the CS state. If this equilibration were fast, it would be indistinguishable from simple collisional encounters which is inconsistent with our data.

Within our scheme there are three relevant electron transfers: (1) electron tranfer between unassociated D and C^{2+}; (2) electron transfer within the D/C^{2+} CT interaction complex; and (3) back electron transfer from $A^{+\cdot}$ to C^{3+}. The increased electronic coupling in (2) means we can safely assume that the rate for (2) is much faster than the rate for (1) (i.e. (2) >> (1)). With this constraint, the value for φ (the quantum yield from the MLCT) will depend on (3). If (2) >> (1) >(3), then the CS state will be formed with unit efficiency regardless of the value of K_{eq}. Likewise if (3) >> (2) >> (1), then no CS state would be formed at all. If (2) >> (3) > (1), the case where all the photo-excited D/C^{2+}-A^{2+} complex reaches the CS state, but none of the photo-excited D + C^{2+}-A^{2+} does, then φ would depend on the fraction of the D/C^{2+} CT interaction present at equilibrium in the ground state; in other words, $\varphi = [D/C^{2+}\text{-}A^{2+}]/[C^{2+}\text{-}A^{2+}]_i$. Substituting this into the ground state equilibrium expression (Equation 28) gives us $K_{eq} = \varphi/(1-\varphi)$. This relationship is not supported by the experimental data for K_{eq} and φ. On the other hand, if (3) $\approx$ (2) >> (1) then φ = (2)/(3) or $\varphi = k_2/k_{-1}$ (Figure 4.9). Thus, in our proposed scheme, the quantum yield from the MLCT is determined by the relative rates of k_2 and k_{-1}. The quantum yield from the ground state (Φ) is largely dependant on the value of K_{eq}.

Conclusions: The data clearly shows that there is a ground state charge transfer interaction between phenothiazine-type donors and the ligands on $Ru(bpy)_3^{2+}$-type chromophores. This interaction exists whether the donor is covalently linked to the chromophore or is free to diffuse in a bimolecular system. The interaction exists whether there is a linked acceptor or no acceptor present.

The data also shows that the CT interaction is primarily responsible for the large quantum yields seen in the linked $D\text{-}C^{2+}\text{-}A^{2+}$ complexes. Furthermore, due to the fortuitous alignment of rates in our system, we have a readily available means of tracking this interaction through the equilibrium constant derived from absolute quantum yields.

These results give a new direction of study for $D\text{-}C^{2+}\text{-}A^{2+}$ triads of similar structure to those outlined in this work. Whereas we were investigating new phenothiazine-type donors to increase the driving force for the forward reaction to the CS state as outlined in Chapter 2, we now know that the formation of the CS state is largely dependant on the equilibrium constant. Therefore, factors that effect the equilibrium of the CT interaction, such as solvent effects, temperature and sterics, will play more of a role in the CS state formation than the oxidation potential of the donor. We can think about substituting in donors such as phenoxazine, which have smaller driving forces for forward electron transfer than phenothiazine (see Chapter 2), yet should form a CT interaction in a like manner and should give high quantum yields to the CS state. Such substitutions should yield more stored energy in the CS state, the forward reaction being less downhill. In fact there is no reason *a priori* that any significant incident photon

energy be lost at this step of the forward electron transfers to the CS state. Furthermore, it has been shown that the lifetimes of the CS state in linked D-C^{2+}-A^{2+} complexes can be increased ~ 10x in moderate magnetic fields.[1] The back electron transfer being spin forbidden (the CS state being a triplet while the ground state is a singlet), the principal mechanism for recombination is interconversion between ^{3}CS state and a ^{1}CS state allowed by spin-orbit coupling through the heavy sulfur atom.[1] Placing the complex in magnetic fields at low as 0.5 mT affects the interconversion rate between these two states.[1] Substituting oxygen for sulfur will provide less spin-orbit coupling through the only spin-orbit active atom in either radical in the CS state. A complex with a phenoxazine donor in a magnetic field should exhibit even larger magnetic field effects than the corresponding complexes with phenothiazine. We are now in the process of investigating the effects on the quantum yield to the CS state of substituting in 44-POZ and 44-PSZ (see Chapter 2) in D-C^{2+}-A^{2+} triads and N-MePOZ and N-MePSZ in bimolecular systems and the magnetic field effects on the quantum yield in these systems as well as repeating some of the above experiments with improved instrument design to minimize degradation of the sample.

ENDNOTES

[1] Klumpp, T; Linsenmann, M.; Larson, S.L.; Limoges, B.R.; Bürssner, D.; Krissinel, E.B.; Elliott, C.M.; Steiner, U.E. *J. Amer. Chem. Soc.*, **1999**, *121*, 1076.

[2] Danielson, E.; Elliott, C.M.; Merkert, J.W.; Meyer, T.J. *J. Amer. Chem. Soc.*, **1987**, *109*, 2519.

[3] Klumpp, T; Linsenmann, M.; Larson, S.L.; Limoges, B.R.; Bürssner, D.; Krissinel, E.B.; Elliott, C.M.; Steiner, U.E. *J. Amer. Chem. Soc.*, **1999**, *121*, 1076.

[4] Cooley, L.F.; Larson, S.; Elliott, C.M. *J. Phys. Chem.*, **1991**, *95*, 10694.

[5] Cooley, L.F., Headford, C.E.L.; Elliott, C.M., Kelley, D.F. *J. Amer. Chem. Soc.*, **1988**, *110*, 6673.

[6] Yonemoto, E. H.; Saupe, G.B.; Schmehl, R.H.; Hubig, S.M.; Riley, R.L.; Iverson, B.L.; Mallouk, T.E. *J. Amer. Chem. Soc.*, **1994**, *116*, 4786.

[7] The time at t=0 in our experiments is the rise time of our signal (~4 ns). During this time, the concentrations of [MLCT] and [CT] states have fallen to zero. In other words $k_1+k_2 \gg (4\ ns)^{-1}$ (see Figures 4.8 and 4.9); and as is mentioned in Chapter 1, $k_1 > (80\ ps)^{-1}$. On the other hand, the concentration of the CS state is at its maximum because $k_3 \ll (4\ ns)^{-1}$.

[8] Atkins, P.W. "Physical Chemistry, 4th ed.", W.H. Freeman and Co., New York, **1990**, pp. 848-849.

[9] It is interesting to note that the PTZ degradation products appear to quench at the diffusion controlled limit in acetonitrile until [D] ≈ 50 mM at which concentration $k_{obs} << k_{diff}$.

[10] No direct measurement of the viscosity was made. Qualitatively the solution flowed at a rate much slower than ethylene glycol, which has a viscosity of over 1000x that of 1,2-DCE.

Appendix A:

Cyclic Voltammograms of Various Donors and Ruthenium Compounds

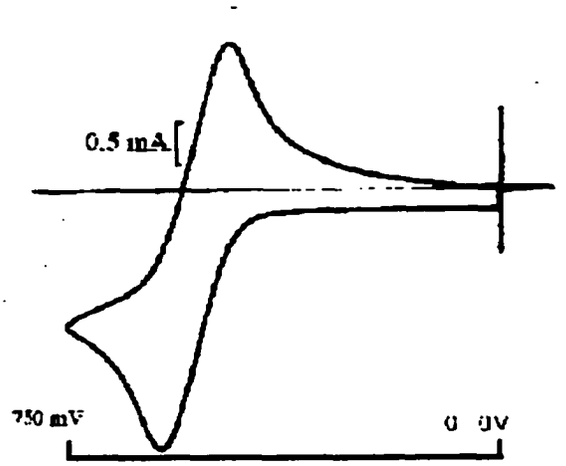

Phenoxazine (POZ)

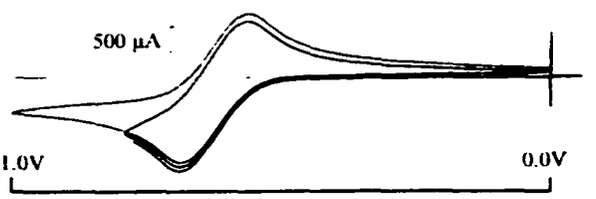

N-methylphenoxazine (N-MePOZ)

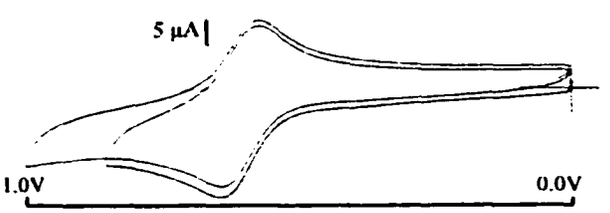

44-POZ

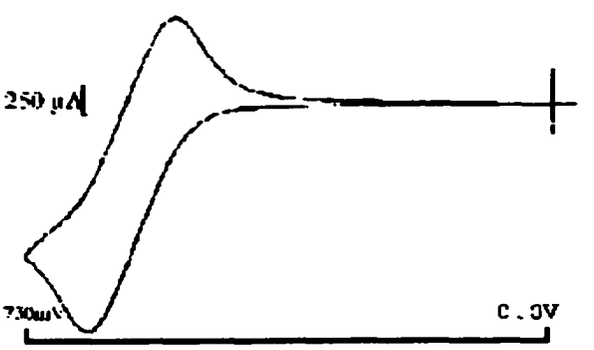

Phenothiazine (PTZ)

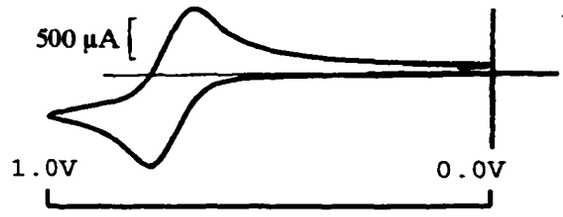

N-methylphenothiazine (N-MePTZ)

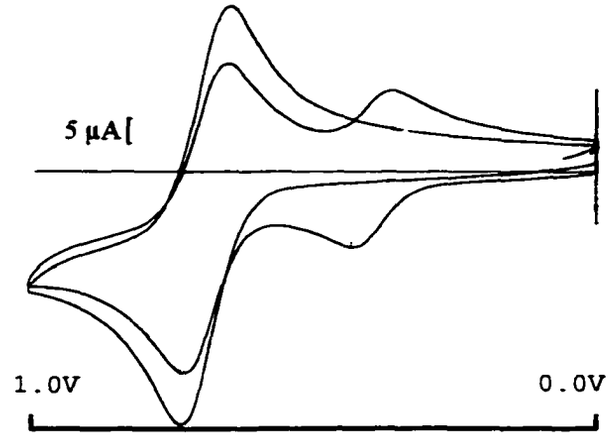

44-PTZ w/ferrocene

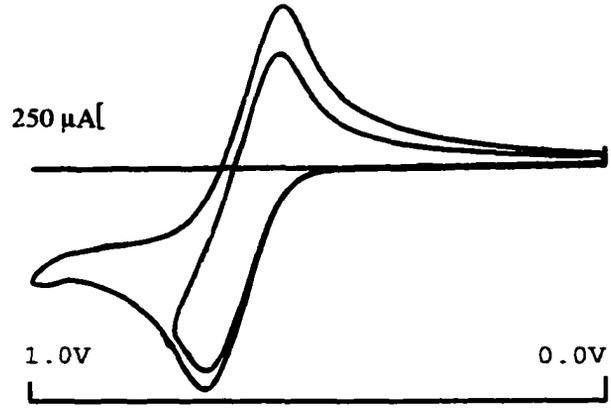

Phenoselenazine (PSZ)

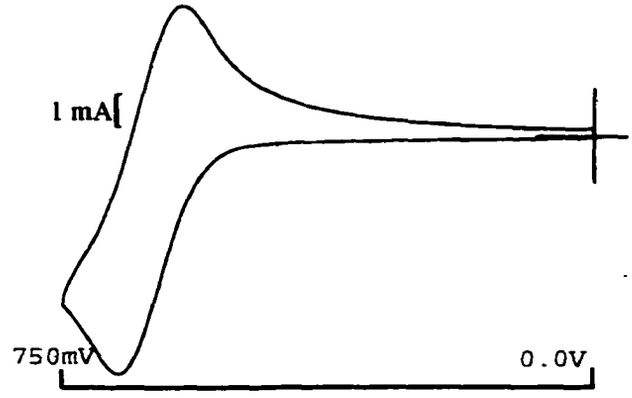

N-methylphenoselenazine (N-MePSZ)

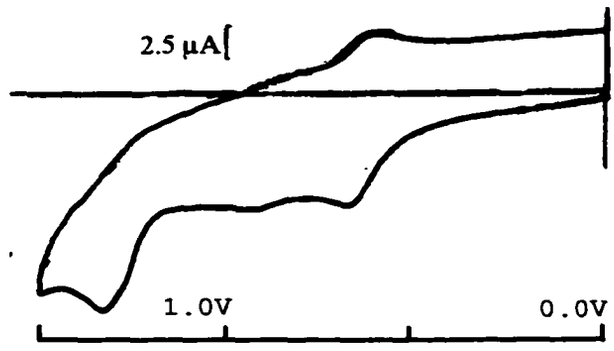

44-PSZ

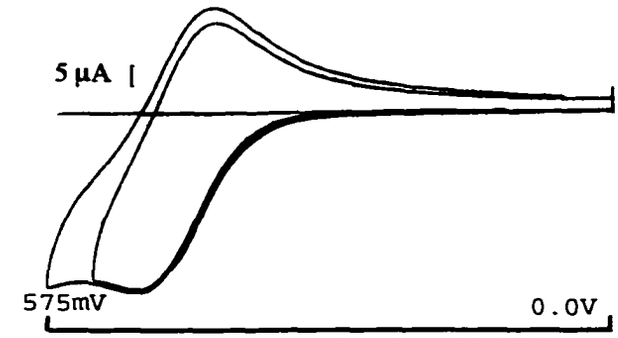

2,4,6,8-Tetramethylphenothiazine (tMePTZ)

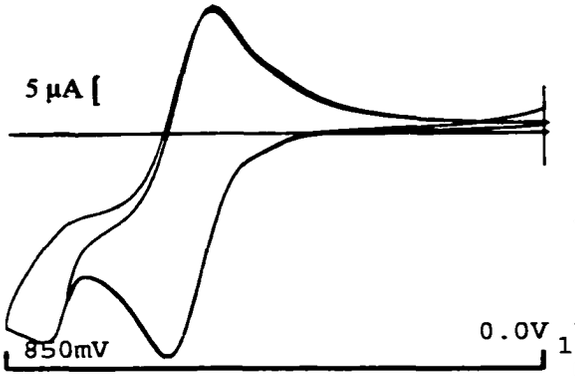

44-tMePTZ

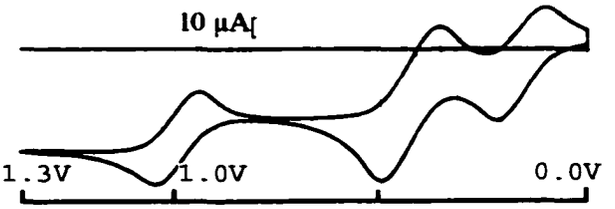

5,10-Dimethyldihydrophenazine (di-Me-PNZ) w/ferrocene

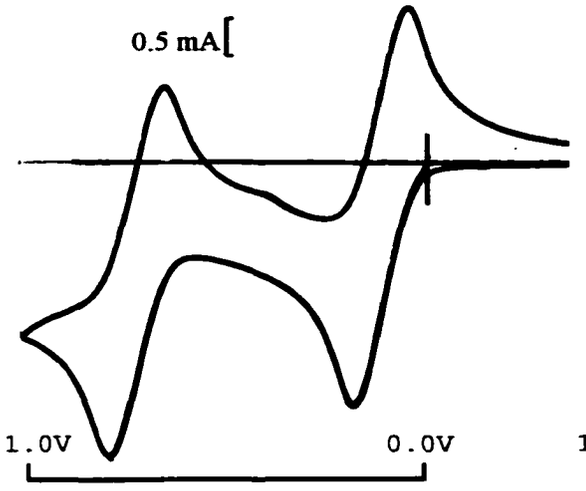

N,N,N'N'-Tetramethylphenylenediamine (TMPD)

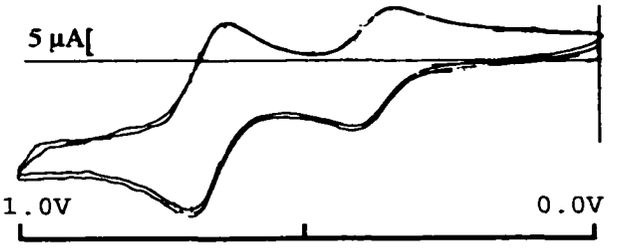

47-PTZ w/ferrocene

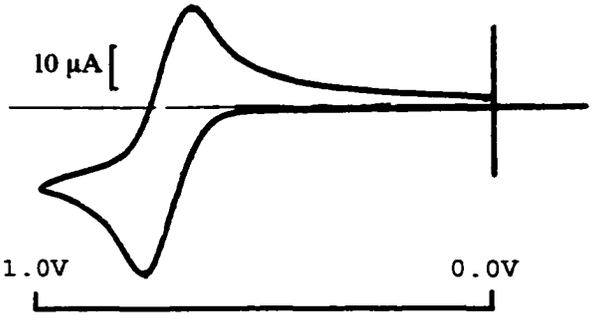

N-neopentylphenothiazine (npPTZ)

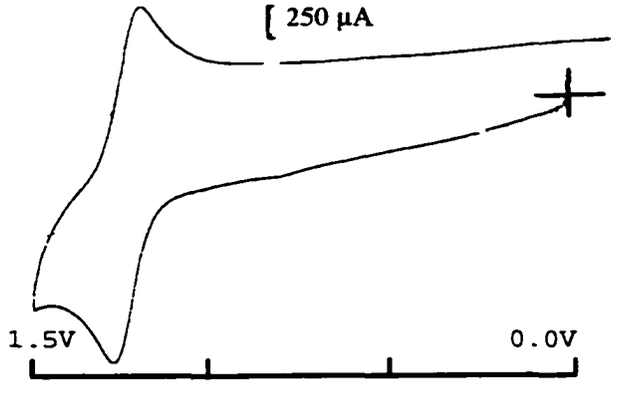

$Ru(dmb)_3(PF_6)_2$

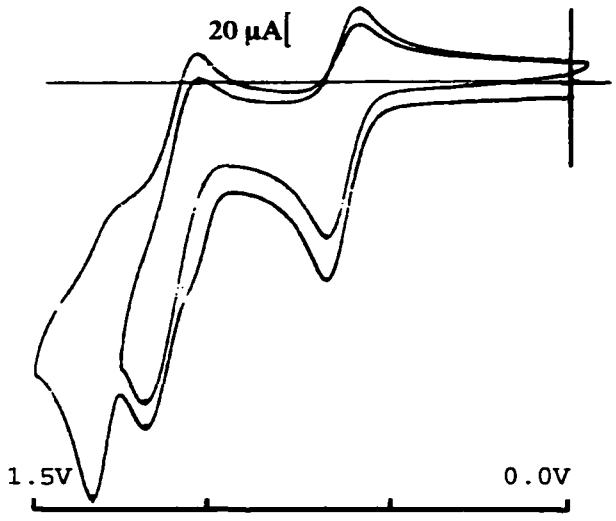

$Ru(dmb)_2(47\text{-}PTZ)(PF_6)_2$

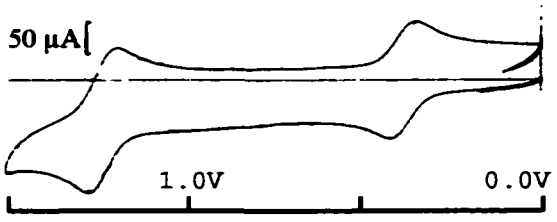

$Ru(phen)_2(dmb)(PF_6)_2$ w/ferrocene

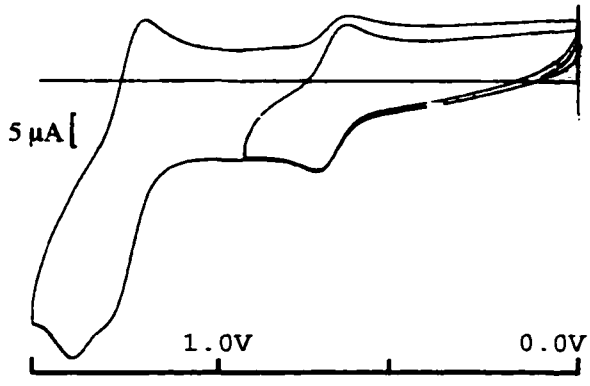

$Ru(phen)_2(47\text{-}PTZ)(PF_6)_2$

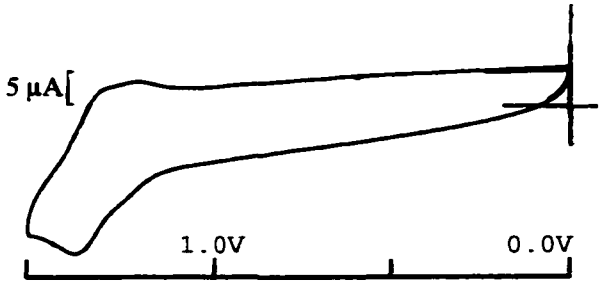

$Ru(dppz)_2(dmb)(PF_6)_2$

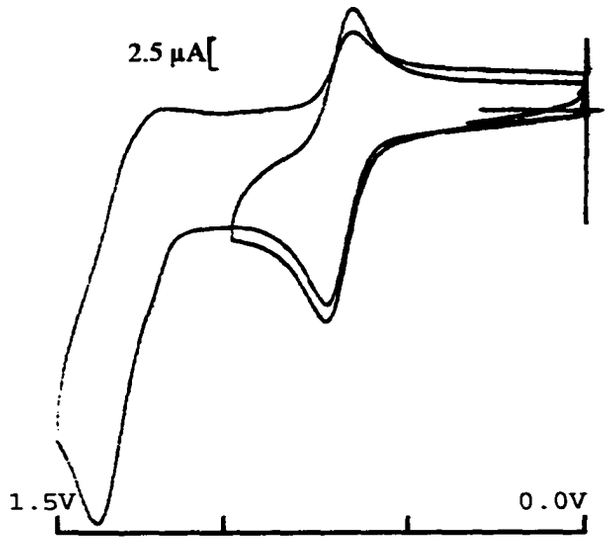

$Ru(dppz)_2(47\text{-}PTZ)(PF_6)_2$

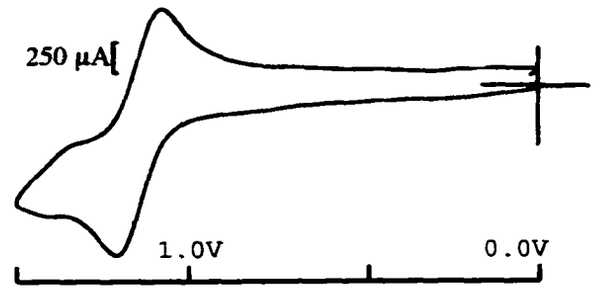

$Ru(tbut)_3(PF_6)_2$

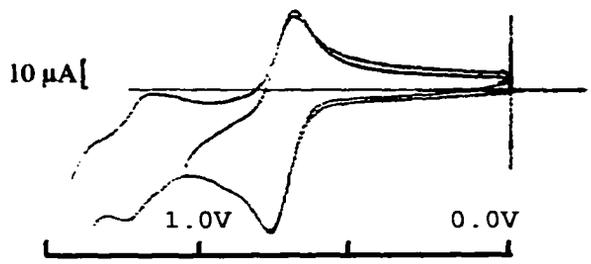

$Ru(tbut)_2(47\text{-}PTZ)(PF_6)_2$

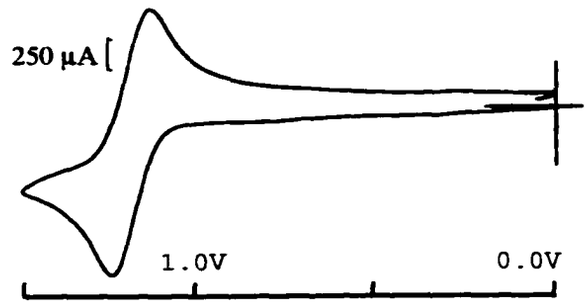

$Ru(\varphi_2\text{-}bpy)_2(dmb)(PF_6)_2$

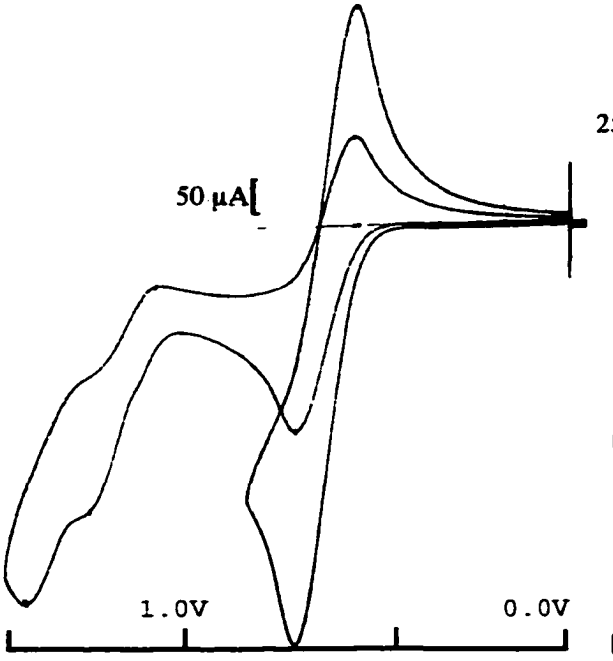

$Ru(\varphi_2\text{-bpy})_2(47\text{-PTZ})(PF_6)_2$

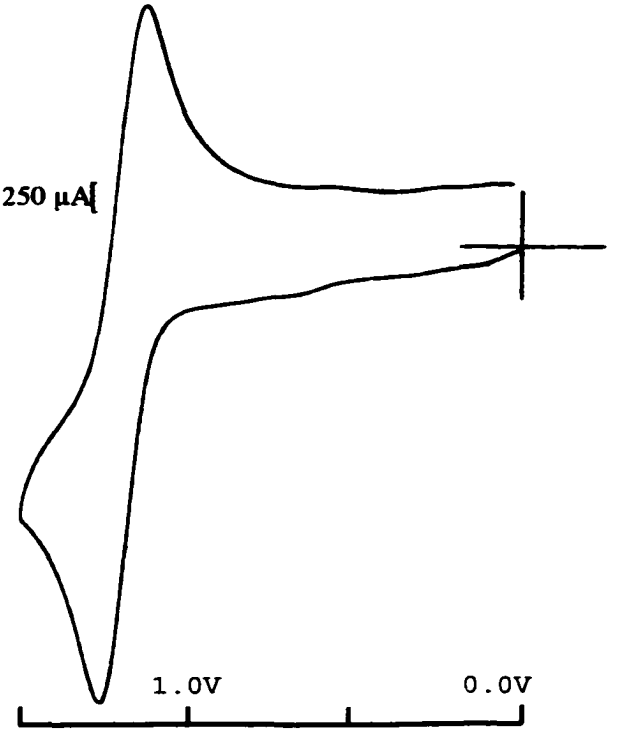

$Ru(\varphi_2\text{-phen})_2(dmb)(PF_6)_2$

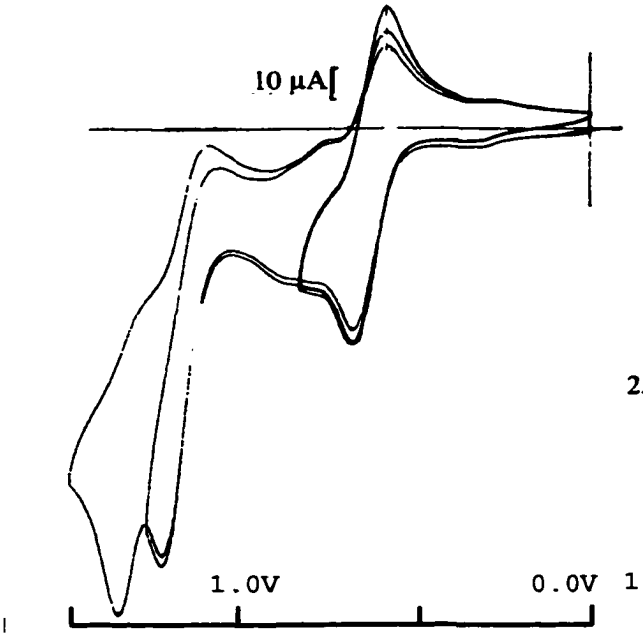

$Ru(\varphi_2\text{-phen})_2(47\text{-PTZ})(PF_6)_2$

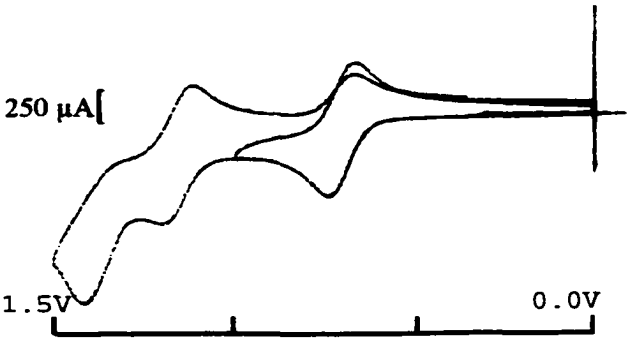

$Ru(i\text{-biq})_2(47\text{-PTZ})(PF_6)_2$

Appendix B:

NMR Spectra of $Ru(phen)_3(PF_6)_2$ + *x* M N-MePTZ and Related Data

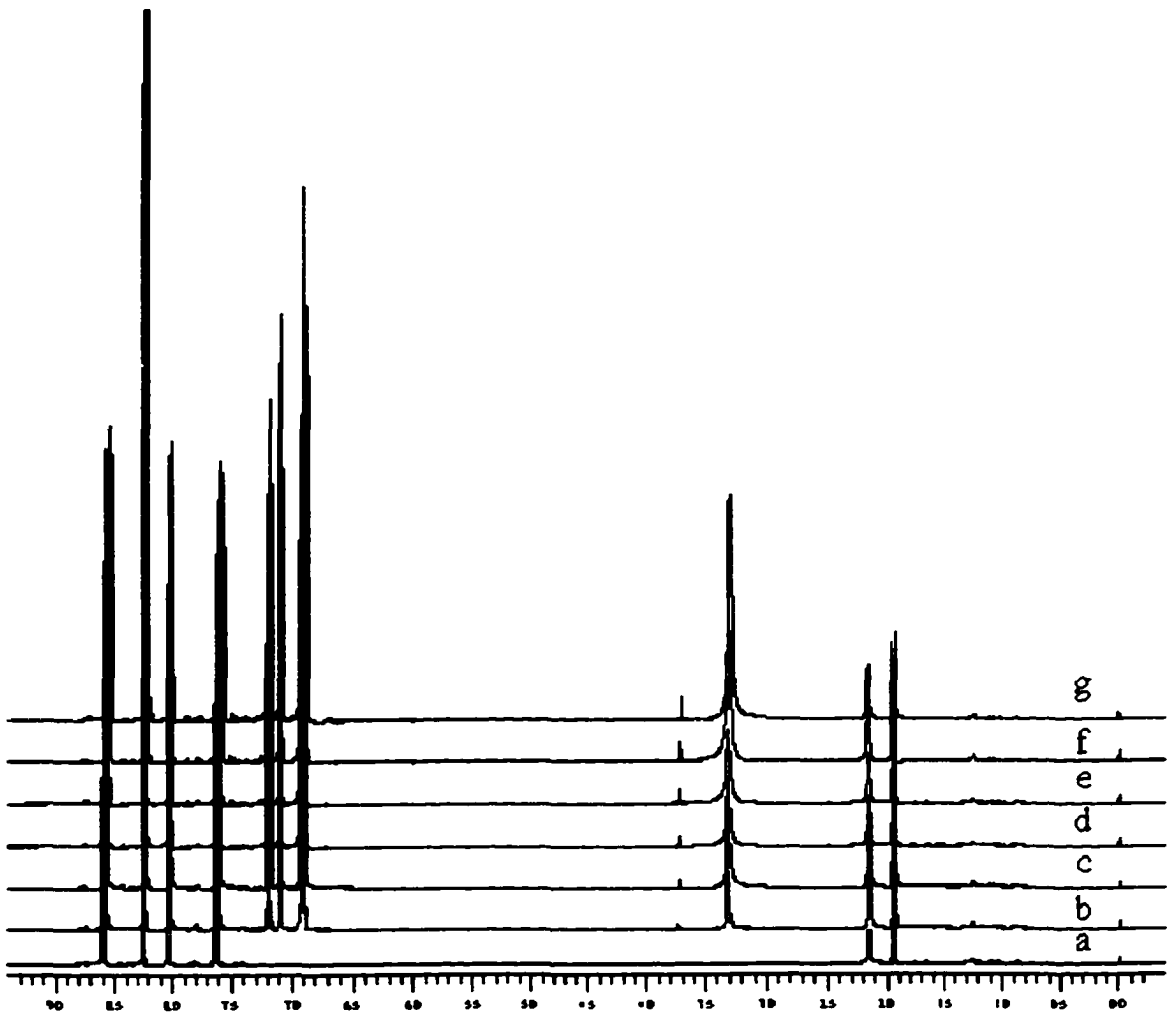

NMR spectra of 10^{-4} M $Ru(phen)_3^{2+}$ + *x* mM N-MePTZ in d_6-acetonitrile; a) 0 mM; b) 27 mM; c) 54 mM; d) 74 mM; e) 98 mM; f) 144 mM; g) 239 mM.

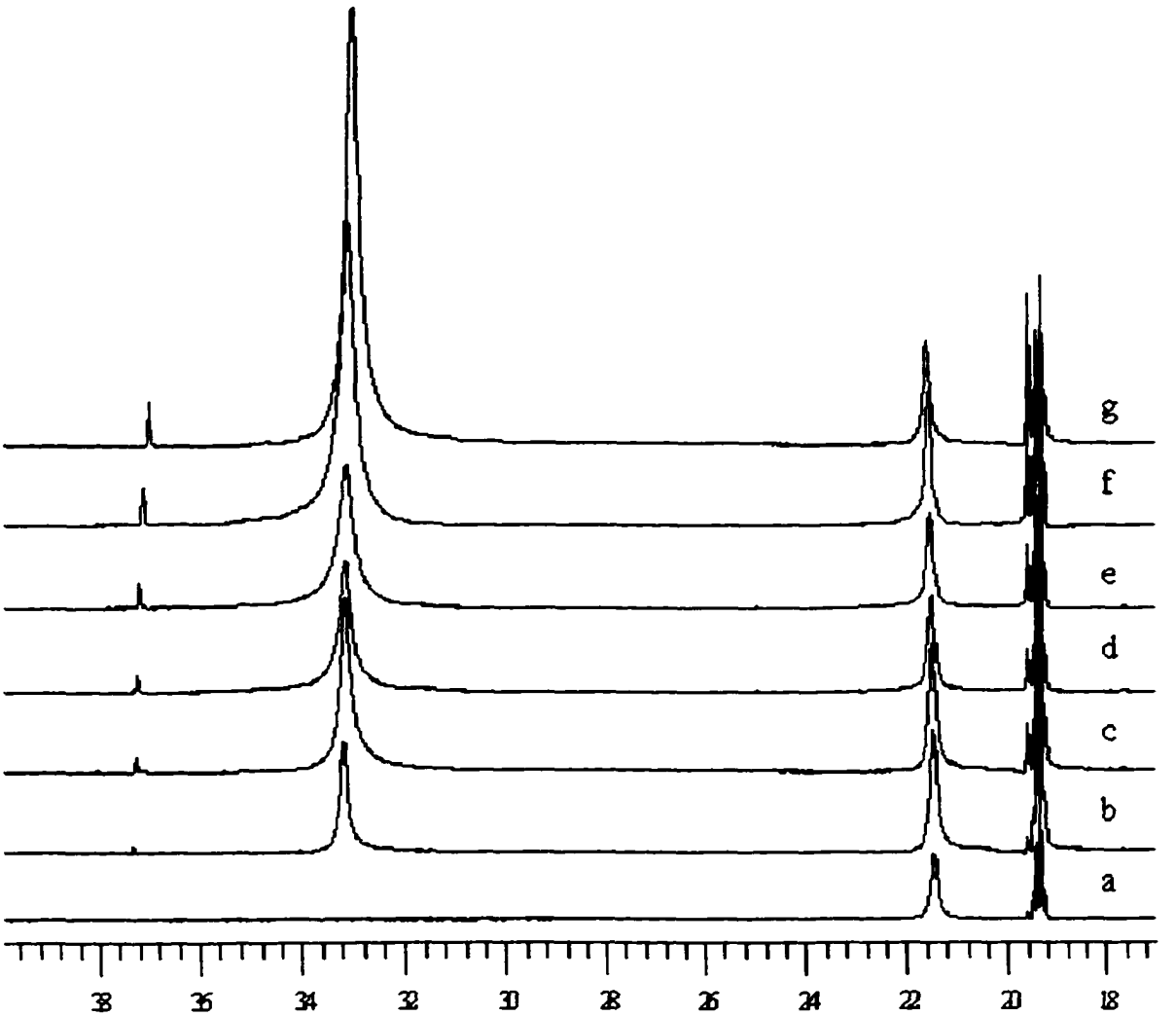

Expansion of the above spectra. The peaks at 1.94 and 2.15 ppm arise from the solvent (the latter arising from a water contaminant). The peak at ~3.32 ppm are the methyl protons from N-MePTZ.

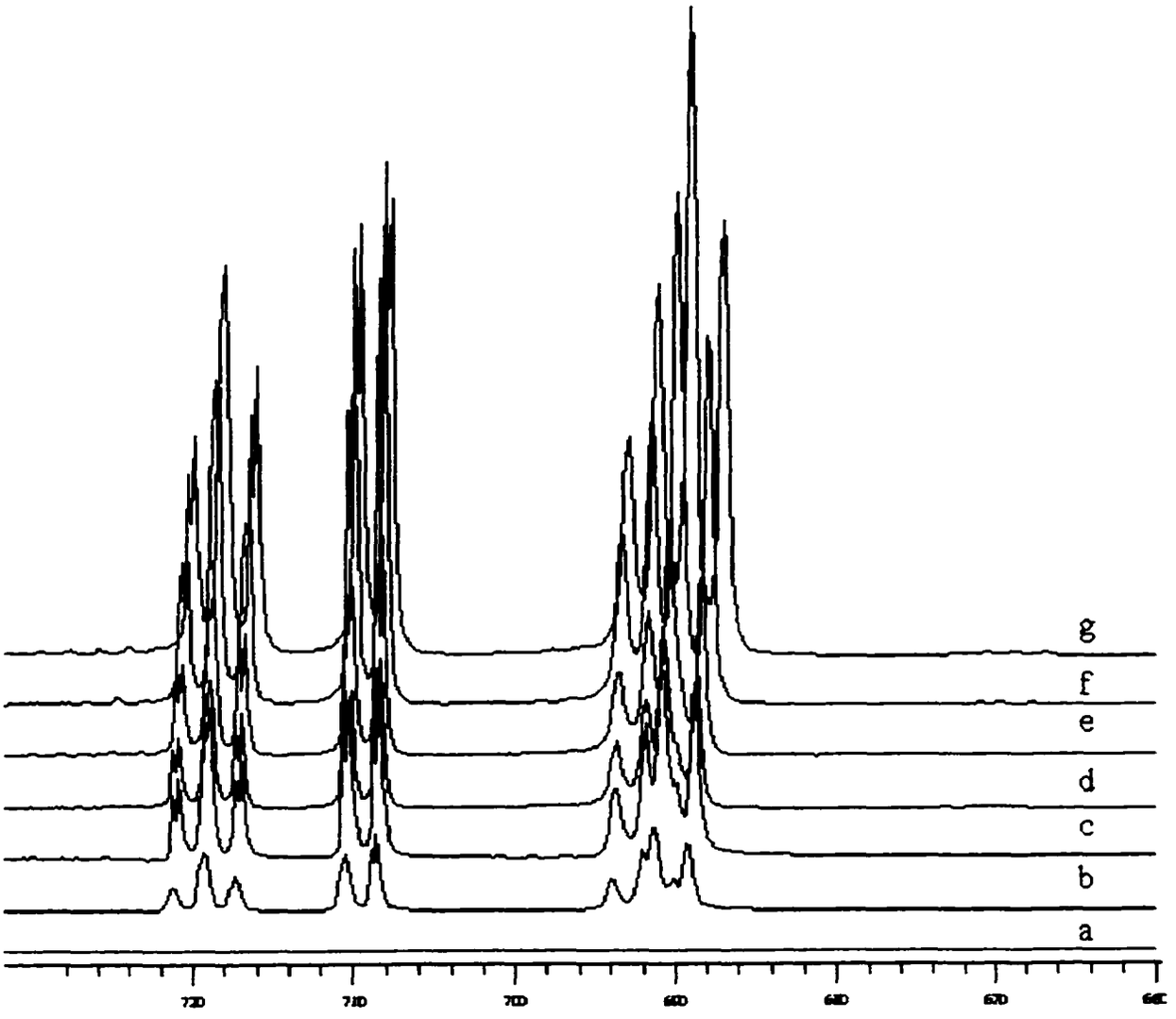

Expansion of the N-MePTZ ring protons.

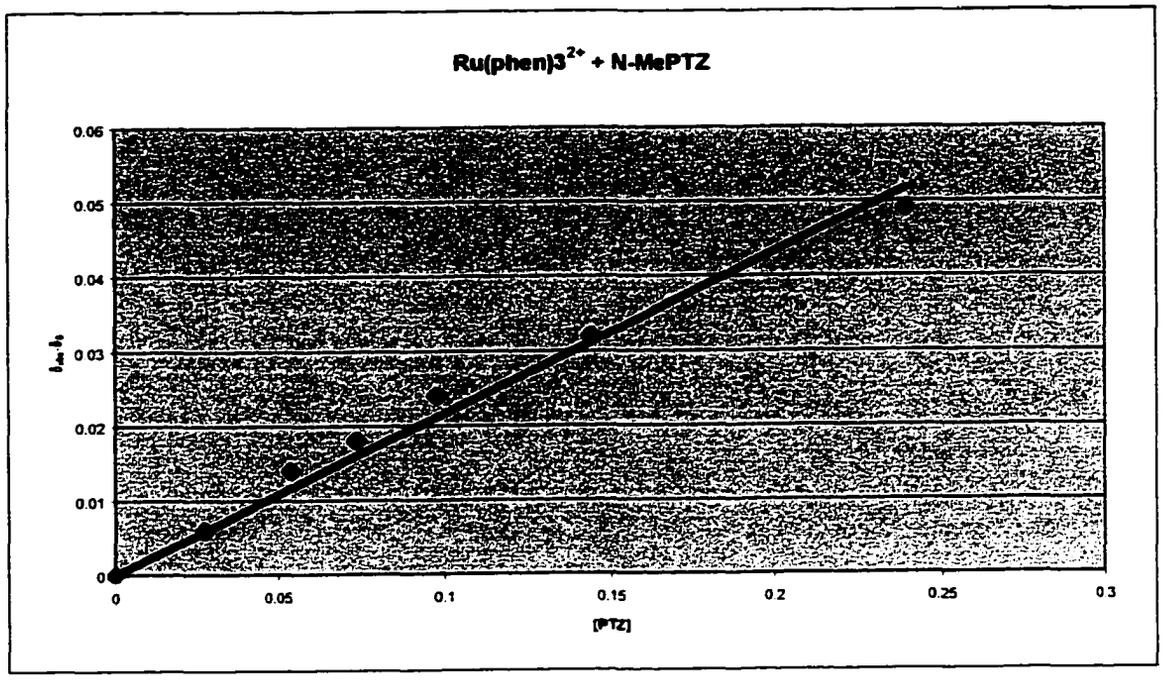

Plot of change in the chemical shift (δ_{obs}-δ_0) of the $H_{5,6}$ protons on the phenanthroline ligands versus the concentration of N-MePTZ.

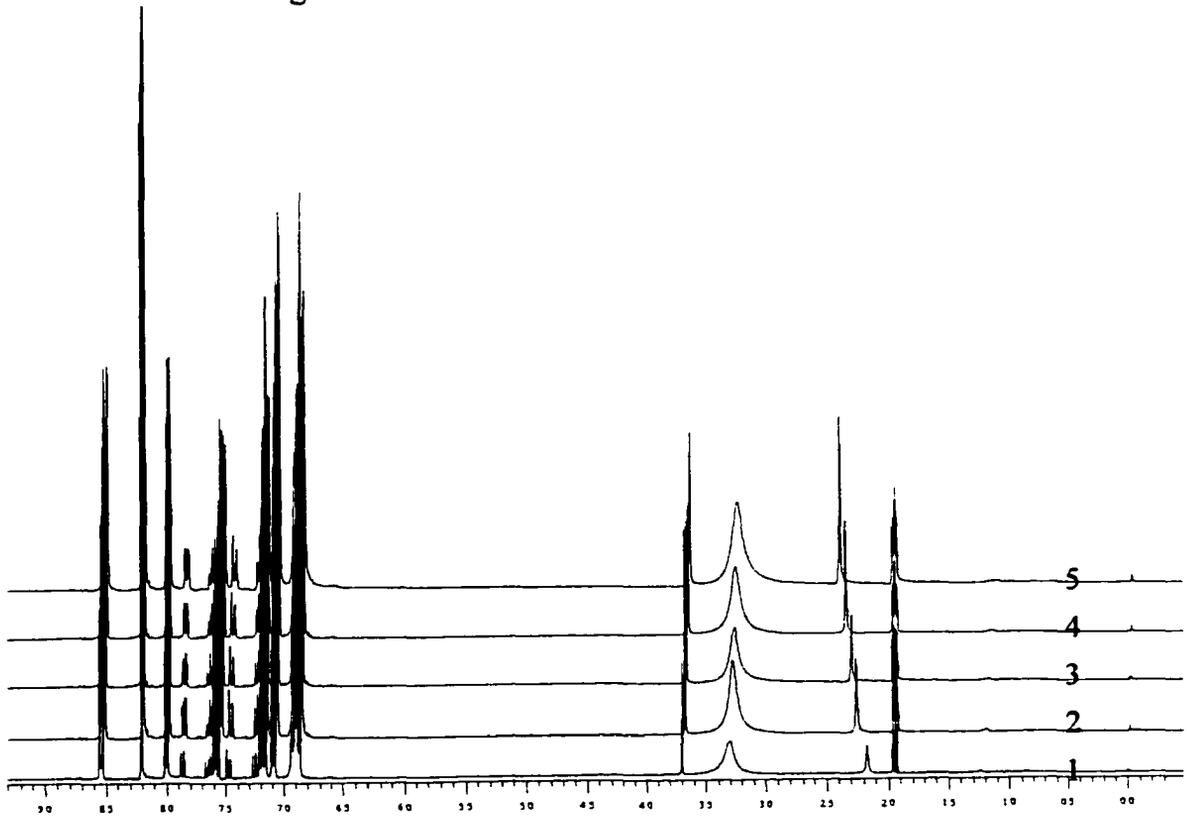

NMR spectra of 10^{-4} M $Ru(phen)_3^{2+}$ + 289 mM N-MePTZ in d_6-acetonitrile at 1) 25°C; 2) 0°C; 3) -10°C; 4) -20°C; 5) -30°C.

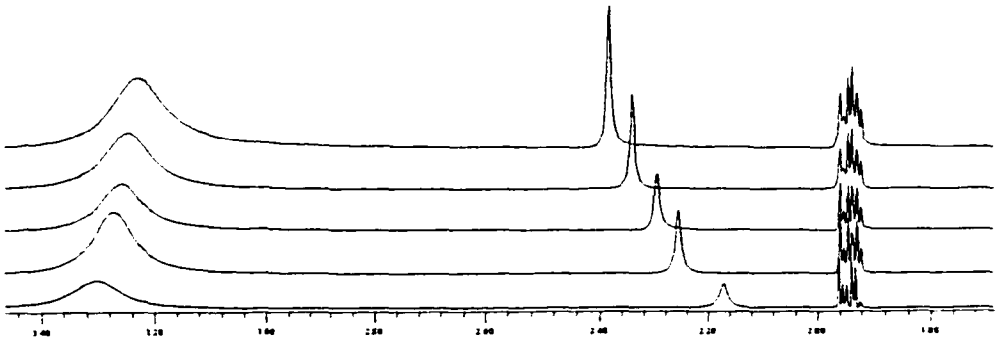

Expansion of the upfield section of the above spectra.

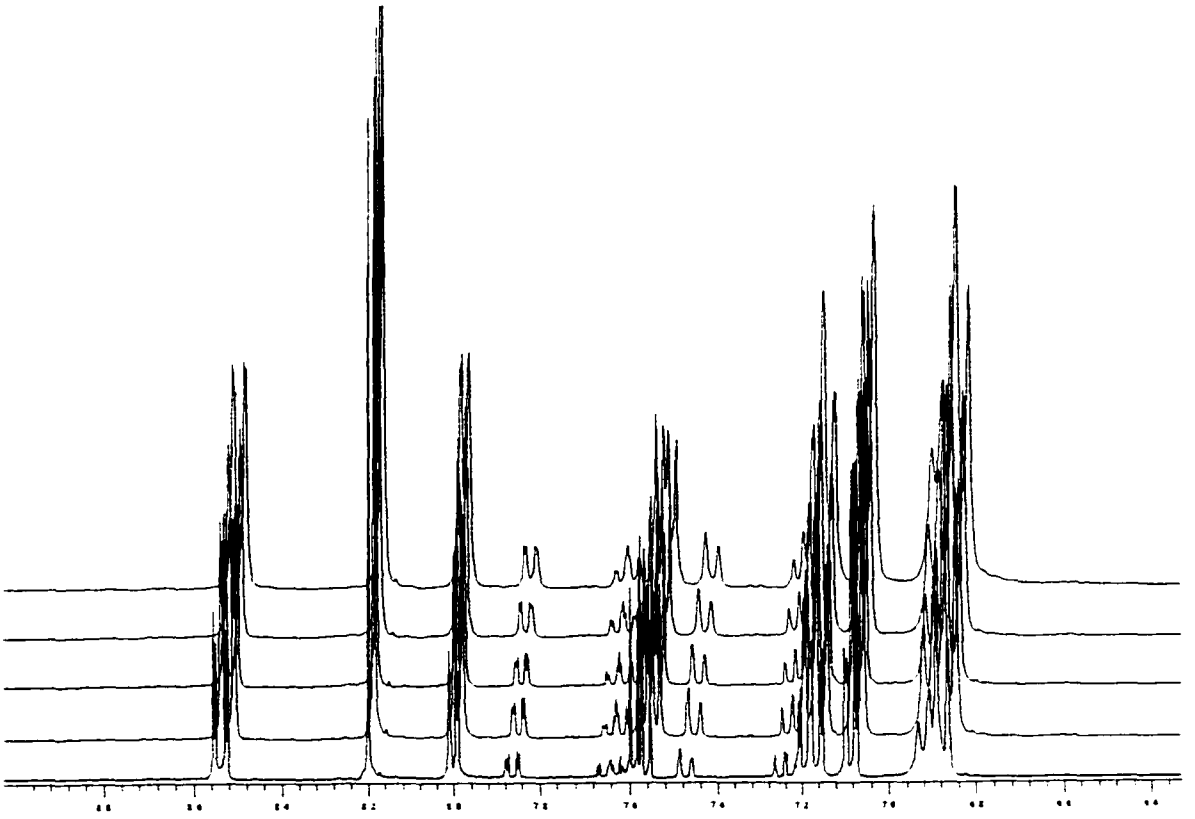

Expansion of the N-MePTZ and phenanthroline ring protons. The multiplets at 7.24, 7.48, 7.64 and 7.85 ppm arise from degradation products of the N-MePTZ.

Appendix C:

Emission Spectra of Selected Ruthenium Complexes

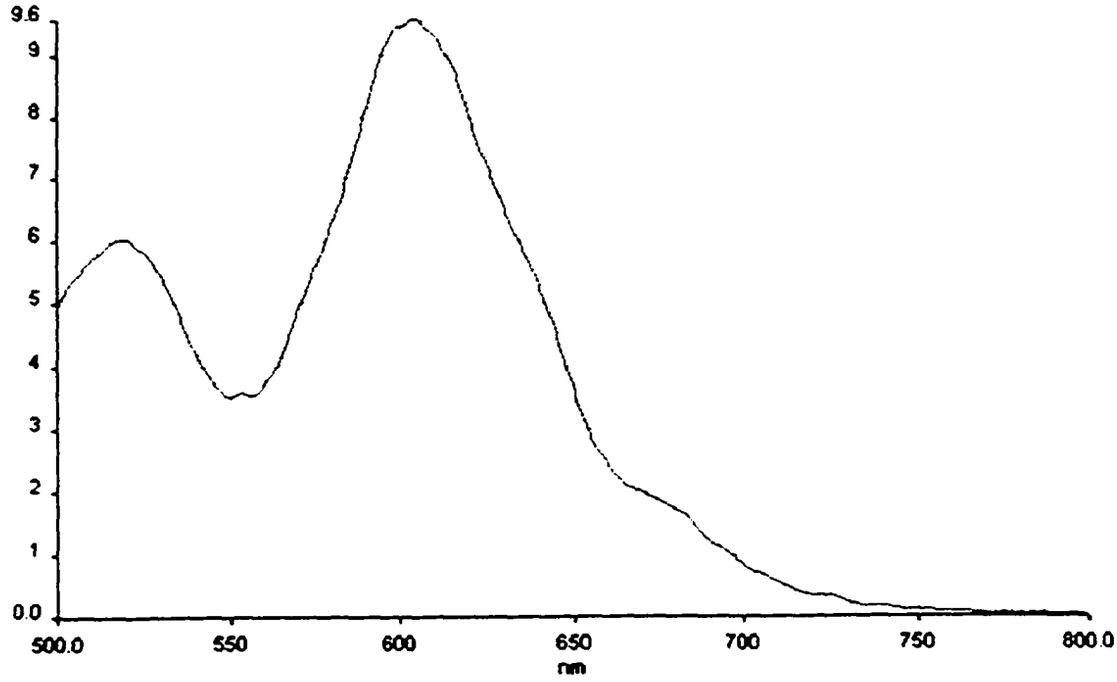

$Ru(44\text{-}tMe\text{-}PTZ)_3(PF_6)_2$

Em_{max}= 604nm Em_{onset}= 542nm

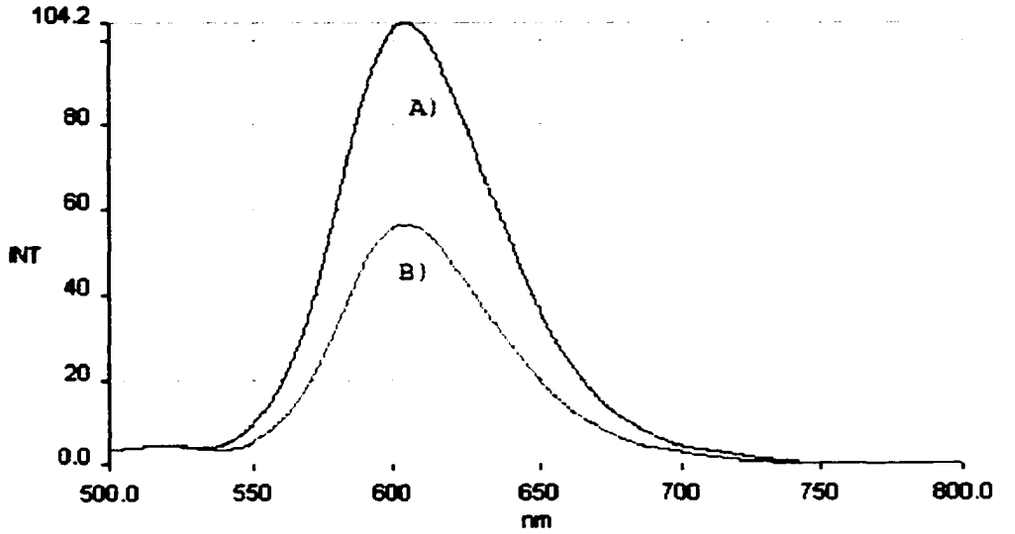

A) $Ru(dmb)_3(PF_6)_2$ B) $Ru(dmb)_2(47\text{-}PTZ)(PF_6)_2$

Em_{max}= 603nm Em_{onset}= 556nm

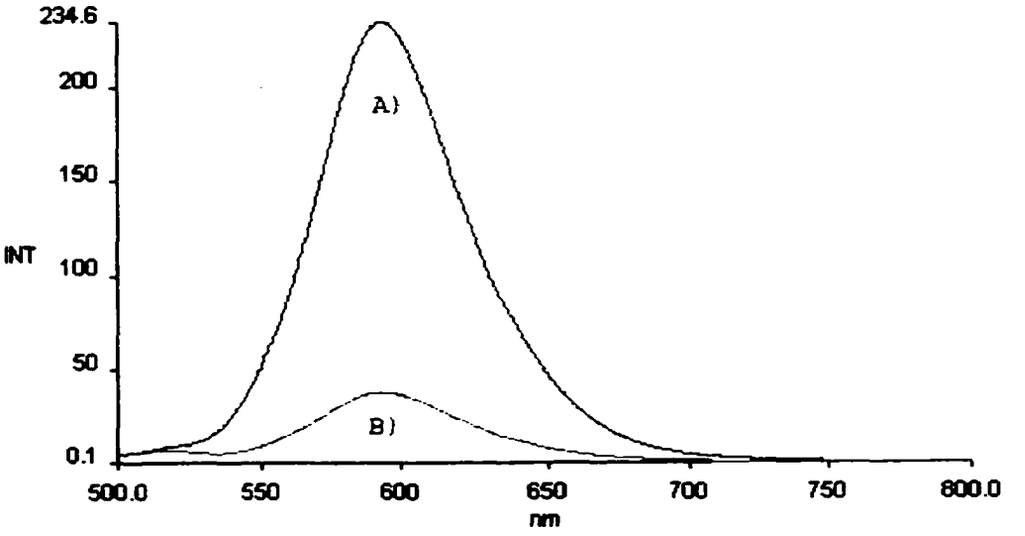

A) $Ru(phen)_2(dmb)(PF_6)_2$ B) $Ru(phen)_2(47\text{-}PTZ)(PF_6)_2$

Em_{max}= 593nm Em_{onset}= 542nm

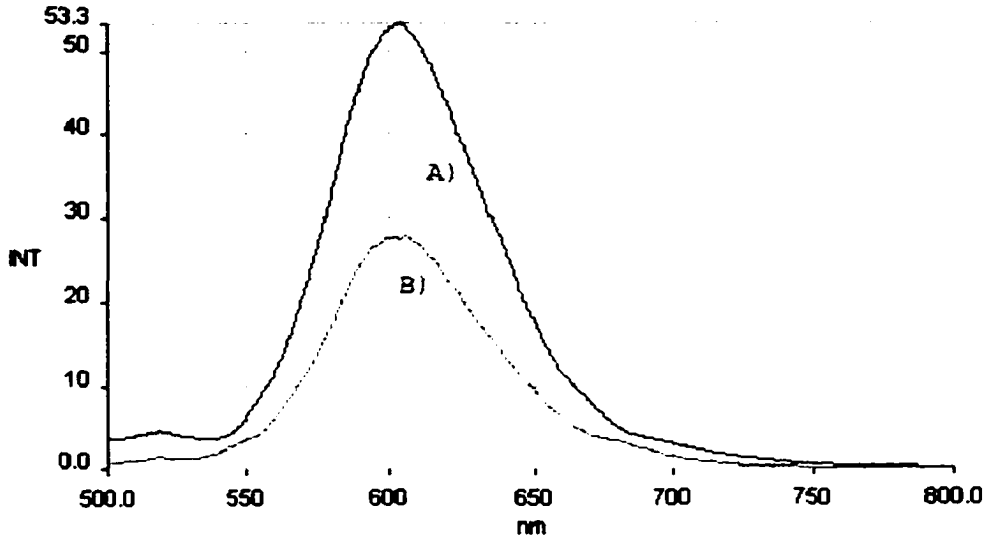

A) $Ru(tbut)_2(dmb)(PF_6)_2$ B) $Ru(tbut)_2(47\text{-}PTZ)(PF_6)_2$

Em_{max}= 603nm Em_{onset}= 554nm

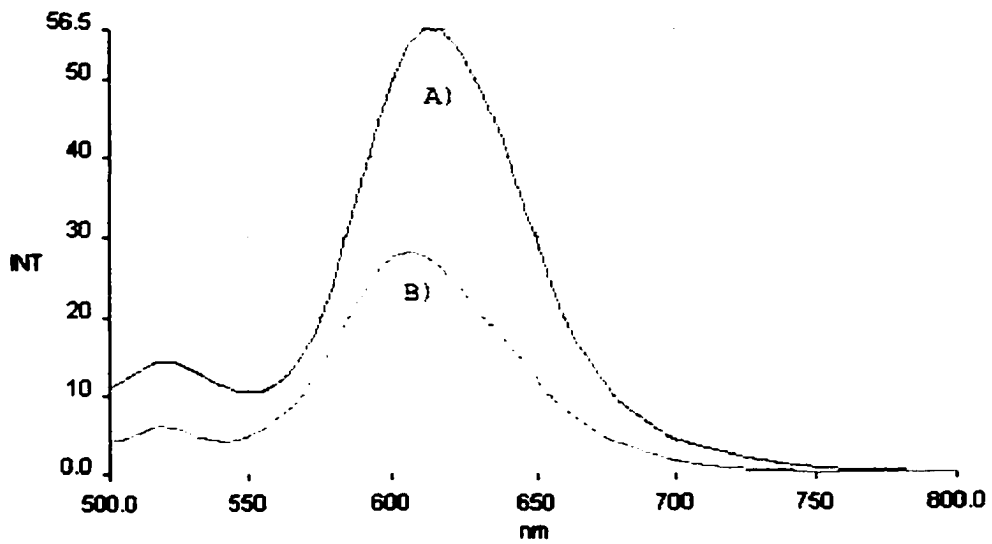

A) $Ru(dppz)_2(dmb)(PF_6)_2$ B) $Ru(dppz)_2(47\text{-}PTZ)(PF_6)_2$

Em_{max}= 615nm Em_{onset}= 560nm

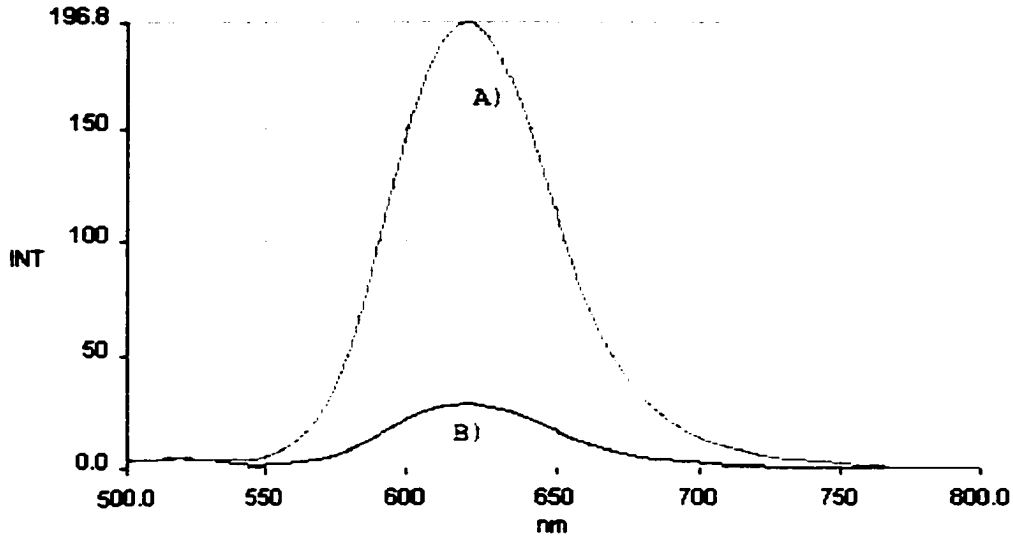

A) $Ru(\varphi_2\text{-}bpy)_2(dmb)(PF_6)_2$ B) $Ru(\varphi_2\text{-}bpy)_2(47\text{-}PTZ)(PF_6)_2$

Em_{max}= 620nm Em_{onset}= 570nm

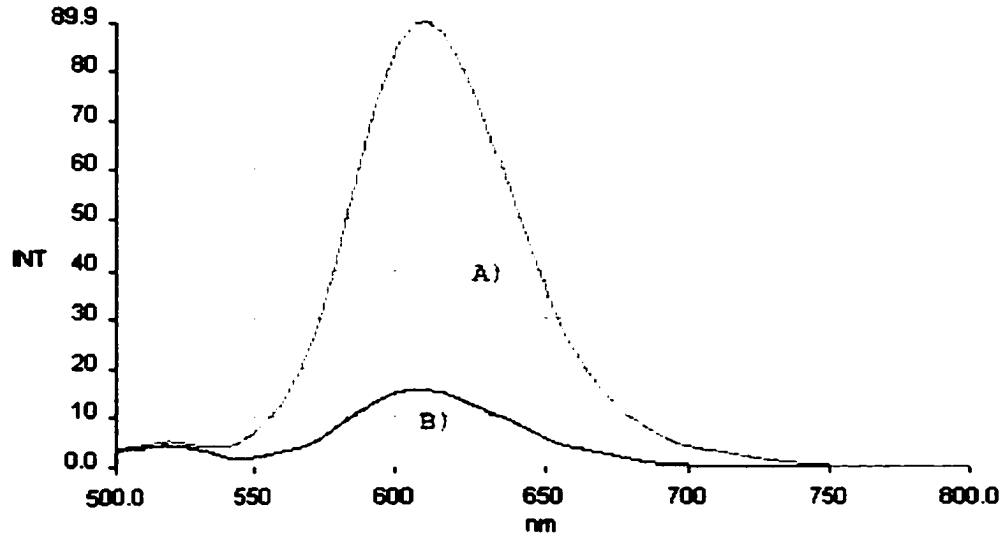

A) $Ru(\varphi_2\text{-}phen)_2(dmb)(PF_6)_2$ B) $Ru(\varphi_2\text{-}phen)_2(47\text{-}PTZ)(PF_6)_2$

Em_{max}= 605nm Em_{onset}= 560nm

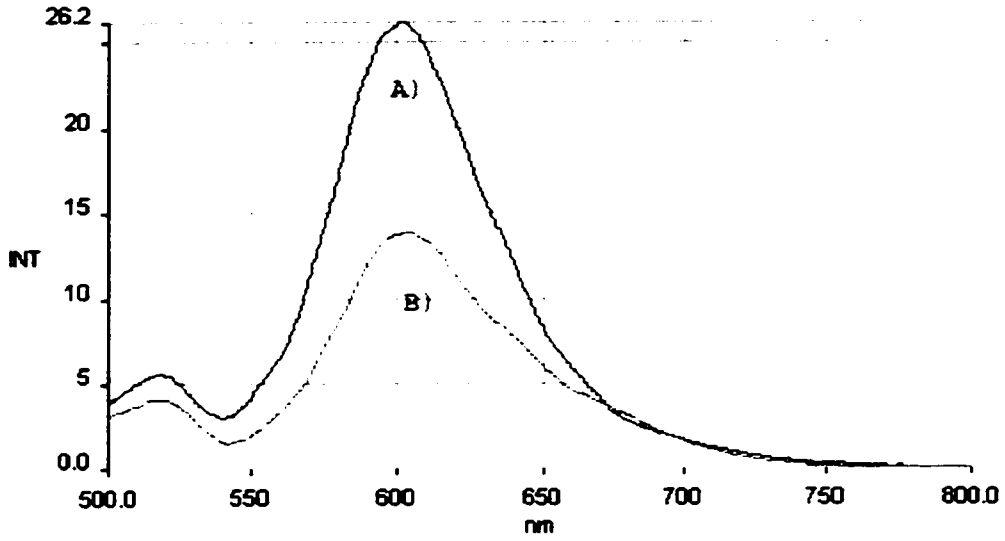

A) $Ru(i\text{-}biq)_2(dmb)(PF_6)_2$ B) $Ru(i\text{-}biq)_2(47\text{-}PTZ)(PF_6)_2$

Em_{max}= 600nm Em_{onset}= 551nm